Minimal models of the tropical climate: theoretical aspects and implication for the future climate change

Gilles Bellon

Thèse de doctorat de l'Université Pierre et Marie Curie
Sciences de l'Environnemment

présentée par

Gilles BELLON

Modélisation minimale du climat tropical : aspects théoriques et implications pour le changement climatique futur

Minimal Models of the Tropical Climate: Theoretical Aspects and Implication for Future Climate Change

Soutenue le 4 octobre 2004 devant le jury composé de :

M. Jean-Philippe	Duvel	Examinateur
M. Michael	Ghil	Co-directeur de thèse
Mme Katia	Laval	Présidente
M. Hervé	Le Treut	Directeur de thèse
M. Serge	Planton	Rapporteur
M. Jean-Luc	Redelsperger	Rapporteur

Laboratoire de Météorologie Dynamique du CNRS, IPSL,
Université Pierre et Marie Curie et Ecole Normale Supérieure,
Paris, France

Remerciements

Je tiens à remercier tout d'abord à Hervé Le Treut et Michael Ghil qui m'ont proposé un sujet de thèse très riche et ont permis le bon déroulement de ce projet, avec notamment une instructive visite d'un an à l'Université de Californie, Los Angeles. Je leur suis très reconnaissant de leurs conseils et de leur soutien constant, ainsi que de l'indépendance dont j'ai bénéficié.

J'ai beaucoup apprécié ma collaboration avec Bjorn Stevens que je remercie pour le temps qu'il a consacré à m'expliquer avec passion les processus de couche limite. Merci aussi à Sylvain Cheinet avec qui j'ai eu de nombreuses discussions à ce sujet, entre mille autres...

Merci à Jun-Ichi Yano pour ses explications et son point de vue critique sur les problèmes de dynamique tropicale. Merci à Rémi Roca pour ses conseils sur les données ayant trait au cycle de l'eau et son énergie communicative.

Je remercie Katia Laval d'avoir accepté de présider mon jury de thèse. Merci à Jean-Philippe Duvel et Jean-Luc Redelsperger d'avoir suivi mon travail au sein du comité de thèse avant de siéger dans le jury, et merci à Serge Planton de les avoir rejoints. Je tiens à remercier particulièrement Serge Planton et Jean-Luc Redelsperger d'avoir mené à bien leur tâche fastidieuse de rapporteurs.

Des conversations avec des chercheurs du groupe de modélisation au LMD-Jussieu ont souvent apporté des éléments très utiles à ma réflexion. Je tiens donc à remercier Sandrine Bony, Laurent Li, Jean-Yves Granpeix, Jean-Louis Dufresne, Frédéric Hourdin et Rémi Tailleux pour leur aide.

Merci à tous ceux qui ont facilité mon travail en apportant leur aide : Martine Mahérou, Catherine Douineau et Marie-Christine Roos pour les aspecs administratifs; Robert Franchisseur, Laurent Fairhead, Véronique Fabart et Frédéric Bongat pour les aspects informatiques.

Je remercie aussi tous ceux qui ont rendu convivial l'environnement de travail sur les différents sites, notamment les joyeuses équipes de doctorants. Un merci particulier à Sylvie, Sébastien, Eric, Armel et Julien qui ont partagé mon bureau, et donc aussi mes enthousiasmes et frustrations de tous les jours.

Je n'oublie pas ma famille qui m'a soutenu dans ce projet. Merci à toutes les équipes d'Equiterre et d'Etudiants et Développement de m'avoir permis de diversifier mes préoccupations. Un salut au passage à Michel et Raph, ainsi que Valérie et Delphine, pour ne pas m'avoir demandé trop souvent quel temps il ferait le lendemain. Et merci à Debra, de juste être là.

Résumé

Cette thèse a pour but d'amener quelques réponses à des questions toujours pendantes sur le climat tropical: pourquoi la température de surface dans les Tropiques présente-t-elle un maximum autour de 30°C, quels sont les processus, à différentes échelles, qui contrôlent la stabilité du climat tropical, et sa faible sensibilité à un changement climatique? L'approche choisie, celle de la modélisation idéalisée, permet d'isoler les principaux mécanismes et de tester ou d'approfondir notre compréhension théorique de ces phénomènes.

Dans l'atmosphère libre, les tropiques sont caractérisés par la faiblesse des gradients horizontaux de température et la bimodalité des profils verticaux d'humidité. Cette bimodalité est couplée avec la dynamique de grande échelle : les zones sèches et subsidentes alternent avec des zones humidifiées par la convection, en ascendance moyenne. Le travail de thèse a débuté par la modélisation simplifiée du climat tropical reposant sur cette image physique : un modèle en boîtes du type Pierrehumbert a été développé.

Ce modèle a confirmé la grande sensibilité du climat tropical aux changements des surfaces relatives occupées par les zones sèches et humides. En particulier, la réponse de la température du modèle à une variation modérée de ces surfaces est de même ordre de grandeur que la réponse à des perturbations radiatives du type du doublement de la concentration atmosphérique en dioxyde de carbone. L'importance de cette sensibilité est expliquée par les rétroactions dynamiques du système : alors que l'intensité de la circulation de grande échelle augmente avec un réchauffement dû à une perturbation radiative et réduit ce réchauffement, la circulation se ralentit avec une augmentation de la surface couverte par la colonne humide.
Par ailleurs, l'influence de la circulation de grande échelle sur les flux de surface s'est révélée importante : ces flux sont proportionnels au vent de surface, lequel dépend notamment de la circulation de grande échelle. Ceci introduit une rétroaction positive entre les flux de surfaces et la circulation de grande échelle qui diminue significativement la sensibilité du modèle à une perturbation radiative et augmente celle à une perturbation de l'aire relative des régions humides.
Enfin, une rapide analyse d'observations montre que, dans le climat présent, la variabilité interannuelle de la température de surface est fortement corrélée à celle de l'aire relative des régions convectives. La variation de cette aire relative peut donc constituer une rétroaction importante dans le climat tropical. Du point de vue de la circulation axisymétrique, la

modification de l'extension de la Zone de Convergence Intertropicale entraînée par un changement de la dynamique de la cellule de Hadley apparaît comme un mécanisme de première importance dans la modulation du climat tropical.

Le contrôle de l'aire relative des zones humides est en partie dynamique, résultant de la compétition entre la dynamique de surface et la circulation verticale thermodynamiquement forcée. Une paramétrisation simple des vents de surface comme fonction des gradients de températures indique que cette rétroaction pourrait moduler significativement la sensibilité de la température de surface à une perturbation, notamment à une perturbation radiative : suivant les hypothèses sur le cycle hydrologique dans le modèle, un réchauffement s'accompagnerait d'une diminution ou une augmentation de l'aire relative occupée par les régions convectives qui limiterait ou accroîtrait ce réchauffement. Ces résultats sont sensibles non seulement à la modélisation du cycle hydrologique du modèle, mais aussi aux paramétrisations dynamique et thermodynamique de la couche limite.

Pour mieux comprendre la répartition des Tropiques en zones humides et en zones sèches, dans la perspective d'évaluer leur réponse à un changement climatique, des réanalyses d'observations ont été utilisées. Il apparaît que la distribution des régions humides en fonction de leur taille caractéristique est bimodale : l'un des mode correspond aux échelles méso à synoptiques (jusqu'à 2000 km), l'autre à l'échelle planétaire des circulations de Hadley et Walker (autour de 5000 km). Notre modèle suggère que l'existence de ces deux modes provient de la sélection d'échelles opérée par la dynamique dans les basses couches de l'atmosphère, dans la mesure où les vents de surface peuvent être paramétrisés par une adaptation des théories linéaires. La bimodalité résulte plus précisément de la compétition entre le terme principal de la divergence du flot de surface, proportionnel au Laplacien de la température, et un deuxième terme dû à la variation du paramètre de Coriolis avec la latitude. Là encore, les résultats sont sensibles à la représentation de la dynamique : si l'existence de la séparation d'échelle repose sur une analyse dimensionnelle robuste, les propriétés des deux modes modélisés sont sensibles à la paramétrisation de la dynamique, et notamment du forçage de pression. Ce forçage semble mal représenté dans les théories linéaires proposées dans la littérature.

Enfin, alors que le forçage radiatif des systèmes convectifs est faible, la nébulosité de la couche limite des alizés constitue un forçage radiatif important dans les zones sèches qui conditionne le climat tropical. De plus, l'épaisseur et la structure verticale de la couche limite contrôlent la convergence de l'humidité dans les basses couches et donc l'intensité de la convection dans les régions humides. Dans la perspective de détailler la représentation de la couche limite dans notre modèle, des parametrisations simplifiées de la convection peu profonde ont été analysées. Cette étude a montré les dangers d'une simplification excessive des profils thermodynamiques verticaux dans la couche limite, et la nécessité d'adopter une approche unifiée de l'ensemble de cette couche en incluant la couche d'inversion qui sert de transition vers la troposphère libre.

Abstract

The goal of this thesis is to find answers to pending questions about the tropical climate: why does the surface temperature exhibit a maximum around 30°C in the tropics, what are the processes, on various scales, that are controlling the stability of the tropical climate and its weak sensitivity to a climate perturbation? The chosen approach, that of idealized modelling, allows one to isolate the main mechanisms, and to test or deepen our theoretical understanding of theses phenomena.

The tropical free troposphere is characterized by weak horizontal gradients of temperature and a marked bimodality in the vertical profiles of humidity. This bimodality is coupled with large-scale dynamics: dry subsiding zones alternate with ascending regions that are humidified by convection. The first step of this PhD project was to build a simple model of the tropical climate based on this physical image, following the approach of Pierrehumbert-type models.

This model confirmed the high sensitivity of the tropical climate to changes of the relative area covered by the dry and moist regions. In particular, the response of the model temperature to a moderate variation of these areas has the same order of magnitude as the response to radiative perturbations such as the doubling of the atmospheric concentration in carbon dioxyde. The magnitude of this sensitivity is explained by the dynamical feedbacks of the system: while the intensity of the large-scale circulation increases with a radiatively-driven warming and reduces this warming, this circulation slows down with an increase of the relative area covered by the moist column.
Furthermore, the influence of the large-scale circulation on the surface fluxes appears significant: these fluxes are proportional to the surface winds which depend on the large-scale circulation. This introduces a positive feedback between the surface fluxes and the large-scale circulation that further disminishes the sensitivity of the model to a radiative perturbation and increases the sensitivity to a change of the relative area of the moist regions.

Moreover, observations show that in the present climate the interannual variability of the surface temperature is well correlated to the variability of the relative area of convective regions. Therefore, the variation of this area could constitute an important feedback

in the tropical climate. From an axisymmetric point of vue, the modification of the latitudinal extent of the Intertropical Convergence Zone that could be caused by a change in the Hadley circulation appears as a key mechanism in the regulation of the tropical climate.

Dynamics play a crucial role in controlling the extent of moist regions: the competition between the near-surface dynamics and the thermodynamically driven vertical circulation is expected to determine this extent. A simple parameterization of the surface winds as a function of the temperature gradients indicates that this feedback could significantly alter the sensitivity of the surface temperature to a radiative perturbation. Depending on the assumptions in the model hydrological cycle, a warming would be accompanied by a decrease or an increase of the relative area covered by the convective zones, which would either limit or increase the warming. This results are sensitive not only to the parameterization of the hydrological cycle, but also to those of the dynamics and thermodynamics of the boundary layer.

Observation reanalyses were used in order to better understand the spatial distribution of the moist and dry regions in the tropics. The size distribution of the moist regions is bimodal: the first mode corresponds to meso and synoptic scales (up to 2000 km), and the other to planetary Hadley/Walker scales (about 5000 km). Our model suggests that the existence of these two modes originates from a scale selection by the low-level dynamics, as far as the surface winds can be parameterized following linear theories. The bimodality in the size distribution arises from the competition between the main term of the divergence, which is proportional to the temperature Laplacian, and the second term due to the change of the Coriolis parameter with latitude. Again, the results are sensitive to the parameterization of the dynamics; the existence of a scale separation relies on a robust dimensional analysis, but the characteristics of the two model modes are sensitive to the parameterization of the pressure forcing. This forcing seems to be the weak point of the linear theories that can be found in the litterature.

Finally, whereas the radiative forcing of the convective clusters is weak, the trade-wind boundary layer cloudiness has a strong radiative forcing in the dry regions. This forcing is thought to be a srong feedback in the tropical climate. Furthermore, the depth and vertical structure of the inversion control the convergence of humidity in the lower troposphere and thus the intensity of the convection in the moist regions. In order to detail the representation of the boundary layer in the model, parameterizations of the shallow convection have been studied. This work shows the limits to the simplification of thermodynamic vertical profiles in the boundary layer, and the necessity of a unified approach including the inversion layer.

Contents

Introduction

Les basses latitudes collectent une part importante de l'énergie solaire reçue par la Terre. De ce fait, la réponse des Tropiques est déterminante dans la sensibilité du climat global: la façon dont le système tropical réémet cette énergie vers l'espace où la transmet aux autres parties du globe conditionne à la fois le climat présent et les possibilités de changements climatiques à venir.

Circulation générale et nébulosité de l'atmosphère tropicale

L'atmosphère tropicale est caractérisée par des circulations zonale et méridionale à l'échelle planétaire. En moyenne zonale, l'air s'élève au dessus de l'Equateur et redescend dans les subtropiques; cette circulation axisymmétrique est appelée cellule de Hadley d'après George Hadley qui, au XVIII^{e} siècle, émit l'hypothèse d'une telle circulation s'étendant jusqu'au Pôle. Elle permet d'exporter l'énergie de la zone équatoriale, qui reçoit un rayonnement solaire important, vers des latitudes plus élevées qui collectent moins d'énergie solaire : en effet, l'énergie transportée vers le Pôle par la branche supérieure de la cellule est, à cause de sa composante d'énergie potentielle de gravité, plus élevée que celle ramenée vers l'Equateur par le courant de surface. Cette circulation est associée à des vents zonaux: la force de Coriolis due à la rotation de la Terre entraîne, en surface, la déviation des alizés vers l'Ouest et, en altitude, le courant de jet à l'extrémité de la cellule vers le Pôle. De plus, ce mouvement des masses d'air participe à l'homogénéité horizontale de la température (Held and Hou 1980). La figure 1 montre la circulation en moyenne zonale de l'atmosphère tropicale. Lors des saisons extêmes, l'ascendance équatoriale se décale vers l'hémisphère d'été, et la cellule estivale s'estompe.

Cette cellule méridienne moyenne est couplée à une dynamique verticale et zonale : la circulation de Walker. Pour la petite histoire, Sir Gilbert Walker était un scientifique britannique qui découvrit les premiers éléments révélant cette circulation en étudiant au début du XX^{e} siècle les facteurs influençant la mousson indienne. En temps normal, à l'Equateur, les ascendances sont concentrés au dessus des continents et le reste de l'atmosphère subside, comme le montre la Figure 2. La variabilité liée à El Niño-Oscillation Australe (ENSO) peut être considérée en première approximation comme des modifications de cette circulation (Philander 1990) : lors des évènements El Niño, la zone d'ascendance d'Océanie se décale vers le centre du Pacifique et entraîne une modification de l'ensemble de la dy-

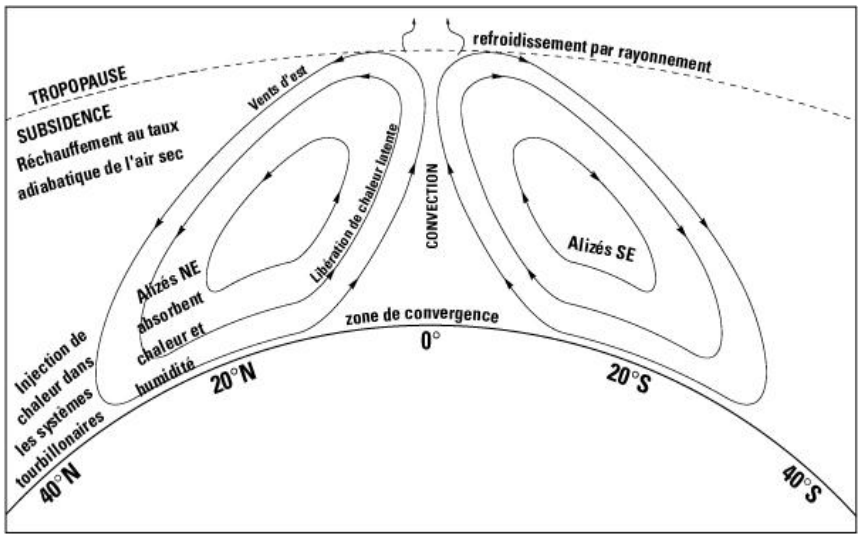

Figure 1: Schéma de la circulation hémisphérique.

namique planétaire (Fig. 2). Lors des évènements La Niña, la circulation moyenne est renforcée.

La dynamique tropicale est profondément liée au cycle hydrologique; en effet, l'énergie nécessaire aux mouvements ascendants est fournie par le dégagement de chaleur latente occasionné par la condensation au sein des nuages convectifs. En retour, la dynamique de surface converge dans les zones de convection et amène la vapeur d'eau nécessaire à la convection. Notamment, la Zone de Convergence Intertropicale (ITCZ) correspond à la branche ascendante de la cellule de Hadley. Cette zone est une bande longitudinale de nuages convectifs à proximité de l'Equateur (Fig 3). Les régions subsidentes sont par contre relativement sèches, la circulation de grande échelle limitant la convection à la couche limite, qui culmine vers 3000m d'altitude. Cette couche limite est chapeautée par l'inversion,

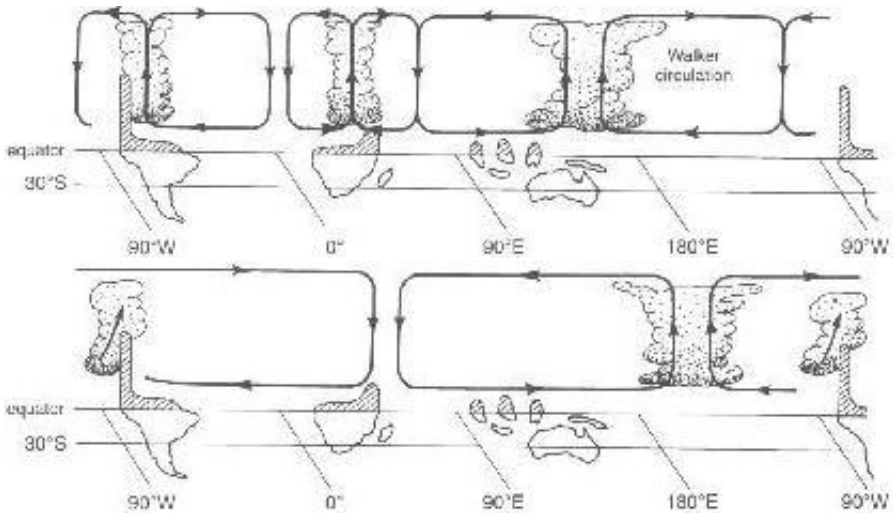

Figure 2: Circulation de Walker: moyenne (en haut) et évènement El Niño (en bas).

une couche stratifiée très stable qui résulte de la compétition entre la subsidence de la troposphère libre et la turbulence sous-jacente. Alors que, dans les zones de convergence, les cumulonimbus convectifs s'élèvent jusqu' à la tropopause autour de 17 à 18 km d'altitude, les nuages sont principalement limités à la partie supérieure de la couche limite dans les régions subsidentes (Fig 4) : loin de l'Equateur et à l'Est des bassins océaniques, l'inversion est relativement basse et des couches nuageuses stratiformes et étendues sont observées : les stratocumulus. En se rapprochant de l'Equateur, la turbulence de couche limite s'organise spatialement en ascendances et en subsidences qui élèvent l'altitude de l'inversion: c'est la convection peu profonde, qui donne naissance aux cumulus. Cette convection peu profonde s'intensifie vers l'Equateur à proximité des zones de convection profonde. On observe aussi des nuages stratiformes élevés, les cirrus, qui proviennent de la dérive de la partie supérieure des nuages convectifs en forme d'enclumes.

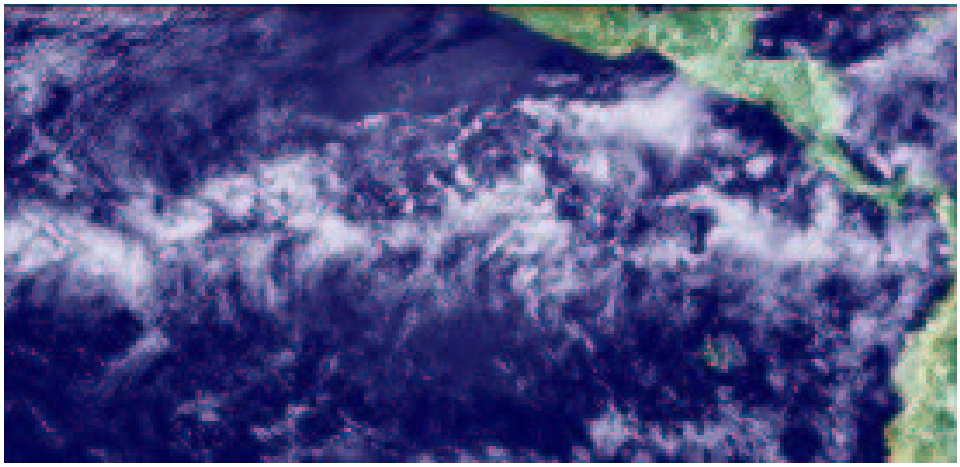

Figure 3: Image satellite (visible) de la Zone de Convergence Intertropicale dans l'Est du Pacifique.

Enfin, le cycle de l'eau interagit avec le rayonnement : dans les régions en convection, l'humidité de l'atmosphére augmente l'effet de serre local et permet à ces régions de collecter plus d'énergie. C'est aussi le cas dans les subtropiques, où la vapeur d'eau conditionne la capacité des zones subsidentes à rayonner vers l'espace et donc la vitesse moyenne de subsidence. Les nuages ont aussi un fort effet radiatif : en réfléchissant la lumière solaire, ils augmentent l'albédo planétaire. Mais ils absorbent aussi le rayonnement infra-rouge, occasionnant un effet de serre additionnel.

Pour des raisons encore mal comprises, un système complexe d'interactions entre la circulation générale, le cycle hydrologique et les processus radiatifs, le climat de la zone tropicale apparaît peu sensible aux perturbations quelle que soit leur nature.

Stabilité du climat tropical dans les observations

La température de surface dans les Tropiques semble plus stable que les températures aux hautes latitudes, et ce sur des échelles de temps très diverses, allant des millions

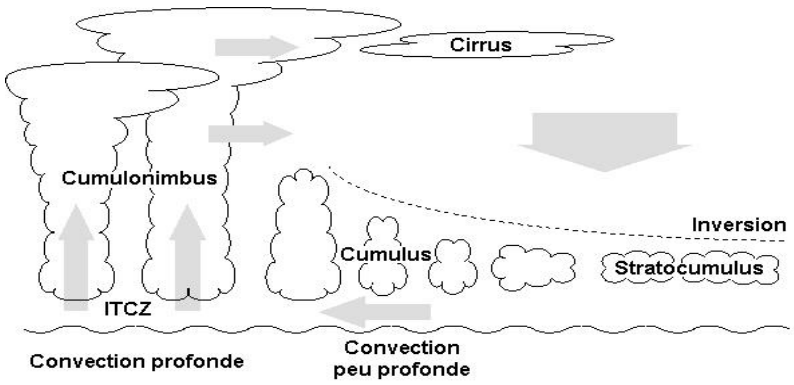

Figure 4: Schéma des différents nuages tropicaux.

d'années aux échelles intrasaisonnières. Il semble qu'aussi loin que l'on puisse remonter, la température des océans tropicaux n'a varié que de quelques degrés.

Au Crétacé, 100 millions d'années avant notre ère, une période très chaude aurait vu des températures jusqu'à 20°C supérieures aux températures actuelles dans les hautes latitudes. Cette période était caractérisée par une concentration atmosphérique en dioxyde de carbone importante et une disposition tectonique différente (c'est à cette époque que l'Océan Atlantique a commencé à s'ouvrir) et ces deux facteurs expliquent la différence de température (Barron and Washington 1985). Néanmoins, les températures des océans tropicaux semblent n'avoir été alors que quelques degrés plus chaudes qu'aujourd'hui (Selwood et al. 1994).

Au sujet d'un évènement plus récent, le dernier maximum glaciaire, une controverse est toujours en cours. Ce maximum a eu lieu il y a une vingtaine de milliers d'années et fait partie des cycles climatiques forcés par les variations des paramètres orbitaux de la révolution de la Terre autour du soleil. A la fin des années 70, les résultats du projet CLIMAP semblaient indiquer que les températures à la surface des océans tropicaux ont peu ou pas évolué depuis vingt mille ans (CLIMAP 1976). Mais ces résutats, fondés sur les fractions isotopiques de l'oxygène dans les carottes sédimentaires marines (forminifères), sont mis en doute par les traces de la ligne des névés (Broecker 1996), par des rapports de concentration de Strontium/Calcium dans les coraux (Gagan et al. 2000) ou encore par des ratios isotopiques de l'oxygène dans les glaciers andins (Thompson 2000). Toutes ces études tendent à prouver que la température tropicale était de l'ordre de 5° plus froide lors du dernier maximum glaciaire que de nos jours. La variation de température depuis cette période aurait donc été glogalement homogène entre l'Equateur et 40° de latitude, cette variation étant plus importantes dans les hautes latitudes. Néanmoins, ces mesures pourraient présenter jusqu'à 50% d'incertitude, notamment à cause des relations empiriques, basées sur des données modernes, qui sont utilisées pour reconstruire l'historique des températures. La modélisation de la sensibilité climatique semble indiquer que le réchauffement des Tropiques depuis le dernier maximum glaciaire est de 2 à 2,5°C (Betts and Ridgway 1992; Crowley 2000). Le débat sur ce réchauffement est lié à un autre portant sur les modifications du

cycle hydrologique dans les Tropiques depuis la période glaciaire : l'atmosphère tropicale aurait été globalement plus sèche, ou simplement plus homogène (Thompson 2000).

Encore plus récemment, l'optimum climatique médiéval (du X^e au XIII^e siècle), suivi du petit age glaciaire (du XVII^e au XVIII^e siècle) auraient vu des températures tropicales éloignées de moins d'un degré des valeurs actuelles (Keigwin 1996), alors que ces variations climatiques, dues à priori à la variation de l'activité volcanique et de l'intensité du soleil (en fait du nombre des taches solaires), ont eu des conséquences importantes sur l'activité humaine dans les moyennes et hautes latitudes de l'hémisphère Nord (colonies Vikings au Groënland au Moyen-Age, famines en Europe au XVII^e).

Sur la période récente où des systèmes d'observation systématique du climat ont été développés (réseaux de stations, campagnes de mesures, satellites, ...), le climat tropical montre un maximum de température proche de 30°C, et ce malgré des variations importantes du cycle hydrologiques, notamment lors des évènements El Niño et La Niña (Philander 1990).

Etude et test de mécanismes: observations et modélisation

Les observations paléoclimatiques disponibles sont insuffisantes pour aller au delà de la spéculation au sujet des rétroactions en jeu dans le système climatique tropical. Il est en effet difficile de tester les hypothèses avec des données sur un nombre de variables limitées en un faible nombre de points du globe. De ce fait, l'identification et la validation des processus clefs du climat tropical passe le plus souvent par l'utilisation des variations géographiques et temporelles (particulièrement interannuelles) du climat sur la période récente d'observations intensives (Ramanathan and Collins 1991; Chou and Neelin 1999; Lindzen et al. 2001; Hartmann et al. 2001). Ce type d'étude repose sur l'hypothèse que les principaux mécanismes sont conservés dans le cadre d'un changement climatique. Cette hypothèse est discutable, surtout lorsqu'il s'agit d'évaluer quantitativement la compétition entre les réponses de différents processus.

Les rétroactions responsables de la faible sensibilité du climat tropical aux perturbations du forçage ont aussi été étudiées en utilisant des modèles d'une complexité variée, allant des modèles en boîtes, qui s'attachent aux principaux bilans des variables atmosphériques, aux Modèles de Circulation Générale (MCG), qui incluent une représentation des processus dynamiques et thermodynamiques sur tout le globe. Ces derniers ont confirmé la moindre sensibilité climatique des Tropiques comparés aux moyennes et hautes latitudes (Meehl et al. 2000), mais les causes de cette caractéristique sont tout aussi difficile à discerner dans les sorties de MCG que dans les observations. De plus, si certains résultats sont communs à de nombreux MCG développés par la communauté internationale, et rejoignent les résultats d'approches simplifiées (Held and Soden 2000; Cess et al. 1990), d'autres aspects liés à la convection et aux nuages diffèrent sensibement entre modèles (Cess et al. 1990; Cess et al. 1996), et ces divergences relativisent la fiabilité de ces modèles pour simuler le climat tropical et sa sensibilité.

La modélisation simplifiée garde donc tout son intérêt pour isoler et comprendre les mécanismes contrôlant la sensibilité du climat tropical, ainsi que pour donner des éléments d'interprétation pour les modèles plus complexes. De fait, dans la littérature scientifique, de nombreuses études utilisent des modèles idéalisés de l'atmosphère et des océans tropicaux.

Rétroactions climatiques dans les Tropiques

Les principaux travaux reposent sur une analyse du bilan énergétique des tropiques. La figure 5 illustre ce bilan; les valeurs des flux sont données en moyenne sur les Tropiques pour le climat présent, à titre indicatif. Ce bilan est couplé dans certains modèles au cycle de l'eau, qui se résume, en moyenne, à l'évaporation, la précipitation et l'export vers les extratropiques.

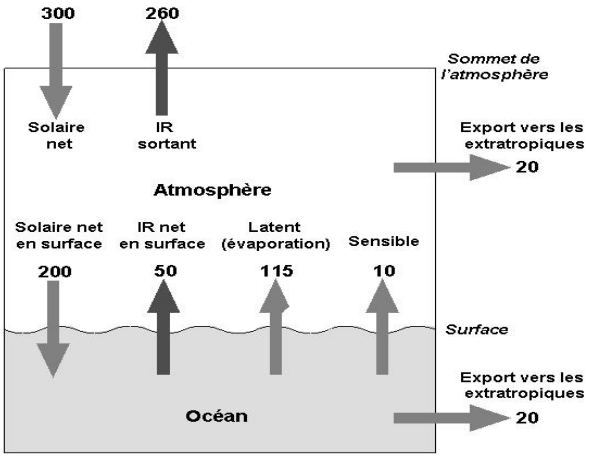

Figure 5: Bilan énergétique des atmosphère et océan tropicaux (flux en Wm^{-2}).

Les principaux termes qui contrôlent la température de l'eau sont le flux solaire en surface, l'évaporation, et dans une moindre mesure le flux infra-rouge (IR) net en surface. Le premier est fortement dépendant de la nébulosité, à cause du pouvoir réfléchissant des nuages. Le second dépend de la température de l'eau en surface, car l'évaporation est, au premier ordre, proportionnelle à la différence entre l'humidité de saturation en surface et l'humidité de l'air dans la couche limite, et la première est fonction croissante et non-linéaire de la température ; au passage, rappelons que les flux de chaleur sensible et latent sont aussi proportionnels au vent de surface. Le troisième flux, infra-rouge, dépend de la température de surface: la loi de Stephan-Boltzman indique que l'émission d'un corps noir est proportionnelle à la puissance 4 de la température. Mais les gaz à effet de serre (dont la vapeur d'eau) et les nuages absorbent une partie de ce flux radiatif, et réémettent à la fois vers l'espace et vers la surface, conditionnant le flux IR net en surface et le flux IR sortant vers l'espace. Ces trois composantes du bilan énergétique sont considérées comme les principaux régulateurs internes de la sensibilité du climat tropical. Le quatrième terme, le flux de chaleur sensible, est faible comparé aux autres, et estimé peu sensible aux variations de température. Mais ce bilan moyen cache les variations latitudinales et

longitudinales qui sont importantes et mettent en jeu les transports horizontaux d'énergie via la dynamique de grande échelle. En effet, les caractéristiques de nébulosité et d'humidité varient géographiquement, comme décrit plus haut, et l'interaction entre les différentes régions est une autre source de mécanismes potentiels pour la régulation de la température de surface.

Les principales rétroactions radiatives-convectives envisagées peuvent se classer en différentes catégories: les rétroactions du ciel clair, des nuages et celles couplées à la dynamique.

Rétroactions radiatives-convectives en ciel clair

La vapeur d'eau est le principal gaz à effet de serre dans l'atmosphère. Les modifications du cycle hydrologique associées à un changement climatique sont donc considérés comme la rétroaction la plus importante du système climatique. La vapeur d'eau absorbe une partie du flux IR incident, et réémet un rayonnement qui dépend de sa température. La température diminuant avec l'altitude dans la troposphère, l'humidité des couches supérieures a un rôle déterminant dans le bilan radiatif du système terrestre, alors que l'impact de l'humidité de la couche limite est plus faible, à cause de sa température proche de celle de la surface (Shine and Sinha 1991). La principale source d'humidité dans la haute troposphère est la convection profonde, qui injecte de la vapeur d'eau et de l'eau condensée dans les couches supérieures. Des rétroactions faisant intervenir des modifications de la convection profonde ont donc été proposées.

Des modèles de complexité variée semblent montrer que le profil d'humidité relative varie peu lors d'un changement climatique (Bony et al. 1995; Held and Soden 2000; **?**). Ceci entraîne une forte rétroaction positive à un réchauffement puisque l'humidité de saturation augmente fortement avec la température et l'absorption IR dépend de l'humidité spécifique. Néanmoins, des mécanismes régulant l'humidité dans la haute troposphère tropicale ont été proposés pour étayer l'idée que cette rétroaction est beaucoup plus faible qu'il n'est communément admis.

Tout d'abord, une théorie qui repose sur les variations de l'altitude du sommet des nuages a été proposée. En effet, la majeure partie du détraînement d'un nuage convectif a lieu à proximité de son sommet, et l'altitude de celui-ci augmente avec un réchauffement de la surface. Comme la température décroît avec l'altitude, la température à laquelle l'air humide est majoritairement détraîné aurait une variation plus faible que celle en surface, voire de signe opposé. L'air détraîné pourrait donc contenir moins d'eau, ce qui assècherait la troposphère libre et constituerait une rétroaction négative (Lindzen 1990). Mais les expériences avec des MCG montrent qu'un réchauffement s'accompagne en effet de l'élévation de l'altitude de détraînement tout en occasionnant une augmentation de l'humidité spécifique (Salathe and Hartmann 2000). En fait, le modèle simplifié de Lindzen (1990) ne prend en compte ni la diversité des altitudes du sommet des nuages, et donc des altitudes de détraînement, ni l'effet de l'advection de grandes échelle dans la régulation de l'humidité dans la haute troposphère (Pierrehumbert and Roca 1998; Sherwood 1996). Ces

processus annulent l'effet de la variation de l'altitude des sommets des nuages.

Mais Lindzen a proposé une autre théorie, qui met en jeu la phase condensée de l'eau. En effet, une grande partie de l'eau qui condense dans les nuages n'atteint jamais le sol sous forme de pluie. Une partie est détraînée et réévaporée dans la haute troposphère, et une partie des précipitations se réévapore au cours de sa chute. Cette réévaporation des précipitations a été avancée comme source principale d'eau dans les régions subsidentes des tropiques (Sun and Lindzen 1993), ce qui suggère le mécanisme suivant. Comme l'efficacité des précipitations (la fraction d'eau condensée qui se transforme en pluie atteignant le sol) semble augmenter avec la température pour des raisons de microphysique nuageuses, la quantité d'eau liquide et solide détraînée serait donc moindre dans un climat plus chaud et ceci entraînerait un assèchement de l'atmosphère libre. Bien que séduisante pour expliquer les incohérences dans les données paléologiques entre la ligne des névés et la température de surface, cette théorie achoppe là encore sur le fait que la circulation de grande échelle, et non pas la précipitation, est déterminante dans l'humidification des zones de subsidence (Pierrehumbert and Roca 1998; Sherwood 1996). Des études utilisant des modèles résolvant explicitement la convection (MRC) n'ont montré aucun effet climatique significatif lié à l'efficacité des précipitations (Tompkins and Craig 1999).

Le consensus scientifique actuel considère que la rétroaction de la vapeur d'eau est positive, bien que son amplitude soit encore mal connue à cause de l'hétérogénéité spatiale de l'humidité, et que c'est la principale rétroaction du climat tropical, fortement destabilisante dans une grande partie des tropiques. De ce fait, la faible sensibilité du climat tropical est encore plus étonnante, et seule l'existence d'une forte rétroaction négative compensant celle de l'humidité peut l'expliquer. Les nuages pourraient causer une telle rétroaction.

Rétroactions radiatives-convectives nuageuses

Le trait le plus frappant du forçage radiatif des nuages dans les tropiques est la faiblesse du forçage net de l'ensemble des nuages convectifs dans le climat présent. En effet, la composante visible et ultra-violette, due à la réflexion du rayonnement solaire vers l'espace, compense la composante IR liée à l'effet de serre additionnel des nuages (Ramanathan et al. 1989). Certains y ont vu l'effet fortuit de l'altitude de la tropopause (Kiehl 1994), ce qui laisse ouvert le champ d'investigation des rétroactions nuageuses. D'autres considèrent que cette compensation est elle-même le fruit de rétroactions complexes implicant la dynamique (Hartmann et al. 2001), ce qui réduit les possibilités d'existence d'une forte rétroaction due aux nuages. La grande diversité des résultats des MCG ne permet pas d'apporter de réponse (Cess et al. 1996).

La première tentative d'explication de la stabilité des températures de surface dans les Tropiques proposait une régulation du flux solaire incident par la réflexion due aux nuages convectifs (Ramanathan and Collins 1991), en utilisant des donnees de l'Expérience sur le Budget Radiatif de la Terre (ERBE) pour les années El Niño/ La Ninã 1987-1988. Cette "hypothèse du thermostat" mettait en avant le fait que la convection profonde devrait augmenter avec la température et entraîner un accroissement de l'albédo dû aux cirrus

issus des enclumes convectives, et donc une diminution du chauffage de la surface par le soleil. Ce mécanisme impliquerait une forte rétroaction négative sur les variations de la température de surface. Cette théorie a été vivement critiquée. Tout d'abord, Ramanathan et Collins (1991) ne prennent en compte que les zones de convection, et considère que la plus grande partie de l'effet de serre dû aux nuages est exportée hors de ces régions par la circulation de grande échelle. Cette réduction de l'influence de la circulation de grande échelle à une action sur un terme précis du bilan radiatif est dommageable à la validité des résultats. En prenant en compte le forçage radiatif complet des cirrus, il apparaît que ceux-ci ont plutôt tendance à réchauffer le système atmosphère-océan dans les données du Projet International sur la Climatologie des Nuages par Satellite ISCCP (Fu et al. 1992; Chou and Neelin 1999). De plus, il semble que l'intensité de la convection dépend davantage de la vitesse verticale de grande échelle que de la température de surface locale (Fu et al. 1992; Bony et al. 1997).

Considérant que l'effet total des cirrus est un chauffage, un autre mécanisme a été proposé : à cause de l'augmentation de l'efficacité des précipitations avec la température, la quantité d'eau liquide dans la haute troposphère tendrait à diminuer avec la température de surface, et l'extension des cirrus diminuerait, permettant au système terrestre d'émettre plus efficacement vers l'espace et de se refroidir (Lindzen et al. 2001). Cette rétroaction négative a été baptisée "Effet Iris" par analogie avec l'iris de l'œil dont la taille varie en fonction de l'intensité lumineuse pour moduler l'énergie reçue par la rétine. Elle a causé une polémique assez vive : plusieurs critiques ont été émises, auxquelles des réponses ont parfois été apportées. Tout d'abord, l'étude de Lindzen et al. (2001) prendrait en compte de nombreux cirrus d'origine extratropicale qui fausseraient l'étude (Hartmann and Michelsen 2002; Lindzen et al. 2002) ; ensuite, l'effet IR des cirrus aurait été surévalué (Fu et al. 2002; Lin et al. 2002; Chou et al. 2002); enfin, à nouveau, les résultats reposent sur le contrôle de la convection par la température de surface en négligeant l'influence de la circulation de grande échelle (Del Genio and Kovari 2002). Le débat sur le sujet n'est pas clos. Il a néanmoins permis de borner l'amplitude potentielle de cette rétroaction qui serait somme toute limitée, si toutefois ce mécanisme existe.

Une théorie alternative suggère que le forçage radiatif des nuages resterait très faible avec un changement climatique à cause de rétroactions dynamiques (Hartmann et al. 2001). Cette théorie s'appuie sur les observations ERBE et ISCCP qui montrent que la convection tropicale, organisée en systèmes méso-échelle, produit divers type de nuages avec une distribution telle entre les types que le forçage moyen est nul. Un modèle simple suggère que cette propriété est maintenue par la dynamique si (i) le forçage radiatif des nuages reste faible dans les régions en subsidence, si (ii) la dynamique de grande échelle est proportionnelle aux gradients de température en surface et si (iii) l'albédo des nuages convectifs est proportionnel à la vitesse ascendante. Ces hypothèses ont été elle aussi vivement débatues. Notamment, la validité de la troisième hypothèse dans le cadre d'un changement climatique a été mise en cause (Chou and Lindzen 2002; Hartmann et al. 2002). D'autre part, le rôle de la température de surface dans le forçage de la dynamique est certainement plus

complexe que ne le stipule le modèle de Hartmann et al. (2001) (Lindzen and Nigam 1987; Yano et al. 2002). Enfin, la première hypothèse nécessite certainement des recherches plus poussées pour être validée.

En effet, alors que le forçage radiatif des nuages hauts a été amplement étudié, les mécanismes associés aux nuages de couche limite sont encore incertains. Pourtant, les nuages bas ont un impact plus significatif sur le bilan radiatif que celui des nuages associés à la convection profonde: en effet, ils occasionnent un faible effet de serre à cause de leur altitude limitée qui entraîne une faible différence de température avec la surface, alors qu'ils accroissent l'albédo tout comme les nuages hauts. En particulier, les nuages stratiformes (stratocumulus) augmentent fortement l'albédo à cause de leur géométrie. L'apparition de ces nuages semble lié à la stablité statique de la basse troposphère (Klein and Hartmann 1993). En s'appuyant sur ces observations, un modèle de l'atmosphère tropicale a été proposé, qui montre que les stratocumulus constituent une forte rétroaction négative à une perturbation de température (Miller 1997). Néanmoins, cette étude tend à surestimer l'extension des régions où peuvent apparaître les stratocumulus, qui sont cantonnés aux bord Est des océans subtropicaux dans le climat présent. En fait, le modèle ne prend pas en compte la possibilité de transition stratus-cumulus. Les petits cumulus sont en effet les nuages les plus courants au dessus des mers tropicales, et ils sont probablement le siège de la majeure partie de la réponse des nuages tropicaux à un changement climatique (Bony et al. 2004).

Rétroactions couplées

Les travaux sur les rétroactions radiatives-convectives ont longtemps considéré la dynamique comme un effet secondaire dans la régulation des températures de surface. Mais la circulation de grande échelle a suscité de plus en plus d'intérêt: le couplage des rétroactions thermodynamiques et dynamiques est apparu vital à la stabilité du climat des faibles latitudes. Hartmann at Michelsen (1993) ont montré que, dans le bilan d'énergie à la surface, la réponse principale à une variation de la température est l'évaporation plutôt que l'albédo des nuages hauts, et que la circulation de grande échelle a un impact important sur celle-ci en ventilant la couche limite. Le couplage entre température moyenne et gradient horizontal de température via la dynamique a donc été proposé comme mécanisme régulateur (Hartmann and Michelsen 1993). Cette rétroaction repose néanmoins sur deux hypothèses fragiles: (i) la proportionnalité entre la circulation et les gradients de surface et (ii) l'augmentation des gradients horizontaux de température avec la température moyenne.

La circulation de grande échelle a aussi un rôle dans le transport de l'énergie. Wallace (1992) a expliqué la distribution des températures de surface observées par le fait que, dans les régions convectives, les variations de températures sont propagées par la convection et la dynamique à l'ensemble de la troposphère libre, alors que dans les régions moins chaudes, en subsidence, les variations de températures sont communiquées à la seule couche limite. De ce fait, les perturbations de la température de surface dans les régions chaudes sont atténuées très efficacement, et la distribution de température montre un maximum proche

de 30°C.

Ce mécanisme est fondamental dans le modèle proposé par Pierrehumbert (1995). Ce modèle en boîtes distingue les régions sèches des zones humides, et explique la stabilité par le couplage des deux boîtes par la dynamique de grande échelle. Les régions où la convection humidifie la troposphère sur toute sa hauteur sont en "effet de serre emballé", c'est-à-dire que l'effet de serre local augmente avec la température de surface et constitue donc une rétroaction positive. L'énergie excédentaire de ces régions est exportée vers les zones sèches, de ciel clair en subsidence, où elle est rayonnée vers l'espace. Cette même circulation transporte l'humidité de la couche limite des régions sèches dans les zones de convergence, et alimente la convection. De plus, l'intensité de la dynamique de grande échelle est contrôlée par le refroidissement radiatif de la troposphère libre sèche. C'est donc l'interaction entre les deux régimes radiatifs qui est au cœur de la régulation du climat tropical.

Cette vision conceptuelle d'un équilibre dynamique entre deux modes radiatifs-convectifs est étayée par un certain nombre d'éléments. Tout d'abord, alors que les gradients horizontaux de température sont faibles dans la troposphère libre tropicale, l'humidité observée est typiquement bimodale (Zhang et al. 2003), ce qui justifie cette modélisation en deux boîtes. Ensuite, l'étude des équilibres radiatifs-convectifs associés à un profil de température donné révèle l'existence de deux profils de transmittivités possibles dans l'infra-rouge (Li et al. 1997; Ide et al. 2001) : l'un correspond à une atmosphère sèche, alors que l'autre correspond à une atmosphère plus humide. Des calculs radiatifs plus poussés montrent que l'équilibre humide est instable, ce qui correspond donc à l'effet de serre emballé, alors que l'équilibre sec est très stable (Nakajima et al. 1992). La dynamique a donc pour effet de coupler deux quasi-équilibres radiatifs-convectifs pour les organiser en système stable. De plus, des expériences deux colonnes utilisant des paramétrisations de la convection et du rayonnement plus détaillées ont montré le rôle de la circulation de grande échelle dans l'inhibition de la convection profonde dans les régions subsidentes (Nilsson and Emanuel 1999) : non seulement la dynamique assure la stabilité du système bicolonne en extrayant l'énergie excédentaire de la colone convective pour la rayonner vers l'espace dans la troposphère libre de la colonne subsidente, mais elle participe aussi à la maintenance de ces deux modes en limitant la convection à la couche limite dans les régions sèches et en alimentant les zones de convergence en humidité nécessaire à la convection.

Pierrehumbert (1995) avait identifié deux paramètres auxquels son modèle est fortement sensible : les aires relatives couvertes par les deux modes radiatifs-convectifs, et l'humidité de la troposphère libre dans la colonne sèche. Ce sont donc deux possibles sources de rétroactions, qui constituent une approche alternative au raisonnement unicolonne pour l'évaluation de la rétroaction de la vapeur d'eau. En utilisant un modèle plus élaboré incluant une représentation du cycle de l'eau, Larson et al. (1999) ont étudié le rôle de la vapeur d'eau et des nuages. Les enclumes convectives ayant un forçage net relativement faible au sommet de l'atmosphère, le modèle montre une faible sensibilité à ce type de nébulosité. Les nuages bas sont traités comme dans le travail de Miller (1997) et les

résultats sont similaires, avec les mêmes limites. L'impact de l'humidité dans la troposphère libre semble faible car, dans le modèle de Larson et al. (1999), l'épaisseur de la couche limite diminue avec l'humidité de la troposphère libre, et les variations de l'effet de serre dues à la couche limite compensent celles liées à l'humidité des hautes couches. Ce résultat est sans doute fortement dépendant de la paramétrisation de la couche limite.

Des travaux récents ont commencé à étudier les facteurs contrôlant l'aire relative des régions humides dans les tropiques (Kelly and Randall 2001; Bretherton and Sobel 2002). Ces recherches s'attachent à la réponse de modèles atmosphériques à deux boîtes à un gradient fixé de temperature de surface. La dynamique y est représentée de façon simple en fonction de ce gradient, et il apparaît que l'extension relative de la colonne convective est fonction décroissante du gradient. En effet, la circulation atmosphérique augmente avec le gradient de température de surface, et comme elle est proportionnelle au refroidissement radiatif de la troposphère libre sèche, l'aire relative de la colonne sèche augmente pour ajuster le rayonnement. La sensibilité climatique de ces modèles n'a pas encore été étudiée, et les rétroactions possibles liées à la variation des aires relatives des régions humide et sèche sont encore inconnues.

Rétroactions océaniques

La température de surface est bien sûr aussi modulée par le transport océanique. La circulation des océans tropicaux est forcée par la dynamique de grande échelle atmosphérique : la quantité de mouvement transmise par la friction des alizés sur la surface entraîne à la fois une partie de la gyre subtropicale et l'affleurement d'eaux de subsurface autour de l'Equateur, par pompage d'Eckmann. L'intensité de la circulation atmosphérique de grande échelle contrôle la vitesse des deux circulations (horizontale et verticale), qui occasionnent un transport d'énergie des zones convectives vers les zones sèches et un export vers les extratropiques. Ce couplage implique une rétroaction négative qui participe à la régulation du climat tropical (Sun and Liu 1996; Clement and Seager 1999; Li et al. 2000).

Problématiques de la thèse

Le modèle de Pierrehumbert (1995) présente une image convaincante du climat tropical, mais l'importance quantitative des différentes rétroactions qui expliquent la faible sensibilité des tropiques aux perturbations du forçage radiatif n'y est pas détaillée. Une expérience menée avec ce type de modèle montre une sensibilité importante à un doublement de la concentration atmosphérique en dioxyde de carbone : la température augmente de 2.5°C (Larson et al. 1999). En incluant la rétroaction des stratocumulus, cette sensibilité est réduite à 1.7°C. Mais les auteurs reconnaissent eux-mêmes que la rétroaction de ces nuages bas est surévaluée du fait que les stratus sont considérés couvrir l'ensemble des régions subsidentes, ce qui n'est pas le cas dans les observations. La sensibilité de ce modèle semble importante, notamment au regard de certains résultats de MCG qui prévoient une

augmentation des températures de surface tropicales d'environ 1°C pour un doublement de CO_2 (Meehl et al. 2000).

De ce fait, plusieurs questions se posent, qui entrent dans l'approche conceptuelle d'un système bicolonne, mais qui ont une portée plus étendue :
(i) Quel sont les rôles de la dynamique dans la régulation de la température de surface? Comment fonctionne le couplage des rétroactions radiatives et dynamiques?
(ii) L'aire relative des zones humides a été identifiée comme un des paramètres clefs du modèle de Pierrehumbert. Dans quelle mesure ce paramètre est une source potentielle de rétroactions significatives pour le climat dans le cadre d'un changement climatique? Et quels sont les processus contrôlant à priori cette extension relative, et notamment, comment appréhender le rôle de la dynamique?
(iii) Comment se distribue cette aire dans les observations? Et quelle est sa variabilité naturelle?
(iv) Quelle est la réponse de la couche limite des zones sèches à une perturbation du forçage de grande échelle? Et comment cette réponse influe sur le climat via la convergence d'humidité dans les régions convectives? De plus, étant donné que les stratus constituent une rétroaction importante, qu'est ce qui conditionne l'apparition de stratocumulus ou de petits cumulus, voire de stratus au sommet de cumulus?

Cette thèse s'attache à apporter un certain nombre de réponses à ces questions. Dans le premier chapitre, les rétroactions associées à la dynamique et à l'aire relative des régions humides seront étudiées. Dans le Chapitre 2, la distribution des régions humides observée sera décrite et une tentative d'explication de cette distribution par une sélection d'origine dynamique sera présentée. Enfin, une étude théorique des perspectives de modélisation simplifiée de la couche limite des alizés sera exposée dans le dernier chapitre.

Chapter 1

Feedbacks in a box model of the tropical climate

Basically, low latitudes are characterized by the homogeneity of the temperature profile, required by the conservation of angular momentum (Held and Hou 1980), and the bimodality of the humidity profiles in the free troposphere (Zhang et al. 2003). This bimodality has been shown to be created by the large-scale circulation (Nilsson and Emanuel 1999) but can also be infered from a purely radiative model (Li et al. 1997; Ide et al. 2001).

Pierrehumbert (1995) used a simple two-box model to show that the coupling between the two humidity profile modes in the Tropics and the large-scale circulation helps maintain the observed tropical climate: the circulation transports the excess of energy from the convecting box, which is in a state of runaway greenhouse, to the subsiding box, where it is radiated away to space. Pierrehumbert's minimal description of the tropical energetics clearly demonstrates that the tropical climate is not determined locally, but globally, and that the interactions between moist and dry regions are an essential part of its stability as well as its variability. Various factors have been shown to affect this radiative-convective two-column equilibrium: low-level clouds (Miller 1997), ocean transport (Clement and Seager 1999), as well as boundary layer properties and the hydrological cycle (Larson et al. 1999).

A model of the same family is developed to study the main potential feedbacks in the tropical climate system. Atmospheric dynamics provides important linkages between the regions of ascending and descending air, and the consequences of their inclusion in the model on the climatic feedbacks are investigated. A slightly different version of this model, with a different representation of the hydrologic cycle, has been used in a previous publication (Bellon et al. 2003): the differences in the formulation and in the results will be pointed out.

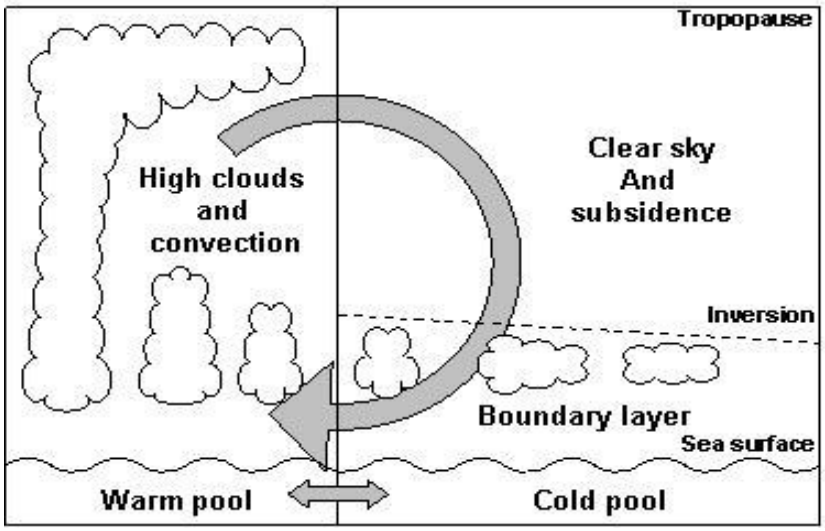

Figure 1.1: Schematic model diagram.

1.1 An idealized model

1.1.1 Description

The model used here (Fig. 1.1) is analogous to those used in previous studies (Pierrehumbert 1995; Larson et al. 1999). One column represents the deep convecting Tropics, with the underlying warm pool, and the other sketches the subsiding regions. The free troposphere in the subsiding column is thermodynamically uncoupled from the boundary layer by the inversion and coupled to the convective column: the temperature profile in the free troposphere is approximatively homogeneous throughout the Tropics (Held and Hou 1980) and the free-tropospheric humidity in the subsiding column mainly originates from the convective column (Pierrehumbert and Roca 1998; Sherwood 1996). Hence, we can define six boxes as follows: the free troposphere, boundary layer and underlying pool for each column. The model emphasizes the role of the boundary layer of non-convecting regions as a reservoir of moist static energy for convection, whereas the dry free troposphere, whose thermodynamic structure is linked to that of the convective regions, controls the radiative input in the boundary layer. The model is primarily designed to represent the equilibrium of the tropical atmosphere, and the physical parameterizations are chosen accordingly.

The subscripts 1, 2, ft and bl are used to designate respectively the convective zone, the subsiding zone, the free troposphere and the boundary layer. The ocean is represented in each column by a 50-m deep, well-mixed layer, a "slab ocean". Considering that 80% of the Tropics are covered by oceans, the continents are neglected in this model. The processes associated with continental influences and land-sea contrasts such as the monsoons cannot be represented by this model.

In the convective column, deep convection ties the temperature profile to a moist adiabat. We approximate roughly this observed feature by a fixed lapse rate Γ (in log-pressure coordinates) and we let the free-tropospheric temperature profile be equal in the

two columns. In the convective column, deep convection also moistens the free troposphere so that the profiles are close to saturation. The observed relative humidity is almost independent of the altitude. In the subsiding column, the observed free-tropospheric relative humidity is also almost constant with height. Here, We set it as exactly constant with height in the entire convecting column and in the dry free-troposphere. In Bellon et al. (2003), the relative humidity in the convective column was fixed and set to 75%, and the free-tropospheric humidity in the subsiding column was considered in quasi-equilibrium with the convective column, and computed from the local equilibrium between detrainment from the moist column and subsidence.

In the subsiding column, the boundary layer is assumed to be non-precipitating and well-mixed: the total water ratio and the moist static energy are independent of height:

$$q_{t2\mathrm{bl}} = q_2(0), \tag{1.1}$$

$$H_{2\mathrm{bl}} = (C_P T + \phi + Lq)_{2\mathrm{bl}} = C_P T_2(0) + Lq_2(0); \tag{1.2}$$

here C_P is the specific heat of air, L the latent heat of vaporization, H the moist static energy, T the temperature, ϕ the geopotential, q the specific humidity, and q_t the total water ratio, while $X(0)$ is the value of quantity X at the surface. The entrainment of mass E_{inv} at the top of the inversion is parameterized using (Sarachik 1985):

$$E_{\mathrm{inv}} = \alpha_s g \frac{LE_2}{C_P \Delta T_{v2}^{\mathrm{inv}}} \approx \alpha_s g \frac{LE_2}{C_P \Delta T_2^{\mathrm{inv}}}; \tag{1.3}$$

here g is the acceleration of gravity, LE_2 is the latent heat flux at the surface, ΔT^{inv} (resp. ΔT_v^{inv}) is the temperature (resp. virtual temperature) jump at the inversion, and α_s is a parameter, taken to be 0.2. At equilibrium, E_{inv} is equal to the total mass flux m between the columns, which determines the equilibrium altitude of the inversion p_{inv}. This parameterization takes the latent heat flux at the surface as a scaling for the buoyancy flux, which drives the shallow convection. The temperature jump at the inversion accounts for the stratification of the stable inversion layer, that limits the depth of the boundary layer. A lot of box models use a more elaborate representation of the boundary layer: the mixing-line model developed by Betts and Miller (1988). As we will point out in Chapter 3, the mixing-line model allows to depart from the mixed-layer approximation, and thus to use more realistic profiles within the boundary layer. But these profiles are arbitrarily chosen by fixing some parameters parameters, and the mixing-line model actually relies on a closure which is similar to the parameterization presented here.

The thermodynamic assumptions are summarized in Figure 1.2.

The large-scale circulation is parameterized by the vertical profile of the mass flux between the two columns, which is chosen to decrease linearly (in log-pressure coordinates) from the inversion (p_{inv}) to the tropopause ($p_{\mathrm{top}} = 150$ mb) to mimic the detrainment of convective anvils. The strength of the circulation is given by the total mass flux m between the columns:

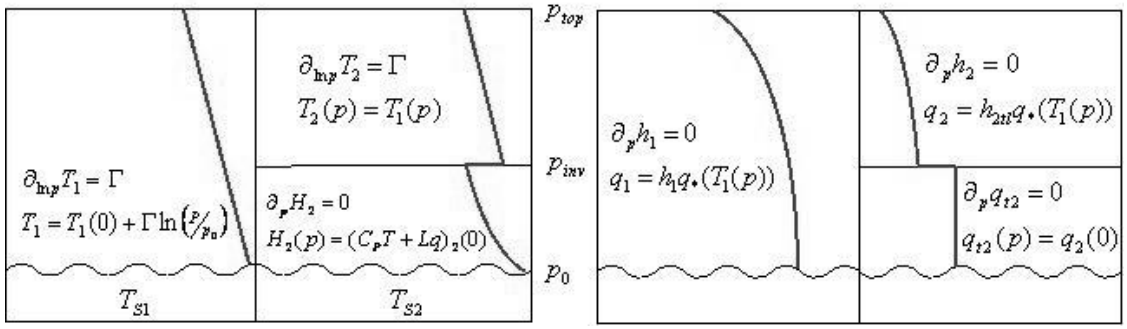

Figure 1.2: Assumptions on the thermodynamic profiles.

$$m = (1 - A_c)\frac{\omega_{\text{inv}}}{g}; \tag{1.4}$$

here, A_c is the relative area covered by the moist, convective column and ω_{inv} is the rate of subsidence at the inversion.

The circulation exports from the convective column, cold, dry air with high potential energy in its upper branch, whereas the lower branch imports into the same column warm, moist surface air. The moist static energy is therewith higher in the upper branch than in the lower, which allows the thermally direct circulation to transport energy from the moist regions to the dry ones.

The model was primarily designed to simulate the tropical climate to a first-order approximation. But it can also describe a mesoscale convective cluster and the surrounding subsidence, as soon as this system can be considered in quasi-equilibrium. Since moist dynamics are essentially transcient on the small scale, only a few small mesoscale systems can be represented by our model. But, on larger scales, convection can be considered in quasi-equilibrium with the large-scale forcing (Arakawa and Schubert 1974). Therefore, our model is relevant to study large mesoscale and synoptic convective perturbations in their mature stage and the associated subsidence.

The budgets of moist static energy H and total water q_t between the six boxes allow us to compute the precipitation rate in the warm pool, the overturning mass flux m, the rate of change of the air and sea surface temperatures, and the rate of change of the humidity in the dry boundary layer, in the dry free troposphere and in the convective column. For simplicity, and since most of the following sections will deal with equilibrium states, the budgets will be presented at equilibrium in the next subsections.

1.1.2 Water Budgets

For the whole atmosphere, the total evaporation equals the precipitation and the export to the extratropics:

$$E_1 + E_2 - P_1 - Q_{\text{exp}} = 0; \tag{1.5}$$

here the E_i are the evaporation amounts in each column and P_1 the precipitation amount in the convective column, while LQ_exp the export of latent heat to the extratropics, which is due to eddies located mainly in the free troposphere, and taken to be 10 Wm^{-2} (Peixoto and Oort 1992).

Ascending large-scale circulation is vital to the onset and the intensity of the deep convection. Following Larson et al. (1999), we parameterize the convective flux of water between the boundary layer and the free troposphere of the convective column as proportionnal to the large-scale circulation. The balance of the boundary layer is thus:

$$m[q_2(0) - (1+\gamma)q_{1\mathrm{inv}}] + E_1 = 0; \tag{1.6}$$

here $q_{1\mathrm{inv}}$ is the humidity in the convective column at p_inv and γ is the proportionality coefficient between the convective and advective fluxes. This parameterization of the convection was not included in Bellon et al. (2003), where the convective flux was implicitely taken to maintain the fixed profile of relative humidity.

The boundary layer in the dry column entrains dry air from the free troposphere, whereas the low-level divergence drives most of the evaporated humidity to the convective column:

$$m[q^+_{2\mathrm{inv}} - q_2(0)] + E_2 = 0; \tag{1.7}$$

X^+_inv is the value of quantity X just above the inversion.

The large-scale circulation dries the subsiding free troposphere, as well as the export to the extratropics, while the detrainment of moist air from the convective column moistens it:

$$m[q_{1m} - q^+_{2\mathrm{inv}}] - Q_\mathrm{exp} = 0; \tag{1.8}$$

here q_{1m} is the average specific humidity detrained from the convective column.

1.1.3 Heat Budgets

At equilibrium, the Tropics receive radiative energy and export it to the extratropics:

$$R_1 + R_{2\mathrm{ft}} + R_{2\mathrm{bl}} - LQ_\mathrm{exp} - F_\mathrm{aexp} - F_\mathrm{oexp} = 0. \tag{1.9}$$

Here R_1, $R_{2\mathrm{ft}}$ and $R_{2\mathrm{bl}}$ are the net radiative contributions, while F_aexp and F_oexp are the atmospheric and oceanic export of energy to the extratropics; the latter two are equal to 10 Wm^{-2} and 20 Wm^{-2}, respectively (Peixoto and Oort 1992), with F_aexp assumed to be concentrated in the free troposphere and F_oexp to be due to upwelling in the subsiding column.

The ocean receives radiative energy from the atmosphere which is mainly returned to the atmosphere as latent and sensible heat. The remaining heat is exported by oceanic transport. The energy budgets for the two oceanic boxes are:

$$-F_\mathrm{oc} - LE_1 - C_P F_1 + R_{1\mathrm{oc}} = 0, \tag{1.10}$$

$$F_\mathrm{oc} - LE_2 - C_P F_2 + R_{2\mathrm{oc}} - F_\mathrm{oexp} = 0. \tag{1.11}$$

Here $F_{\rm oc}$ is the oceanic heat transport from the warm pool to the cold one, the $C_P F_{\rm i}$ are the sensible surface heat fluxes, and the $R_{\rm ioc}$ are the net downward radiative fluxes at the surface.

The oceanic transport is parameterized as a diffusive flux:

$$F_{\rm oc} = m_{\rm oc} C_{P\rm oc} (T_{S1} - T_{S2}), \tag{1.12}$$

where the $T_{\rm Si}$ are the SSTs in each of the two pools, $C_{P\rm oc}$ the specific heat of liquid water, and $m_{\rm oc}$ the rate of water exchange between the pools.

The boundary-layer budget equilibrates radiation, surface fluxes, and large-scale transport:

$$m\left[(S^+_{\rm inv} + Lq^+_{2\rm inv}) - (C_P T_2(0) + Lq_2(0))\right] + C_P F_2 + LE_2 + R_{2\rm bl} = 0, \tag{1.13}$$

where $S^+_{\rm inv} = (C_P T^+_{\rm inv} + \phi_{\rm inv})$ is the static energy at the top of the inversion.

In the free troposphere the radiative cooling and export compensates the diabatic compression:

$$m\left[(S_{1\rm m} + Lq_{1\rm m}) - (S^+_{\rm inv} + Lq^+_{2\rm inv})\right] + R_{2\rm ft} + F_{\rm aexp} = 0, \tag{1.14}$$

where $S_{1\rm m} = (C_P T + \phi)_{1\rm m}$ is the average static energy detrained from the convective column.

1.1.4 Radiation

We chose to develop a simple radiation code that remains at the level of simplicity of our model. The goal of this parameterization is to represent the IR water-vapor feedback of in each box, particularly in the dry free troposphere, since it has been identified as a key-variable by Pierrehumbert (1995), and to parameterize very simply the other processes. Among them, the cloud radiative forcing is parameterized to take into account the main effects, without the ambition to assess their response to a climatic perturbation. We thus implemented the following radiation code: for the incoming solar radiation, the clear-sky diffusivity is neglected; for the infrared (IR) radiation, the surface is considered as a black body and the atmosphere as a grey body. The absorption a of the latter is parameterized as a function of humidity:

$$a = \rho(\alpha q + \beta); \tag{1.15}$$

here ρ is the air density, α a proportionality constant and β a parameter that represents the absorption of atmospheric trace constituents. The IR contribution is integrated for each box following Fouquart (1988).

The radiative effect of clouds is fixed: the low clouds below the inversion are represented by an additional albedo of 0.1, and the modification of IR absorption by condensation is

neglected. The convective clouds reflect the incoming solar radiation and also add to the greenhouse effect. These clouds'net forcing at the top of the atmosphere is still a controversial issue (Hartmann et al. 2001; Chou and Lindzen 2002) but its magnitude seems small. We thus neglect this net forcing. The main effect of these clouds is to redistribute the heat by cooling the ocean while warming the atmosphere. Following recent works (Bretherton and Sobel 2002), we parameterize this effect as an additional warming (cooling) of the atmosphere (ocean) proportional to the precipitation, $(-)rLP_1$, where r is a parameter set to 0.2. This latter effect was not taken into account in Bellon et al. (2003).

1.1.5 Surface Fluxes

The surfaces fluxes of sensible heat C_PF and latent heat LE are parameterized using bulk formulas:

$$C_PF = \rho_s C_d V_s C_P[T_s - T(0)], \tag{1.16}$$

$$LE = \rho_s C_d V_s L[q_*(T_s) - q(0)], \tag{1.17}$$

where ρ_s is the density of the surface air, V_s the surface wind, T_s the SST, $T(0)$ the surface-air temperature, C_d a drag coefficient equal to 0.0013, and q_* the saturated specific humidity. The total surface heat flux is given by $F_S = LE + C_PF$ and is dominated by the latent heat flux LE (about 90% of the total in the Tropics).

In reality, the surface wind V_s depends on the large-scale circulation and this dependence introduces a wind-induced surface heat exchange (WISHE) effect (Emanuel et al. 1994), also called evaporation-wind effect (Neelin et al. 1987): the surface fluxes increase with the intensity of the large-scale circulation, an effect that warms the entire atmosphere. This dependence is complex and difficult to parameterize at our model's level of simplicity: the large-scale circulation is related to the divergence of the wind in the lower troposphere, but the nondivergent component of the surface wind and the small-scale fluctuations cannot be explicitly modeled. We thus choose to arbitrarily link the surface wind to the large-scale circulation as follows:

$$V_s = (1 - \lambda)V_{s_0} + \lambda\eta m. \tag{1.18}$$

Here V_{s_0} is a constant reference wind, equal to 6.5 ms^{-1}, and η is a proportionality coefficient set to 2.10^3 $\mathrm{kg}^{-1}\mathrm{m}^3$. λ is a parameter describing the dependence of the surface wind on the large-scale circulation: if λ=0, the surface wind is independent of the large-scale circulation, while for λ=1 the surface wind is proportional to the large-scale circulation.

1.2 Equilibrium state and seasonal cycle

1.2.1 Methodology

Computing the heat and water capacities according to the thermodynamic hypothesis, the model described in Section 1.1 can be integrated in time until it reaches an equilibrium. In this case, the model evolves exponentially towards the equilibrium. The model was also integrated in time with a time-dependent periodic forcing, as described in Section 1.2.3, until it reaches periodicity. For some sensitivity studies (in Sections 1.5 and 1.6, as well as in Chapter 2), the software PitCon will be used (Rheinboldt and Burkardt 1983): this Fortran program allows one to study the sensitivity of an equilibrium to a parameter by continuity.

1.2.2 Reference equilibrium

Table 1.1 lists the values of the parameters used to obtain this reference equilibrium. The atmospheric and oceanic exports to the extratropics are assumed to be equal and fixed. The results are given in Table 1.2 : they are close to the climatological values as well as to the results of other models (Larson et al. 1999; Miller 1997; Clement and Seager 1999).

Parameter	Value
Area of the convective column A_c	33 %
Proportionality constant λ in Eq. (5)	0.35
Oceanic export to the extratropics	20 W m^{-2}
Latent export to the extratropics	10 W m^{-2}
Sensible export to the extratropics	10 W m^{-2}
Insolation C_s	360 W m^{-2}
Surface albedo	0.06
α	5.0 10^{-2} kg^{-1} m^2
β	1.5 10^{-4} kg^{-1} m^2

Table 1.1: Values of the model parameters in the reference equilibrium

1.2.3 Time-dependent forcing

Although the model is designed to study the climatic equilibrium, we wish to test its behavior in response to a time-dependent forcing. If the model stays in quasi equilibrium with the forcing, the response might be somewhat realistic. If not, this experiment can shed some light on the different timescales at play in the system. In any case, it is interesting to study the time-dependent response in order to understand the limits of the model. We choose to investigate a pseudo-annual cycle. In the Tropics, the seasonal cycle is weak: the annual variation of the incoming solar radiation is small compared to its variations at

Variable	Warm pool	Cold pool
T_s, the SST	301.7 K	298.8 K
$T(0)$, the surface-air temperature	301.2 K	297.3 K
$q(0)$, the surface specific humidity	16.9 g kg^{-1}	13.9 g kg^{-1}
RH, the free-tropospheric relative humidity	72.7%	18.3%
ω_{inv}, the subsidence rate	—	41.1 mb day^{-1}
p_{inv}, the altitude of the inversion	—	801 mb
Precipitation rate	4.91 m yr^{-1}	—
C_PF, the sensible surface heat flux	4 W m^{-2}	13 W m^{-2}
LE, the latent surface heat flux	135 W m^{-2}	125 W m^{-2}
m, the large-scale overturning	$3.25\ 10^{-3}$ kg m^{-2} s^{-1}	

Table 1.2: Results for the reference equilibrium

higher latitudes. Still, between the equinoxes and the solstices, the spatial distribution of the insolation varies as well as the geographic location of the Intertropical Convergence Zone (ITCZ). Over the ocean, the latter tends to follow the maximum of insolation, even if it stays closer to the Equator (Tomas and Webster 1997). In an equinoxial situation, the convective regions tend to be over the Equator, and the subsiding ones are symmetrically distributed on both sides of the Equator. Inversely, at the solstice, the ascending branch of the Hadley circulation is in the summer hemisphere, while the descending branch is mainly located in the winter hemisphere. In the first case the difference in insolation between convective and subsiding region is smaller than in the second case, as shown in Figure 1.3. This seasonal evolution is less true in the East of the oceanic basins, where the ITCZ tends to stay slightly North of the Equator, but we focus on the zonally-averaged, axisymmetric situation.

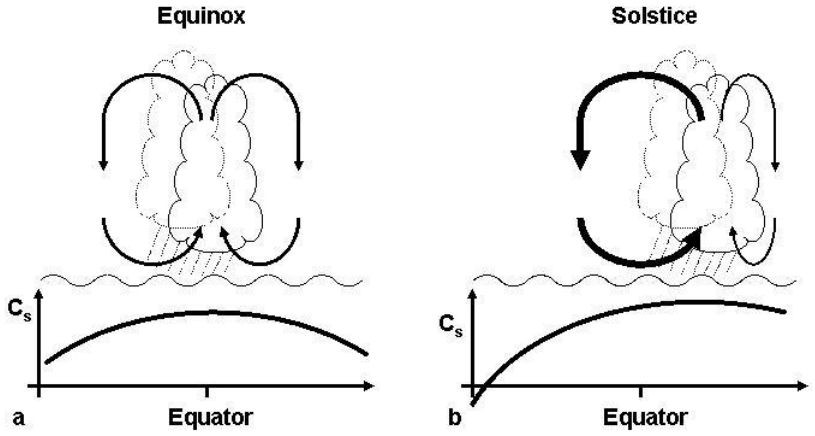

Figure 1.3: Differences in the latitude of the convergence zone and in the insolation between (a) equinoxes and (b) solstices.

To study the response of the model to the seasonal variation of the insolation, we

can apply a time-dependent solar forcing: the average incoming solar flux constant is kept constant, but the difference in insolation between the moist and dry boxes is 180-day periodic to roughly mimic its variation between two equinoxes. Figure 1.4 shows the forcing and the response of the SST in the cold and warm pools.

The temperature of both the warm and cold pools is higher than the equilibrium temperature: because the input of energy is increased in the convective column, which is less able to radiate energy to space than the subsiding column, the asymmetry of the forcing between the two columns tend to heat the system.

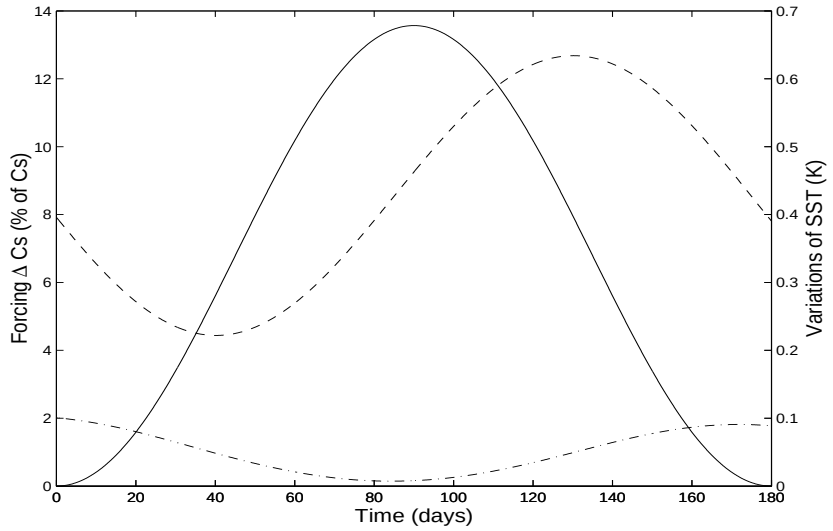

Figure 1.4: Response of the model for a 180-day periodic solar forcing; solid: difference of insolation between the two columns; perturbation of the warm (dashed) and cold (dash-dotted) pool SSTs relative to the symmetric equilibrium.

Furthermore, the response of each column illustrates their fundamental nature. On one hand, in the moist column, the response of the outgoing radiation and the surface fluxes is slow compared to the rate of change of the solar forcing because of (i) the runaway greenhouse state; and (ii) the slowness of the export to the subsiding regions. The time evolution of the temperature is thus driven by the solar heating and the SST is in quadrature with the forcing. On the other hand, in the dry column, the response of the radiative-convective processes is much faster because of the clear sky; consequently the SST is almost in phase with the forcing.

This time-dependent experiment shows one of the limits of the model: the behavior of each column is driven by the local radiative-convective state and the large-scale circulation only modulates these responses. On this seasonal timescale, the two-column system is far from the quasi-equilibrium. On the contrary, observations tend to show that the Hadley Cell circulation is in quasi-equilibrium with the heating (Lindzen and Hou 1988). This suggests that, in the tropical climate, the response of the large-scale circulation to the seasonal cycle is fast, and keeps the temperature in quasi-equilibrium; that would imply that, on the planetary and seasonal scales, the large-scale circulation is not controlled by

the radiative cooling of the subsiding regions. This thermodynamic control is only valid on longer, climatic timescales.

1.3 Sensitivity to the horizontal transport of energy

The tropical atmosphere exports energy to the extratropics mainly through eddies that develop between the subtropics and the mid-latitudes. This transport is thus controlled by dynamical intabilities that are difficult to model in a simplified framework like ours. Nevertheless, we can study the sensitivity of our model to the parameters of export of heat to the extratropics.

Two kinds of perturbations are considered. In a first experiment a prescribed transport of sensible heat is added to the free-tropospheric component of the subsiding area. This additional flux may be positive (energy gain by the subsiding area) or negative (energy loss); for the reference equilibrium, this transport was taken to be -10 W m^{-2}. The results are

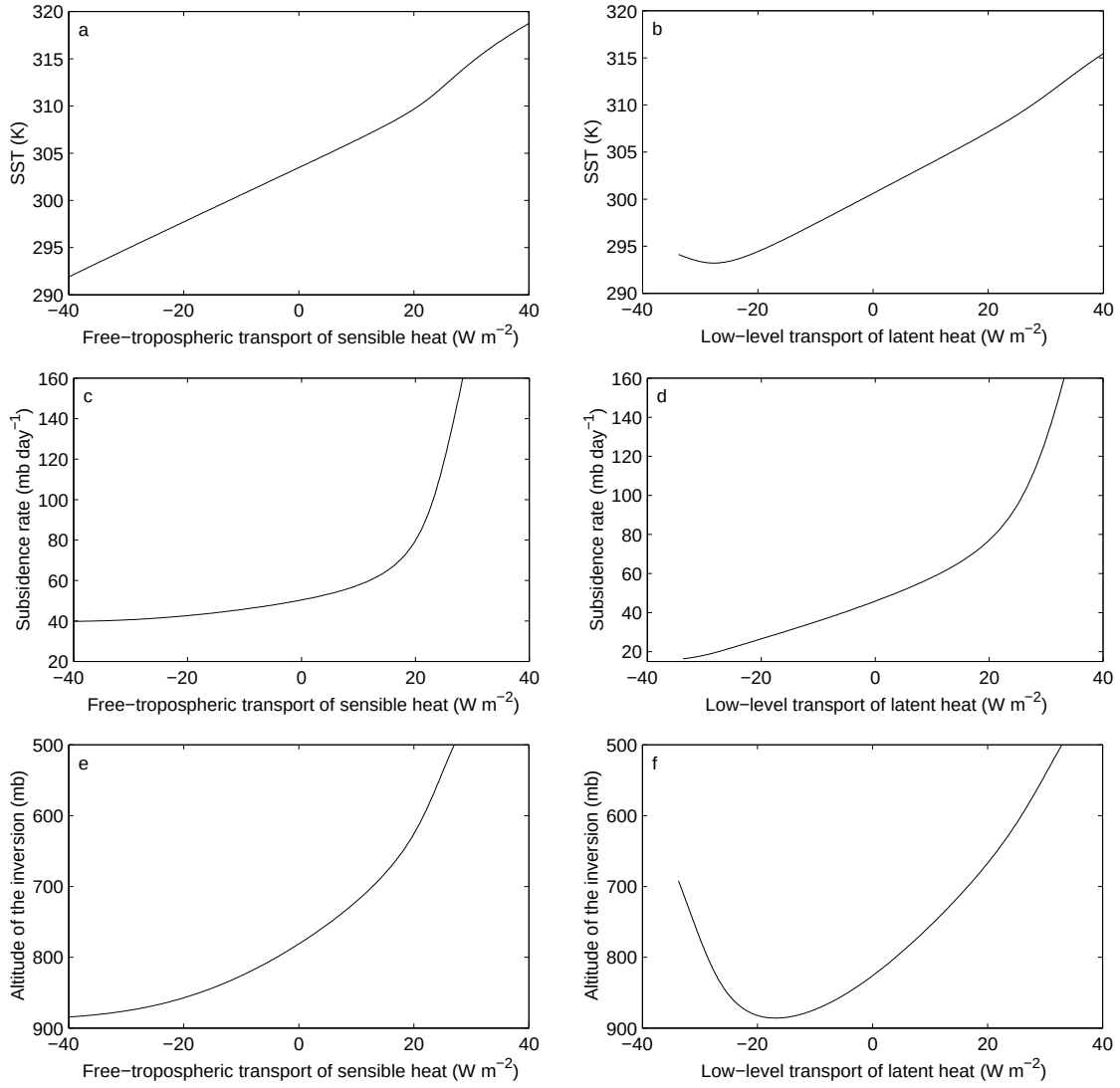

Figure 1.5: Sensivity of the model average SST (a, b), subsidence rate in the dry free troposphere (c,d) and altitude of the inversion (e, f) to the free-tropospheric export of sensible heat (a, c, e) and to the low-level export of latent heat (b, d, f) to the extratropics.

shown in Figure 1.5; the SST, subsidence rate in the clear-sky region and the altitude of the inversion increase with a gain of energy. The simulated impact on the SST is largely linear (Fig. 1.5.a), but the complexity of the model response appears clearly in the strong non-linearity of the large-scale circulation response (Fig. 1.5.c), or in the response of the altitude of the inversion in the descending branch (Fig. 1.5.e). Overall, around the reference equilibrium, an increase of the energy export to the extratropics cools the tropical climate. But the subsidence rate, and thus the overturning circulation, decreases. Consequently, the transport of energy within the tropical system decreases. This dynamical feedback reduces the temperature perturbation, because the excess of energy in the runaway greenhouse column is less efficiently transported to the subsiding column, where it can be radiated to space. Very similar results were obtained by varying the free-tropospheric latent heat export to the extratropics (not shown).

A second set of results corresponds to the prescription of a latent heat flux in the boundary layer of the subsiding area. In the reference equilibrium, this flux was taken to be zero. Exchanges between the tropics and extratropics in the low levels are thought to be small, but since the boundary layer is quite moist, a small perturbation of the dynamics could lead to a significant perturbation of the latent heat transport from the tropics to the extratropics in the lower atmosphere. For an input of latent energy in the boundary layer of the subsiding column, the results of this sensitivity study are close to those obtained by varying the sensible heat horizontal transport: whereas the response of the temperature to an input of latent energy is close to linear (Fig 1.5.b), the response in the intensity of the large-scale circulation and altitude of the inversion exhibits a strong non-linearity (Fig 1.5.d and 1.5.f). Furthermore, an export (e.g. negative transport) of moisture to the extratropics tends to shut down the overturning circulation, and this effect dominates the response of the tropical climate if the transport gets smaller than -20 W m^{-2}: the average temperature and the altitude of the inversion start to increase with decreasing transport of latent heat, because the two model columns become weakly coupled.

The non-linearity of these responses is linked to the response of the boundary layer in the subsiding column of the model (Fig 1.5.e and 1.5.f). For a large input of energy (more than 20 W $m^{-2)}$, the shallow convection intensifies and extracts more energy from the ocean via the evaporation, to the point that it can't really be considered shallow anymore. The thermodynamically-controlled circulation is thus strongly enhanced. The threshold of 20 W m^{-2} and slope of the curves above this threshold are certainly dependent on the parameterization of the cloud-topped boundary layer. Therefore, a better understanding and modeling of the boundary layer is certainly needed (see Chapter 3). Nevertheless, the deepening of the boundary layer is expected to be a strong feedback (Bony et al. 2004).

This sensivity studies can also be considered in the context of multiple two-column tropical systems. The Walker circulation can be seen as an ensemble of three of these systems, with ascending regions above the continents, and descending regions over the oceans. These three systems can interact and exchange energy through their subsiding regions, and the non-linear sensitivities to energy transports illustrate the complexity of

this coupling. Furthermore, these exchanges of energy between two-column systems is certainly vital to the variablity of the Indian monsoon, where a convective zone over the equatorial ocean is in competition with another one over the continent around 20° of latitude (Webster et al. 1997; Le Treut and Bellon 2004).

1.4 Sensitivity to radiative and areal perturbations

The sensitivity of this type of model to the warm pool's relative area A_c is significant, according to previous studies (Pierrehumbert 1995; Larson et al. 1999); Figure 1.6 shows the sensitivity of the warm and cold pool temperature to a variation of the relative extent of the convective column, that is analogous to Fig. 3 in Larson et al. (1999).

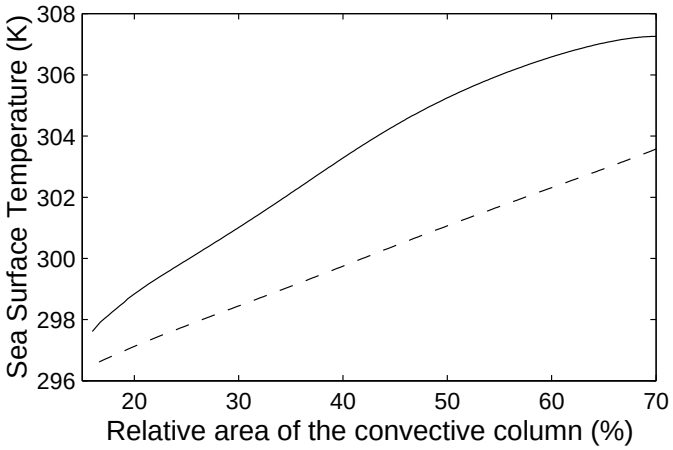

Figure 1.6: Sensitivity of the model SST to a change of the relative area of the warm pool; solid: warm pool; dashed: cold pool.

Therefore, it seems interesting to investigate how the temperature is related to A_c in the reanalyses. Furthermore, we could assess the importance of this sensitivity compared to the sensitivity to radiative perturbations.

1.4.1 Link between the extent of convergence zones and the SST in the observations

Here, we use the monthly means of the National Center for Environmental Prediction/National Center for Atmospheric Research (NCEP/NCAR) reanalysis 2 (Kistler et al. 2001) for the temperature at 400 mb, the vertical velocity at 500 mb, and the precipitable water (PW: the column-integrated water content of the atmosphere). We also use the monthly means of the National Oceanic and Atmospheric Administration (NOAA) Optimum Interpolation (also called "Reynolds") surface temperature (Reynolds et al. 2002). The latter set of data is available from November 1981 to present on a 1°x1° grid, while the former is available from 1979 to present on a 2.5°x2.5° grid. We will use the dataset from November 1981 to December 2002, averaged on the NCEP grid.

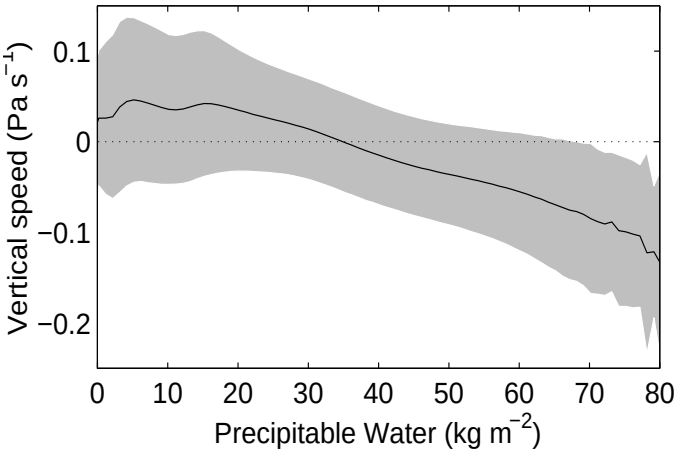

Figure 1.7: Average vertical velocity of the tropical gridpoints as a function of their precipitable water; the shaded zone shows the standard deviation.

To avoid to take into account extratropical air masses, we define the tropics as the zone including the equator where the free-tropospheric horizontal gradients are weak. In practice, the limit of the tropical region is taken where the 400 mb meridional gradient of temperature exceeds a threshold of 0.5 degK/deg lat. An experiment using the temperature difference between the Equator and the limit of the Tropics at 400mb, instead of the temperature gradient, as a criterion for the definition of the tropics gives similar results (not shown).

We discriminate the moist regions from the dry ones using the precipitable water: gridpoints with a precipitable water superior to 45 kg m^{-2} are considered to be part of the convective zone, while dryer gridpoints are part of the subsiding region. The PW threshold is chosen close to the value for which the average vertical at 500 mb velocity is zero. Figure 1.7 shows the observed 500 mb vertical speed as a function of the precipitable water, and the 45 kg m^{-2} threshold appears as a reasonable choice. We obtain values of A_c that are about 0.3, which is the typical value (Pierrehumbert 1995; Larson et al. 1999).

The observed interannual variations of the spatially-averaged tropical surface temperature and the relative area of the moist region (defined as the ratio of the area covered by the convective regions over the total area of the Tropics) are shown in Figure 1.8. The long-term mean seasonal cycle has been removed, by considering anomalies from the long-term monthly mean. The time series of the monthly average surface temperature and the monthly A_c are well correlated, with a correlation coefficient of 0.65. The El Niño-Southern Oscillation (ENSO) warm events and their cold counterpart La Niña events are quite noticeable in 1982-1983, 1987-1988, 1997-1998 and we can see the begining of the 2002-2003 event at the end of the series. The signal of the 1992-1993 event is very weak, but it is so in both time series. In general, warm events are associated with a larger convection zone. Roughly, a change of 4% in the relative area of the convergence zone is associated with half-a-degree perturbation of the average tropical surface temperature. It matches approximately the sensitivity of our model (see Fig. 1.6). It seems that, on

interannual timescales, the hydrologic cycle can be thought to be in quasi-equilibrium with the tropical temperature. Thus the El Niño and La Niña events might be considered as quasi-equilibria that a two-column model can describe: the warm events correspond to a widening of the warm pool towards the Central Pacific, and the cold ones to a shrinking of A_c. The area covered by moist regions also appears as a potential diagnostic variable for General Circulation Models.

The same computation excluding the continental values gives similar results.

The observed long-term mean seasonal cycles of A_c and surface temperature are shown in Figure 1.9. They exhibit a strong monsoonal signal: there is a maximum of temperature followed by a maximum A_c that are due to the Asian and African monsoons. Furthermore, there is a secondary maximum of SST during the Southern Hemisphere Spring. Actually, the warming of the surface during intermediate seasons is associated with the weakening of the large-scale circulation: the Hadley cell is supposed to slow down when the heating is centered over the Equator (Lindzen and Nigam 1987), thus decreasing the export of heat from the deep tropics to the subtropics. The regulation of the temperature by the large-scale circulation is consequently reduced. It corresponds also to the warming preceding the onset of the monsoon. The asymmetry between the two temperature maxima is due to the different characteristics of the Northern Hemisphere and Southern Hemisphere monsoons.

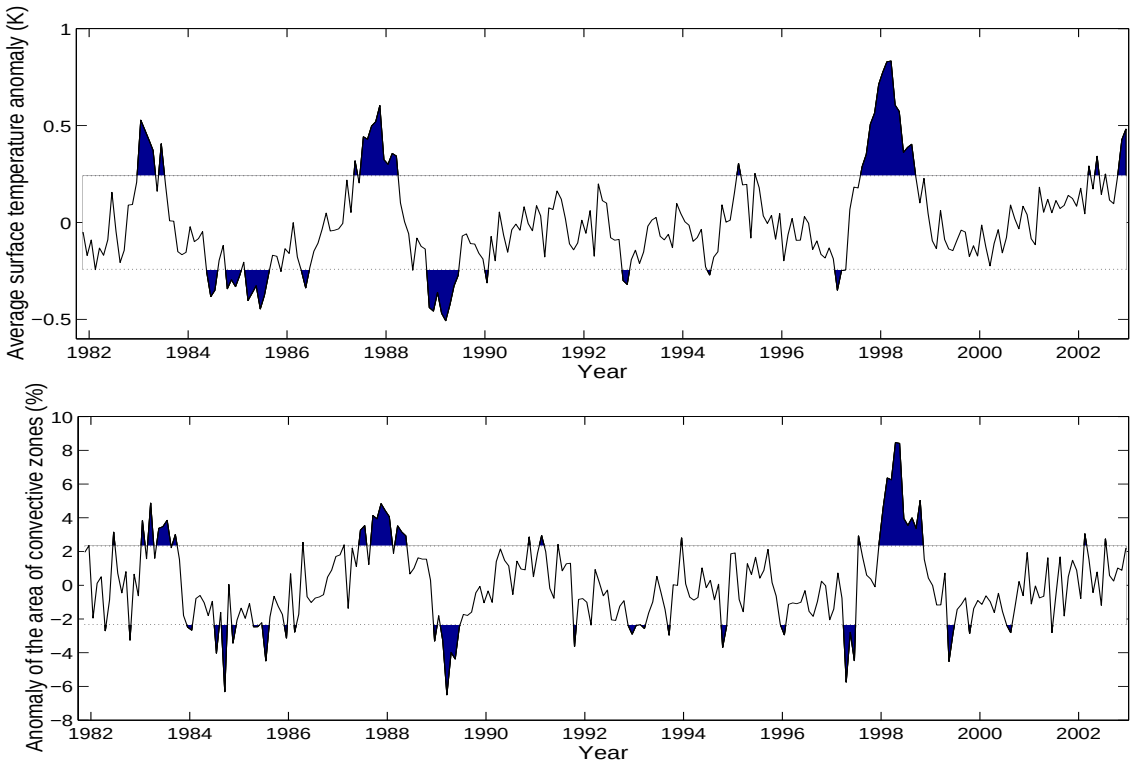

Figure 1.8: Interannual variability of the tropical surface temperature (upper panel) and the relative area covered by the moist region (lower panel); the standard deviations are indicated by the dotted horizontal lines.

The increase of A_c with the onset of the monsoons can be seen after the temperature maximum in the Northern Hemisphere. The interaction between land and ocean is crucial to the development of the monsoons (Webster et al. 1997), or at least to its poleward extension (Neelin and Chou 2001). The geography and topography of the continents thus play an important role in the seasonal cycle that explains part of the asymmetry between summer and winter.

Not surprisingly, the two cycles are not very well correlated. Actually, there is a strong lag-correlation with a lag of about two months (Fig. 1.9, right panel): the surface temperature leads the extent of the convective zone. The lag-time results not only from the adjustment of the hydrologic cycle to the seasonal forcing, but also from the land-sea interaction and hydrologic contrast. We can also notice a strong anticorrelation with a lag of 6 months, which is linked to the interaction between the summer and winter monsoons.

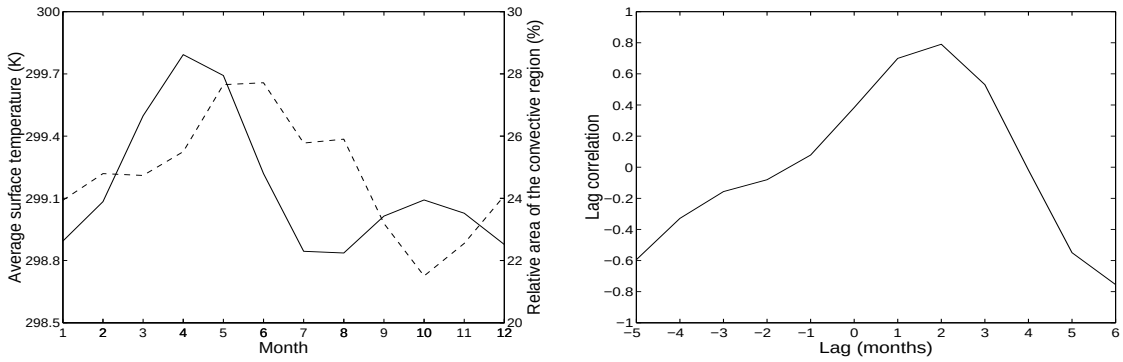

Figure 1.9: Left panel: annual cycle of the surface temperature (solid) and relative area of the convective region (dashed); right panel: lag correlation between the two, the time-lag is counted positively when the temperature is leading A_c.

This analysis shows that, although the zonally-averaged circulation of the tropical atmosphere appears in quasi-equilibrium with the radiative forcing during its seasonal cycle (Lindzen and Hou 1988), the whole tropical climate is not in quasi-equilibrium. In fact, the variations of the surface temperature seem to lead those of the extent of the moist regions. The monsoons break the axisymmetry; therefore, it is not surprising that their signal in temperature and humidity does not match the results from axisymmetric models.

We have already discussed in Section 1.2.3 the limits of our model in simulating the seasonal cycle. In that section, the model SST lagged the solar forcing. The results of the present section, with maxima of average SST in the Spring, further strengthen our conclusion on the specificity of our model, which is better suited to study the equilibria of the tropical atmosphere. While the interannual variability of the water cycle and SST seems to be reasonably represented by our model equilibrium, the seasonal cycle cannot be considered as a thermodynamic quasi-equilibrium.

1.4.2 Comparison of the sensitivity to areal and radiative perturbations: three experiments

The observations, as well as simple models, show the relevance of the feedbacks associated with the relative extent of the convergence regions; it is interesting, therefore, to compare the orders of magnitude of the model sensitivities with respect to A_c and to radiative perturbations. To do so, we study three cases: a 5%-increase of the convective column area (A_c=38%, Case A_c+5), a doubling of carbon dioxide concentration in the atmosphere (β=1.7.10^{-4} kg^{-1} m^2, Case 2·CO_2) and an increase of the insolation (C_s=365Wm^{-2}); the latter Case C_s+5 corresponds roughly to the radiative forcing at the tropopause caused by a CO_2 doubling.

Change in	T_s (K)	ω_{inv}	m	T_s–$T(0)$ (K)
A_c+5	+0.94	+3.6	-1.5 10^{-4}	-0.5
2·CO_2	+1.34	+5.4	+4.4 10^{-4}	-1.8
C_s+5	+0.97	+2.0	+1.5 10^{-4}	-0.7

Table 1.3: Model sensitivity to areal or radiative perturbations. The columns represent the change in T_s, the average SST; the change of ω_{inv} (in mb day^{-1}); the change of the overturning circulation m (in kg m^{-2} s^{-1}); and the change in the temperature difference $T_s - T(0)$ between the SST and the surface-air temperature.

As expected, an SST increase is obtained in all three cases (see Table 1.3). In our model, a doubling of the CO_2 concentration gives an increase in SST of more than 1.3^{o}C, 40% larger than a 5-W m^{-2} perturbation in the solar constant C_s; the change caused by a 5% increase of the convective column's area is of the same order of magnitude as the latter. Actually, the strength m of the overturning circulation increases with a positive radiative perturbation, because the radiative cooling of the dry free troposphere, and thus ω_{inv}, increase; consequently, the transport of energy from the convective zone to the subsiding one, where it can be radiated to space, increases. This dynamical feedback reduces the warming perturbation. Inversely, in the Case A_c+5, the change in the area of the subsiding region compensates the change in the subsidence rate and the strength m of the overturning circulation decreases slightly. The warming is thus enhanced by the large-scale feedback and reaches the same order of magnitude as the warming due to a radiative perturbation. These feedbacks are illustrated in Figure 1.10.

1.5 Feedbacks associated with the surface flux

Because of the nonlinearity of the Clausius-Clapeyron equation and the dominance of the evaporation in the surface heat flux F_S, changes in F_S provide a strong negative feedback for a change in SST, if $T_s - T(0)$ and V_s remain constant (Hartmann and Michelsen 1993). Our model suggests that the sea–air temperature difference $T_s - T(0)$ decreases with a warming (see the last column in Table 1.3). A direct consequence is that $T(0)$, and hence

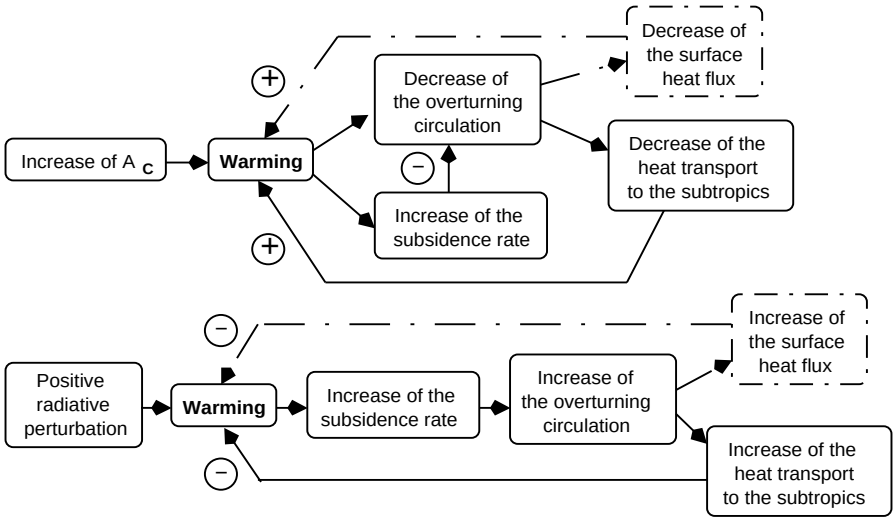

Figure 1.10: Feedback loops for an areal or radiative perturbation. Plus: positive feedback; minus: negative feedback. Dash-dotted: feedback added by the dependence of the surface wind on the large-scale circulation

the entire atmosphere, warm more than the underlying SST. This enhanced atmospheric warming has two effects: (i) the average outgoing IR flux at the top of the atmosphere increases, thus providing a negative feedback on the temperature of the whole system (i.e. the atmosphere acts as a buffer); and (ii) the surface fluxes and thus the corresponding negative feedback are reduced.

Furthermore, the large-scale circulation interacts with the surface fluxes by ventilating the boundary layer, but it also has an impact on the surface wind V_s (Emanuel et al. 1994). The latter effect has been shown to have a potential impact on the global climate stability and sensitivity through the angular momentum transport between the tropics and extratropics (Bates 1999). But the large-scale tropical circulation is another mechanism that influences the surface flux through the surface wind speed. To study this influence in detail, we plot in Figure 1.11 the SST changes as a function of λ, the parameter that describes the dependence of V_s on m (see Equation 1.18), for the three cases described in the previous section.

In our model, the wind-induced surface heat exchange (WISHE) introduces an additional feedback whose sign and magnitude depend directly on the sensitivity of the large-scale circulation to the perturbation: an increase of m enhances the surface heat flux F_S. Increasing F_S allows, in turn, a cooling of the global system because it transfers the heat from the ocean to the atmosphere, where it can be exported by the large-scale circulation to clear-sky regions and radiated to space. From the previous section, it follows that WISHE exerts a negative feedback for a radiative perturbation, while it has a positive feedback for a change in A_c (see Figure 1.10). WISHE can eliminate up to a third of the warming due

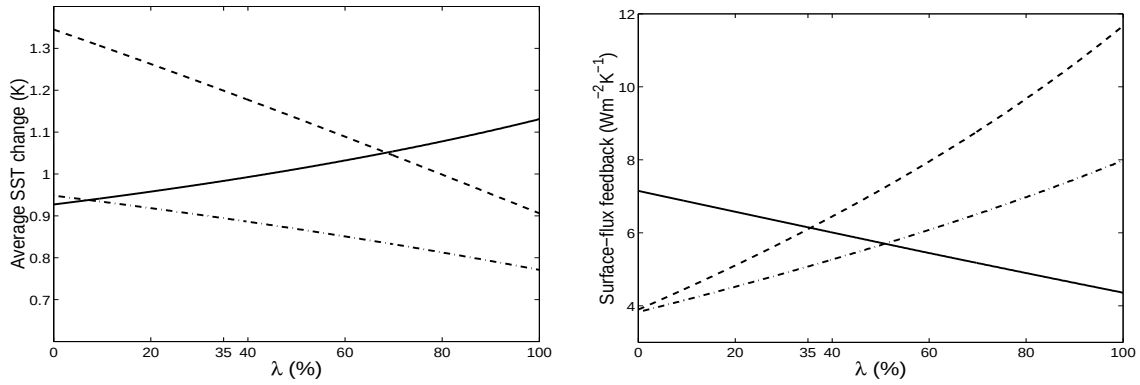

Figure 1.11: Sensitivity of the warming (left panel) and of the surface-flux feedback (right panel) on the parameterization of the surface wind; Case A_c+10: solid line; Case $2{\cdot}CO_2$: dashed line; Case C_s+5: dash-dotted line.

to a radiative perturbation (see Figure 1.11).

We can characterize the magnitude of the surface flux feedback by the surface heat flux increase normalized by the temperature change: $\partial F_S/\partial T$. The Hartmann and Michelsen (1993) model takes into account the ventilation of the boundary layer by the large-scale circulation and gives a surface flux feedback of 7.9 W m^{-2} K^{-1}. Our model gives a slightly smaller feedback for λ=0, of 4 to 7.2 W m^{-2} K^{-1}. The difference between the two models is explained by the decrease of the air–sea temperature difference in ours, while this difference is fixed in (Hartmann and Michelsen 1993).

In our model, the surface flux feedback changes almost linearly with λ; it increases significantly for a radiative perturbation while it decreases for a perturbation of the area as shown in Figure 1.11. Consequently, the surface-wind dependence on the large-scale circulation increases the negative feedback associated with the surface flux and reduces substantially our model's sensitivity to radiative perturbations. Besides, this dependence increases the sensitivity to A_c relative to the sensitivity with respect to a radiative perturbation.

1.6 Potential Area feedback

Our model's sensitivity to the relative areas occupied by the two types of radiative-convective and dynamical behavior — moist and ascending vs. dry and descending — in the tropical atmosphere is quite substantial. This sensitivity suggests the presence of an important and as-yet unexplored feedback in Earth's tropical climate, that could contribute to maintain the "lid" on tropical SSTs. But whether the relative area A_c of the convective region would actually increase or decrease as a response to global warming is not clear.

On the planetary scale, dynamical processes must play an important role in controlling A_c: recent papers (Kelly and Randall 2001; Bretherton and Sobel 2002) are a first step

in a further study of this role, analyzing the atmospheric response to prescribed SST gradients. The mass flux associated to the low-level convergence is supposed to equilibrate the thermodynamically-controled vertical circulation. The competition between the change of the large-scale circulation imposed by the clear-sky thermodynamics and the change of the low-level convergence is therefore a key process in determining the relative extent of the convective and subsiding regions.

The dynamics in the lower levels of the tropical atmosphere are at least partially controled by the surface temperature gradients (Lindzen and Nigam 1987). As a zero-order model, we can consider that the low-level wind is proportional to the surface temperature difference between the boxes as it is assumed in other studies (Hartmann et al. 2001; Kelly and Randall 2001):

$$V_s = \nu \Delta T_{\rm s}, \tag{1.19}$$

where $\Delta T_{\rm s} = T_{\rm s1} - T_{\rm s2}$ is the SST difference between the warm and old pool; from the reference equilibrium, we can get the proportionality coefficient ν=2.3 $\mathrm{ms^{-1}K^{-1}}$. Considering that the horizontal wind is independent of the altitude within the boundary layer, the mass flux m between the columns can then be written:

$$m = \frac{p_{\rm s} - p_{\rm inv}}{g} V_s = \frac{p_{\rm s} - p_{\rm inv}}{g} \nu \Delta T_{\rm s}, \tag{1.20}$$

where $p_{\rm s}$ is the surface pressure.

Using this simple parameterization, we conduct again the two experiments of an increase of the solar incoming radiation C_s+5 and a doubling of carbon dioxyde 2·CO_2. We call them C_s+5' and 2·CO_2'. Table 1.4 gives the results for these 4 experiments (some are reminders from Table 1.3).

Change in	A_c	$T_{\rm s}$ (K)	$\Delta T_{\rm s}$ (K)	$p_{\rm inv}$	$\omega_{\rm inv}$	m
2·CO_2	0	+1.34	-1.0	-65	+5.4	+4.4 10^{-4}
C_s+5	0	+0.97	-0.3	-40	+2.0	+1.5 10^{-4}
2·CO_2'	+2.5	+1.94	-0.8	-100	+6.4	+3.4 10^{-4}
C_s+5'	0	+0.97	-0.3	-40	+2.0	+1.5 10^{-4}

Table 1.4: Model sensitivity to radiative perturbations with and without a parameterization of the low-level flow. The columns represent the change in A_c; the change in T_s; the change in the SST difference $\Delta T_{\rm s}$ between the warm and cold pool; the change of the altitude $p_{\rm inv}$ of the inversion (in mb); the change $\omega_{\rm inv}$ (in mb/day); and the change of m (in kg $\mathrm{m^{-2}}$ $\mathrm{s^{-1}}$).

While the relative area of the convective column doesn't change when relaxing the constraint of fixed relative area of the moist column in the case of an increase of C_s, it increases for a doubling of carbon dioxyde. This increase causes a further warming of 0.6 K, almost half of the original warming in Case 2·CO_2.

From Equations (1.4) and (1.20), we see that the change in A_c results from the competition between the change of the radiatively controled $\omega_{\rm inv}$ and the change in the product of

SST difference ΔT_s and the depth of the boundary layer $p_s - p_{inv}$. Here, ΔT_s decreases with a warming: the surface wind is slower in a warmer climate. This decrease is compensated by the increase of the boundary layer depth in Case 'C_s+5', whereas the product of ΔT_s and $p_s - p_{inv}$ decreases in Case '2·CO_2', which yields a decrease of the relative area of the subsiding column $1 - A_c$.

The model area feedback is thus sensitive to (i) the parameterization of the altitude of the inversion; and (ii) the differential sensitivity of the columns. The latter is controled by the radiative response of the columns, in which the water vapor feedback is crucial. The same experiment using the Bellon et al. (2003) model exhibits an increase of the SST difference between the columns with a warming, which leads to a moderation of the warming (not shown). This different behaviors arises from the simpler representations of the free-tropospheric hydrological cycle and cloud forcing, which yield to different water-vapor and cloud feedbacks and a different response in the differential heating between the columns.

Therefore, the simplicity of the model does not allow to conclude about the sign of the feedback, but it illustrates how crucial it is: the order of magnitude of the potential feedback invites further investigation with models of higher complexity.

1.7 Discussion

Our work shows that, as far as the relative area occupied by the moist regions can be considered constant, the dynamics are a strong negative feedbacks for climate changes related to radiative perturbations. Indeed, the role of the large-scale dynamics are crucial in exporting the energy from the runaway greenhouse regions to the subsiding ones where it can be radiated to space, and this overturning circulation intensifies with a warming associated with a change of radiative parameters. The large-scale circulation has also an influence on the tropical climate through the evaporation-wind feedback, which reduces the sensitivity of the surface temperature.

The role of the dynamics in controlling some of the parameters such as the export to the extratropics and the relative extent A_c of the convective zone might be as important as the effects described above. On one hand, the non-linearity of the response of our model to the export to the extratropics shows that the interaction between different convective regions might have a strong impact on the overall sensitivity of the tropical climate. And distinct moist regions can be observed in the tropics, during the monsoon or simply in the average Walker circulation. On the other hand, the role of the near-surface dynamics in creating convergence zones is expected to control A_c. Including a very simple parameterization of the surface flow in our model showed that this effect could create a positive feedback on the warming caused by a doubling of CO_2. But this parameterization is very sensitive to the modelling of the boundary layer and the differential heating of the columns, and particularly to the water vapor feedback. For instance, an opposite feedback was obtained with the model in Bellon et al. (2003), which includes a slightly different representation of

the hydrological cycle and cloud forcing.

A better understanding of the processes controlling A_c is thus needed to conclude about the sensitivity of the tropical climate in this two-column framework. Among these processes, the near-surface dynamics and the shallow convection in the boundary layer of the subsiding column are already identified and will receive some attention in Chapter 2 and 3. The free-tropospheric hydrological cycle has also an impact on the sensitivity of A_c to radiative perturbations, while A_c itself is a part of the signal of the hydrological processes. This is a strong motivation for a basic study of the observed moist regions, which will be undertaken in Chapter 2.

Chapter 2

Scale separation for humidity-bimodal systems

Observed tropospheric water vapor in the tropics is commonly bimodal (Zhang et al. 2003): the distribution of the tropospheric humidity exhibits a moist mode and a dry mode. According to Zhang et al. (2003), the bimodality arises from the difference of the timescales of processes that control the vertical and horizontal transport of water vapor. The injection of water vapor in the free-troposphere by deep convection is very fast (a few hours) and is responsible for a moist mode. The bimodality arises if the timescale of the drying by radiatively-driven subsidence, which tends to create a dry mode, is shorter than the timescale associated to horizontal mixing, which tends to homogeneize the humidity distribution. Therefore, this bimodality can be seen in data on short timescales (3h to 1 day) with mesoscale definition and in monthly means on the planetary scale as well.

Consequently, the model of an ascending moist column associated with a subsiding column can thus represent not only the Hadley/Walker circulation on long timescales but also a mesoscale bimodal system on timescales of about a day. Furthermore, the circulation between the two columns is similar: the moist convective regions are in average ascent. The relatively dry air detrained at high altitude from the clouds descends in surrounding clear-sky regions, and the low-level flow brings boundary-layer air back to the moist convective regions. A limitation of the model is that it is better suited to describe equilibrium situations. But most of the tropical convection in the Tropics is organized in mesoscale clusters that can be considered in quasi-equilibrium with the large scale forcing (Arakawa and Schubert 1974). Furthermore, the processes in the subsiding regions are slow, and a quasi-equilibrium model can be expected to represent a fair amount of bimodal systems.

Understanding the spatial distribution of two-column moist-vs-dry system in the tropics can give some insight in the regulation of the tropical climate. Indeed, the distribution of the sizes of these two-column system is likely to influence the radiative-convective equilibrium of the tropical climate as a whole. Studying the processes controlling the extent

of moist regions and their interaction with their subsiding counterparts is actually an alternative approach to study the water vapor feedback: although part of the humidity of the subtropics is of extratropical origin, the main source of water vapor in the tropical free troposphere is the convection. In non-convective regions, the large-scale advection is responsible for most of the Upper-Tropospheric Humidity (UTH) by transporting water vapor from convective to subsiding regions (Pierrehumbert and Roca 1998; Sherwood 1996; Zhu et al. 2000). How convection is spatially organized and how convective and subsiding regions interact are thus important issues in the process of unravelling the factors controlling the UTH and the associated radiative feedback, and this interaction is expected to depend on the size of the two-column systems. As a first step in addressing these issues, this chapter is focusing on the size distribution and the spectral properties of the moist regions, as well as their modelling.

While the spectral properties of the humidity field has not been investigated, the convective clouds have been extensively studied in the Atlantic Ocean (Machado et al. 1992), in the Pacific warm pool (Mapes and Houze 1993), in the Indian Ocean (Roca and Ramanathan 2000; Roca et al. 2002), and in larger regions (Machado and Rossow 1993). The cloud clusters have been shown to be continuously distributed up to sizes of 10^6 km^2 (characteristic size of 1000 km) with different distributions depending on regions (Machado and Rossow 1993; Roca and Ramanathan 2000). Furthermore, the mesoscale convective structures have been shown to be highly correlated with the UTH (Roca et al. 2002).

Nevertheless, considering the difference of timescales between processes due to convection (a few hours) and the subsidence drying (a day or two), the humidity spatial structures are likely to evolve on longer timescales than the clouds and a different spatial distribution might appear, with different spectral characteristics.

Since subsiding regions corresponding to different ascending zones are often connected, it is difficult to determine which moist region a dry gridpoint is coupled to. The moist regions tend to be more convex and easier to discriminate. Section 1 is thus dedicated to study the size distribution of the moist regions, without trying to couple them to the corresponding subsiding branch.

The thermodynamical model used in Chapter 1 does not specify any horizontal scale for the extension of the two-column moist-vs-dry system. Therefore, the dynamics of the tropical troposphere might be expected to control the extension of the systems that can be represented by such a model. In Section 2, a parameterization of the low-level flow is included in the model. In Section 3, we ascertain a posteriori the limits of our representation of the dynamics.

2.1 Observed convective regions in the tropical troposphere: a scale separation

2.1.1 Data and methodology

NCEP/NCAR reanalyses 2 of daily mean precipitable water (PW) are used. We will also use the NCEP/NCAR reanalyzed daily relative humidity averaged between 600mb and 300mb, that we will further use to quantify the Upper Tropospheric Humidity and the NOAA daily Outgoing Longwave Radiation (OLR) (Liebmann and Smith 1996). The OLR dataset is available from 1974 to present, but some data are missing during 1978 and the data before 1978 exhibits a large offset from the data afterwards. It thus seems safer to use the period of 24 years from 1979 to 2002 for the three datasets. We limit our analysis to the tropics which are defined here as the region between 30°S and 30°N of latitude. The datasets are defined on a 2.5°x2.5° grid. While the PW contains information exclusively about the water content of the atmosphere, the UTH and OLR are more complex signals: the UTH depends on the temperature of the free troposphere through the saturated humidity, and the OLR contains information about the surface temperature and the temperature profiles, as well as the cloudiness and type of clouds in the column. Nevertheless, small OLRs are well correlated with moist regions.

To study the properties of the moist regions (Section 2.1.3), we will use two additional datasets: the weekly NOAA Optimum Interpolation SST and the daily NCEP/NCAR reanalyszed 500mb vertical speed. The former dataset is available on a 1°x1° grid for weekly means from November 1981 to present (Reynolds et al. 2002). For a given moist region on a given day (in the period of available SST data), we will approximate the average underlying SST by the spatial average of the weekly SST in the region. We will also use the vertical speed (from 1979 to 2002) to compute the total vertical flux of mass in the moist region at 500mb, which will be considered as a good proxy for the intensity of the large-scale circulation.

We focus on the long-term mean distribution: for each day, the number and size of the moist regions is computed and the results are averaged over the 24-year period. The contribution of each moist region is thus weighted by the length of its life cycle. The moist regions that have a long life cycle and can be considered in quasi-equilibrium during their mature stage are thus better taken into account than the transcient, rapidly disappearing ones. Besides, moist regions with more than 50% of their area over the oceans are considered oceanic and the others are considered continental.

The method used to discriminate moist regions from background points is similar to those used to initialize tracking analysis (Hodges 1994). For a given threshold of PW, UTH or OLR, a moist region is defined by the group of points moister than the threshold (i.e. with a larger PW, UTH or a lower OLR), that are connected. Due to the coarse definition of data, connexion is defined as four-way connection, which means that the gridpoints have

one of their sides in common (as opposed to the eight-way connection that allows the gridpoints to be connected by their corners). Furthermore, in order to avoid to join in the same moist region two big moist zones that are connected by a narrow band whereas they are unlikely to be thermodynamically or dynamically coupled, two regions will be considered distinct if the size of the contact between the two is inferior to half the characteristic size of both regions. The characteristic size of a region is defined as the radius R_c of the disc of same area.

More precisely, the segmentation method is the Connected Component Labeling (Rosenfeld and Kak 1976) that is based on the use of a quad-tree data structure and neighbor finding techniques (Samet 1989). The data is first extrapolated to a rectangle of 2^nx2^m gridpoints, taking into account the longitudinal periodicity of the data (the moist regions cut in two parts by the longitudinal border of the data are reproduced in the 2^nx2^m rectangle on one and only one side of the original rectangle). The data is then converted into a hierarchy of levels: the level i contains information about the 2^ix2^i gridpoint squares, and particularly if the squares are within, outside or containing a part of a moist region. The levels are linked by a quad tree that keeps the information on the parent (2^{i+1}x2^{i+1} square that contains the considered 2^ix2^i square) and offsprings (2^{i-1}x2^{i-1} squares that are included in the considered 2^ix2^i square). This quad tree structure is efficient to limit the computation of the connected moist squares, without limiting this computation to convex moist regions. A neighbor finding routine is then applied to the quad tree to classify the moist squares into connected families. Each family is then considered as a moist region.

2.1.2 Results

Figure 2.1.a shows the frequency of occurence of the moist regions for the threshhold of PW used in Chapter 1 (PW = 45 kg m^{-2}). The number of oceanic moist regions are almost an order of magnitud larger than the number of the continental ones, mainly because of the relative extent of continents and oceans in the tropics, but also because of the reduced local moisture source. Furthermore, the size of the tropical continents limits the size of moist regions over land, and these don't exceed 2500 km while the moist regions over sea can extend up to 5500 km. Both over the continents and the oceans, the number of moist regions decreases with their characteristic size R_c, but this decrease appears to be smaller for an interval of large values of R_c (R_c between 1500 and 2000 km over land; R_c between 2500 and 3500 km over the ocean). Consequently, the distribution of the total moist area exhibits two modes (Fig. 2.1.b), one for mesoscale and synoptic-scale regions that correspond to the size of convective clusters and superclusters, and one on scales that correspond to the large-scale of the ITCZ and the Hadley/Walker circulation. This bimodality results from the distribution of the oceanic moist regions: the size of the continental system doesn't exceed the size of superclusters, but we can see a strong signal of continental-scale moistening around 1500 km than is linked to monsoonal activity.

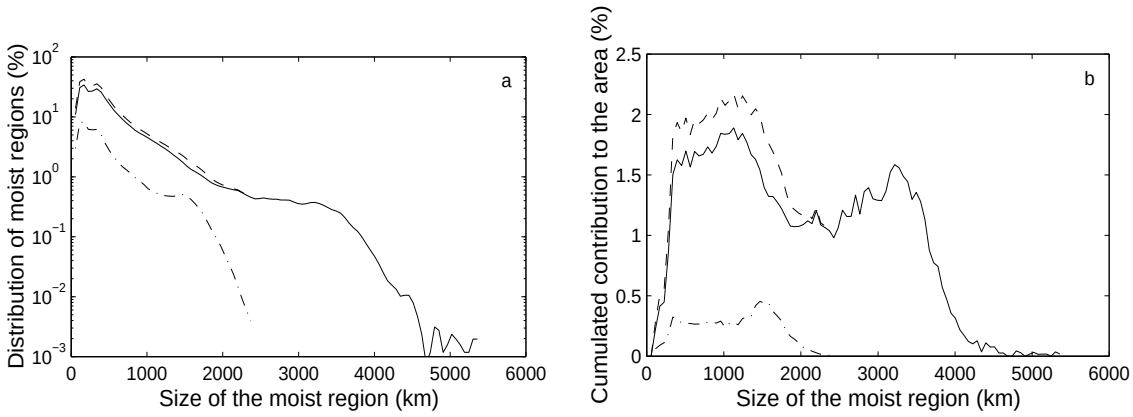

Figure 2.1: Distribution of (a) the number of moist regions and (b) the contribution to the total moist area as a function of the characteristic size of the moist region; solid: oceanic moist regions; dash-dotted: continental moist regions; and dashed: total.

Of course, this distribution is expected to be sensitive to the chosen threshold. Figure 2.2.a shows the cumulated contribution of moist regions to the total area covered by the moist zones as a function of their size and the chosen threshold. For a very high threshold, only small regions can be considered humid: they are regions of intense convection organized on the meso and synoptic scales. The second mode appears for threshold under 50 kg m^{-2} for characteristic sizes about 3000 km, and we can note that it is an independent mode: it cannot be considered as a consequence of a widening of some very moist regions by the decrease of the threshold. The large regions are actually an organization on the large-scale of various smaller scale moist regions connected by regions of moderate humidity, but still moister than subsident regions that typically exhibit precipitable waters around 30 kg m^{-2}. It is actually the signature of the ascending branches of the Hadley/Walker circulation in the daily data. A third mode appears for thresholds under 40 kg m^{-2} and a characteristic scale of about 6000 km. This mode is the signature of the whole tropics.

Figures 2.2.b and 2.2.c show the same study with the UTH and OLR datasets. Both datasets exhibit a meso/synoptic-scale mode and a large-scale one. Nevertheless, the latter is smaller than in the PW data. The UTH second mode is at smaller characteristic sizes (around 3000 km) than the PW large-scale mode. This tends to show that only a part of the large-scale humid regions - as determined by PW - is very moist in the upper troposphere and that very deep convection occurs only in part of these regions, while the convection in the rest is less intense. For UTH and OLR, the second mode doesn't extend beyond 5000km, and neither the OLR nor the UTH data exhibits the third tropical-scale mode, which is expected since the boundary layer humidity has no or only a weak signature in these datasets.

The OLR synoptic-scale mode exhibits also a fork around 1500km: some synoptic systems are widened by the lowering of the threshold, while some are not. This could be the signature of the cirrus clouds that are still connected to the convective anvil that

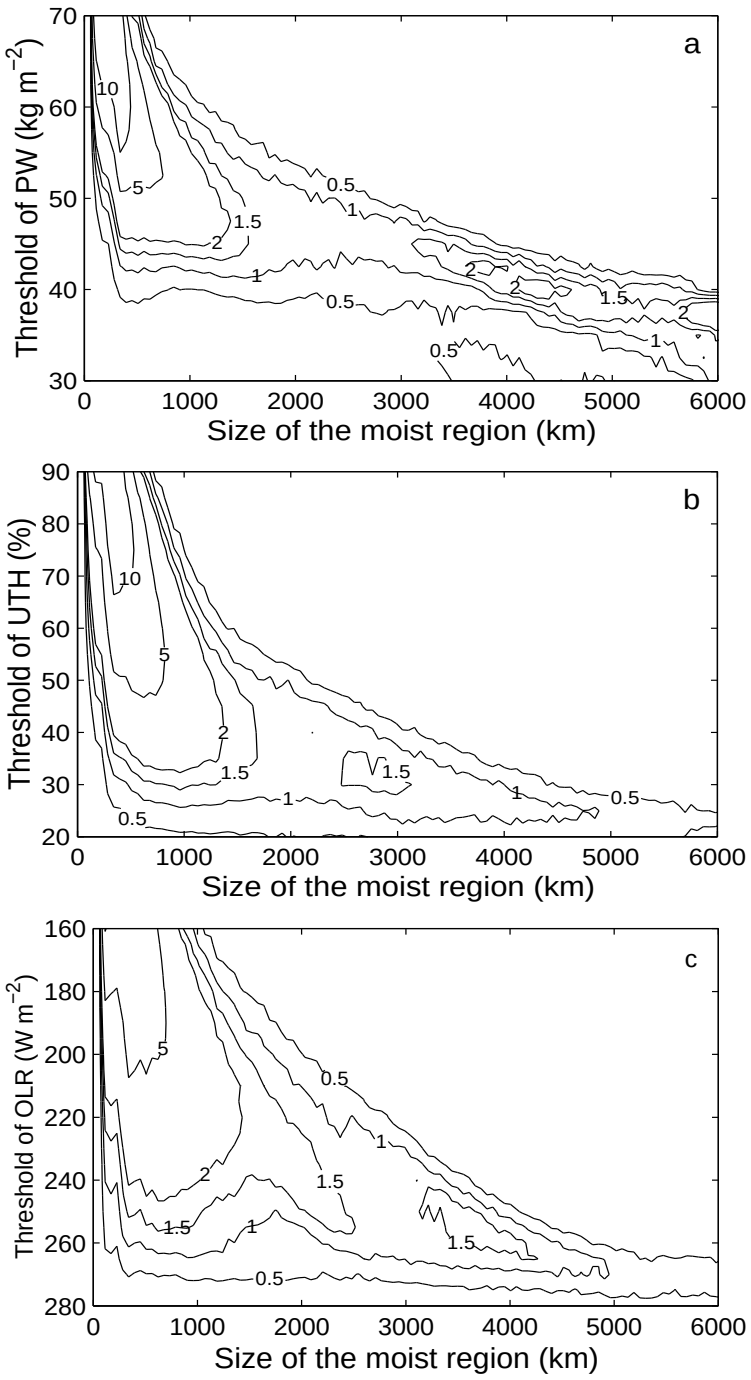

Figure 2.2: Distribution of the contribution to the total moist area as a function of the characteristic size of the moist region and the discriminating threshold, in per cents of the total moist area for the given threshold, for (a) PW, (b) UTH and (c) OLR.

generates them. These high clouds have a strong signature in the OLR because of their low temperature, while their water content is weak and their signal is thus weak in the PW data.

The existence of a scale separation raises doubts about the theories that consider convection to be identically organized on different space scales. These theories claimed that the convection is organized in auto-similar or fractal structures (Lovejoy 1982; Cahalan and Joseph 1988), and it does not seem consistent with the fact that the size distribution of the regions humidified by convection exhibits a scale separation.

2.1.3 Spectral properties: underlying SST and ascending mass-flux

Using the initial threshold of PW (45 kg m^{-2}) to discriminate the moist regions from the dry background, we study the dependence of some properties of the moist regions on their sizes: the underlying SST and the large-scale circulation.

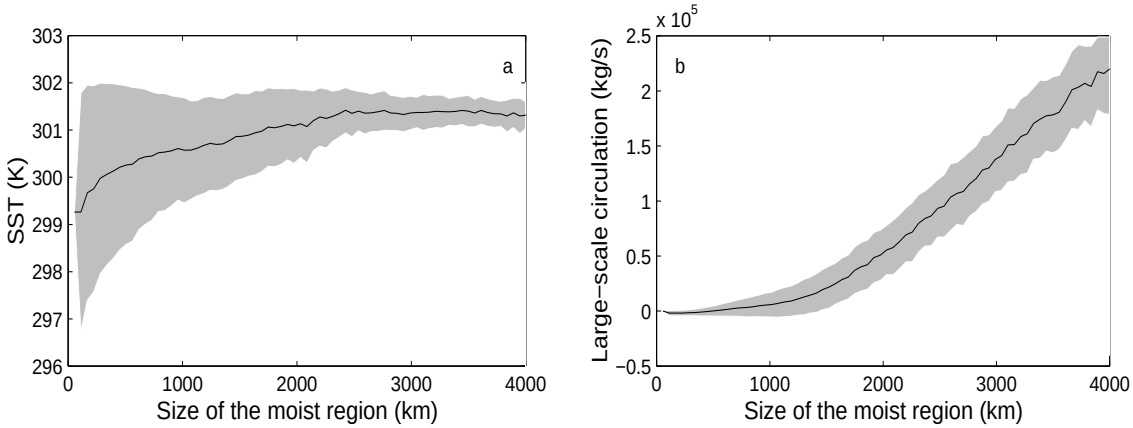

Figure 2.3: (a) Average SST and (b) large-scale ascending circulation in a moist region as a function of its characteristic size.

Figure 2.3 shows that the SST in moist regions is increasing with the size of the region, and the variability among regions of the same size is much more important for small regions: a high SST, above 301K, is necessary to the development of a large-scale moist region, while on smaller scale, other factors participate to the control of the convective moistening. Among those factors, the humidity convergence might be more dependent on the SST on the large scale than on the synoptic scale.

Unlike the SST, the large-scale circulation exhibits two distinct regimes: the ascending mass flux increases slowly with the extent of the region up to sizes about 1500 km, which is approximately the scale of separation between the two modes of the distribution (see Fig. 2.1). For larger typical radii, the large scale circulation increases faster with R_c. This is a bit counterintuitive since the synoptic-scale regions are expected to be more intensely convecting than the larger ones. But this actually confirms that the large-scale moist regions are intrinsequely linked to the global circulation, while the synoptic-scale systems are more likely to develop in weakly ascending zones.

2.2 A prospective toy model

As we noted above, to some extent, the moist regions described above can be modeled as the convective column of the model used in Chapter 1. Of course, the observed moist regions, and particularly the synoptic-scale ones, are unlikely to be in steady state. However, we can consider that the convection is in quasi-equilibrium with the large-scale circulation, and that our simple thermodynamic model can approximate the thermodynamics of a moist region and the surrounding connected subsidence. A simple parameterization of the dynamics in the two-column model used in Chapter 1 will allow to study which scales can be represented by this model and how sensitive to their horizontal extent the moist-dry systems are.

2.2.1 A steady-state theory for the low-level winds

Two simple theories have been developed to describe the steady state large-scale circulation in the Tropics. They both describe this circulation as a perturbation from a state of rest and are thus linear, although the dynamics of the tropical free troposphere is essentially non-linear (Yano et al. 2002): while the first-order low-level winds are determined by a balance of the pressure forcing, the Coriolis acceleration and the friction, the firts-order free-tropospheric circulation is controlled by the balance between the pressure forcing, the Coriolis acceleration and the non-linear advection.

The first simple steady-state theory of the tropical was developped by Gill (1980). This linear theory decribes the internal modes of a two-layer atmosphere with a lid at the tropopause, forced by a prescribed diabatic heating exclusively attributed to convection. This forcing was later parameterized in terms of the SST through the surface flux and the low-level moisture convergence (Zebiak 1982).

The second theory claims that the low-level winds are forced by the SST gradients (Lindzen and Nigam 1987). Temperatures in the whole boundary layer are supposed to be tied to the SST by turbulent vertical mixing. The horizontal temperature gradients imply pressure gradients that force the low-level winds. In this model, the role of the convection is limited to quickly venting the low-level convergence in convective regions.

The two models have been proven to be mathematically identical (Neelin 1989): a recombination of the parameters yields the same equations. The Gill model results are actually better in the boundary layer than in the rest of the free troposphere; this is not surprising considering that the free-tropospheric circulation is non-linear. Furthermore, these models are mathematically equivalent to a reduced-gravity (RG) model developped more recently (Battisti et al. 1999). The latter will be described hereafter.

The RG model features a well mixed boundary layer of constant virtual potential temperature tied to the SST and topped by an inversion of constant amplitude ΔT_{inv}. The depth of the boundary layer is variable. The low-level winds are considered as perturbations from a reference state of rest with a given surface temperature and depth of the boundary layer. They are forced by the horizontal variations of the pressure resulting from

the gradients of virtual potential temperature.

In this model, the linear momentum equation can be written:

$$\epsilon_d \mathbf{u} + f\mathbf{k} \times \mathbf{u} = -\nabla\Phi, \tag{2.1}$$

where $\mathbf{u}$ is the mass-weighted average boundary-layer horizontal velocity, f the local Coriolis parameter and ϵ_d a drag coefficient accounting for the friction on the surface. In the Tropics, the mechanical damping is observed to happen on a timescale of one to two days: ϵ_d^{-1}= 1-2 days. In fact, the friction term is non linear, and the drag coefficient is often considered proportional to the surface wind speed $|\mathbf{u}|$; we will further comment on this in Section 3.

Φ is the perturbation of the vertically-averaged pressure, which will further be called potential, whose perturbation can be expressed by linearizing the integral of the hydrostatic equation over the boundary layer:

$$\Phi = g'H' - \Gamma_{bl} T_s'. \tag{2.2}$$

Here, T_s' is the perturbation of the surface temperature from the reference temperature T_{s0}, H' is the perturbation of the depth of the boundary layer from the reference depth H_0, Γ_{bl} is a thermodynamic integral coefficient accounting for the vertical variation of the temperature in the well-mixed boundary layer and $g' = g\Delta T_{inv}/T_{s0}$ is the reduced gravity. The first term on the right hand side (RHS) of Equation 2.2 is linked to the variation of the depth of the inversion layer and it is analogous to the forcing in the classical shallow water equations. It was called "back-pressure" term in Lindzen and Nigam (1987). The second term is accounting for the thermally induced differences of pressure within the boundary layer.

Furthermore, the height of the boundary layer is assumed to relax towards the reference state in the absence of large-scale forcing, with a timescale τ that depends on the state (convecting or not convecting) of the atmosphere. The mass balance of the boundary layer can thus be written:

$$0 = -H_0 \, \nabla \cdot \mathbf{u} - \frac{H'}{\tau}. \tag{2.3}$$

In the absence of deep convection, the relaxation time for the boundary layer perturbations is observed to be close to the drag time. The mechanical and thermal dissipation time are thus taken to be the same: $\tau = \epsilon_d^{-1}$. In convecting regions, the venting of the boundary layer is faster, happening on the timescale of the deep convection $\tau = \epsilon_m^{-1}$= 3-12 hours. Here, the reduced-gravity model departs from the formulation of Lindzen and Nigam (1987): in their work, τ is taken to be of the order of 30 minutes everywhere. This timescale seems physically small, even in convective regions.

The expression of the potentiel Φ can be simplified and unified:

$$\Phi = -\Gamma_{bl} \, T_s' - \frac{c^2}{\epsilon_d}(1 - \beta') \, \nabla \cdot \mathbf{u}, \tag{2.4}$$

where $c = \sqrt{g'H_0}$ is the atmospheric wave speed and β' accounts for the effect of convection, if needed:

$$\begin{aligned} \beta' &= 1 - \epsilon_d \epsilon_m^{-1} && \text{if the atmosphere is convecting,} \\ &= 0 && \text{otherwise.} \end{aligned}$$

Equations (2.1) and (2.4) contain the complete theory, and allow one to compute the surface wind from the SST field. Let's note that these two equations are independent, and that Equation (2.1) is just the linear form of the momentum equation and it is thus quite robust, while Equation (2.4) relies on various approximations and parameterizations.

From Equation 2.1, the surface wind can be written in terms of a geostrophic component and a friction component:

$$\mathbf{u} = \frac{f}{\epsilon_d^2 + f^2}\mathbf{k} \times \nabla\Phi - \frac{\epsilon_d}{\epsilon_d^2 + f^2}\nabla\Phi. \tag{2.5}$$

The firts term of the RHS is the geostrophic term, while the second is the friction term. Considered on a f-plane, this equation suggests that the divergent (friction) component of the wind is proportionnal to the gradient of potential, which is in turn related to the gradient of temperature and the gradient of convergence. The divergence can be written:

$$\nabla \cdot \mathbf{u} = -\frac{\epsilon_d}{\epsilon_d^2 + f^2}\nabla^2\Phi. \tag{2.6}$$

Close to the Equator, a β-plane is more relevant, and the variation of the Coriolis parameter with latitude introduces a dependence of the divergence on the potential gradient:

$$\nabla \cdot \mathbf{u} = -\frac{\epsilon_d}{\epsilon_d^2 + f^2}\nabla^2\Phi + \frac{\beta_c\,\mathbf{j}}{\left(\epsilon_d^2 + f^2\right)^2} \cdot \left[2\epsilon_d f \nabla\Phi + \left(\epsilon_d^2 - f^2\right)\mathbf{k} \times \nabla\Phi\right], \tag{2.7}$$

where β_c is the rate of change of the Coriolis parameter with latitude.

Following Lindzen and Nigam (1987), we will call the first term on the RHS of Equation 2.7 "Laplacian" divergence, and the second term "Beta" divergence. The first term is proportional to the Laplacian of Φ, while the Beta divergence is proportional to the gradient of Φ. Therefore, the competition between these two terms is a potential mechanism for the selection of horizontal scales.

2.2.2 Parameterization of the surface dynamics

We adapt the theory described in the previous section to our two-column framework in order to represent the surface flow. Of course, by applying a two-dimensional model to a one dimensional two-gridpoint system, we loose part of the complexity in the dynamics. At the level of simplicity of our model, the parameterization of the surface flow cannot be much more refined and the model has to be considered explorative.

In the subsiding colum of the model, the average divergence in the boundary layer can be written:

$$\overline{\nabla \cdot \mathbf{u}} = \frac{\omega_{\rm inv}}{p_{\rm s} - p_{\rm inv}}, \tag{2.8}$$

where $\omega_{\rm inv}$ is the subsidence rate at the inversion and $p_{\rm s}$ ($p_{\rm inv}$) is the surface (inversion) pressure, as defined in Chapter 1. The overline indicates the horizontal averaging over the column.

In order to include a parameterization of the surface convergence, we use the reduced-gravity model described in the previous Section. We first rewrite Equation 2.7 in the form:

$$\nabla \cdot \mathbf{u} = -\frac{\epsilon_d}{\epsilon_d^2 + f^2}\left(\nabla^2\Phi - \frac{\beta_c \xi}{\epsilon_d}|\nabla\Phi|\right), \tag{2.9}$$

with

$$\xi = \frac{2\epsilon_d f}{\epsilon_d^2 + f^2}\ \mathbf{j}\cdot\frac{\nabla\Phi}{|\nabla\Phi|} + \frac{\epsilon_d^2 - f^2}{\epsilon_d^2 + f^2}\ \mathbf{j}\cdot\frac{\mathbf{k}\times\nabla\Phi}{|\nabla\Phi|}. \tag{2.10}$$

ξ is a geometrical and geographical parameter: it depends on the latitude and the direction of the gradient of potential ($|\xi| \leq 1$). Considering that the Laplacian is of the order of the variation of the potential over the square of the horizontal scale, and that the gradient is of the order of the variation over the horizontal scale, a competition between scales is possible.

As an example, we plot in Figure 2.4 the average reanalyzed ξ for the moist regions defined by a threshold of humidity of PW = 45 kg m^{-2}, using the weekly NOAA Optimum Interpolation SST and the NCEP/NCAR daily reanalysis 2 for the period from November 1981 to December 2002. For each day and each moist region, Φ is computed with the SST of the corresponding week. Details of this calculation will be explained in the next section. The average observed ξ is around 0.2, except for regions of characteristic size around 1500 km, where ξ tends to be closer to zero. This critical characteristic scale corresponds to the maximum extent of synoptic moist regions, and also to the scale of dynamical regime change (see Fig. 2.3). We can conclude that moist regions of characteristic radius around 1500 km tend to be associated with a weak Beta convergence.

To include a simple parameterization of the divergence in our simple model, we average Equation 2.9 over a subsiding region of a two-column system. To keep our parameterization as simple as possible, we average the surface divergence applying three further assumptions:
(i) the first-order terms in β_c that are due to the variations of $\epsilon_d^2 + f^2$ and independent of the Φ gradient are negligible in front of the terms proportional to this gradient,
(ii) the second-order terms in β_c are negligible compared to the zero- and first-order terms, and
(iii) the gradient is proportional to the potential difference $\Delta\Phi$ between the moist and dry regions divided the horizontal extent R of the total system and the Laplacian is proportional to the gradient divided by R:

$$|\nabla\Phi| \propto \frac{\Delta\Phi}{R} \qquad \nabla^2\Phi \propto \frac{\Delta\Phi}{R^2} \tag{2.11}$$

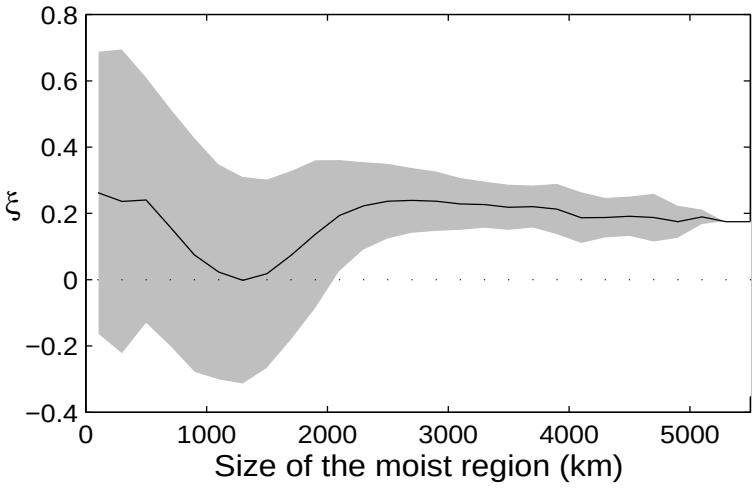

Figure 2.4: Average parameter ξ computed from the reanalysis and the Reynolds SST, as a function of the characteristic size of the moist region; standard deviation is indicated by the shaded region.

The average divergence can thus be expressed:

$$\frac{\omega_{\text{inv}}}{p_{\text{s}} - p_{\text{inv}}} = \overline{\nabla \cdot \mathbf{u}} = -\mu\left(\frac{\Delta\Phi}{R^2} - k\frac{\Delta\Phi}{R}\right), \tag{2.12}$$

with

$$\mu \propto \frac{\epsilon_d}{\epsilon_d^2 + f^2} \qquad k \propto \frac{\beta_c \xi}{\epsilon_d}; \tag{2.13}$$

μ is of the order of a week (μ=6.5 days at the Equator for a sinusoidal temperature perturbation and ϵ_d^{-1}=1 day) and $|k|$ of the order of 10^{-7}-10^{-6}. While μ is a mixed friction-Coriolis coefficient, k accounts for the geometrical asymmetry of the region, and the asymmetry between the region and the potential field. Note that Equation (2.12) is independent of the parameterization of $\Delta\Phi$.

$\Delta\Phi$ is the difference of pressure between the column averaged over the boundary layer. Following the reduced-gravity theory, it can be parameterized as follows:

$$\Delta\Phi = -\Gamma_{bl}(T_{S1} - T_{S2}) + c^2\left(\frac{1}{\epsilon_m}\frac{1 - A_c}{A_c} + \frac{1}{\epsilon_d}\right)\frac{\omega_{\text{inv}}}{p_{\text{s}} - p_{\text{inv}}}, \tag{2.14}$$

where the divergence in the convertive column has been replaced $-\frac{1-A_c}{A_c}\frac{\omega_{\text{inv}}}{p_{\text{s}}-p_{\text{inv}}}$ to comply to the mass balance.

For a given thermodynamical state of the two-column model, Equation (2.12) is equivalent to a binomial equation in R. We can thus expect the model including the parameterization of the surface dynamics to have mutiple equilibria and to select specific scales of equilibrium. Furthermore, as the large-scale circulation is expected to be non-zero, a scale separation can be expected for $R = 1/k$.

2.2.3 Model results

The additional Equation (2.12) and the parameterization of Φ (2.14) are included in the model of Chapter 1 and allow one to compute interactively the relative area A_c of the convective column. The sensitivity of the model to its horizontal extent is studied using PitCon, with the parameters indicated in Table 2.1. Figure 2.5.a shows the model SST as a function of the horizontal extent R of the whole two-column system (solid line): a scale separation can be seen for R between 2500 and 4000 km. Note that this scale separation is not the same as the concept usually used in GCM modelling to discriminate between subgrid and large-scale processes: the synoptic scale is already larger than the typical GCM subgrid scale. For smaller R, a warm equilibrium can be found between 299 and 306K, corresponding to a relative area A_c of about 50%. For larger R, a cooler equilibrium can be found, with A_c about 20%. Because of the difference of range of A_c, the scale separation doesn't appear if the model SST is plotted as a function of the extent of the convective column $R_c = \sqrt{A_c}R$ (Fig. 2.5.b): the warm synoptic-scale and cool large-scale modes overlap. Nevertheless, they present the characteristic sizes of the two modes seen in the reanalyses (see Figure 2.2).

Parameter	Value
ϵ_d^{-1}	1 day
ϵ_m^{-1}	6 hours
Γ_{bl}	50 $m^2 s^{-2} K^{-1}$
c	18 ms^{-1}
μ	8 days
k	3.10^{-7}

Table 2.1: Values of the parameters used in the computation

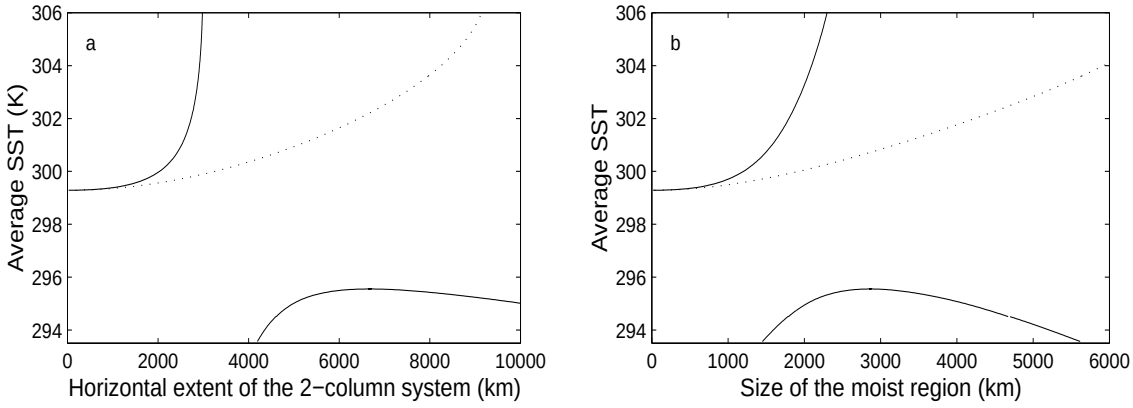

Figure 2.5: Model average SST as a function of the horizontal scale of (a) the two-colum system and (b) the moist column; solid: case (μ, k)=(8 days, 3.10^{-7} m^{-1}); dotted: same with k=0.

The SST results are not in good agreement with the reanalysis that tended to show

higher temperature for larger moist regions (see Figure 2.3). Besides, very high temperatures (above 304K) are quite unrealistic. Nevertheless, the distribution of observed SST underneath a small region is very wide and encompasses an important part of the results of our model. Furthermore, the two modes exhibit distinct humidity and dynamical regime (Figure 2.6): the model synoptic-scale regions are moister than the large-scale ones, and the overturning mass-flux increases faster with R_c for the large-scale regions than for the smaller ones. This resembles the observed regimes (see Figures 2.2 and 2.3), thought the model relative humidity tend to be large compared to the observed UTH values. The existence of two distinct modes, the existence of a scale separation for the size of the two-column system, and the agreement of the humidity and dynamical regimes with the reanalyses suggest that such a toy model might be able to explain the two observed modes in the size distribution of the moist regions.

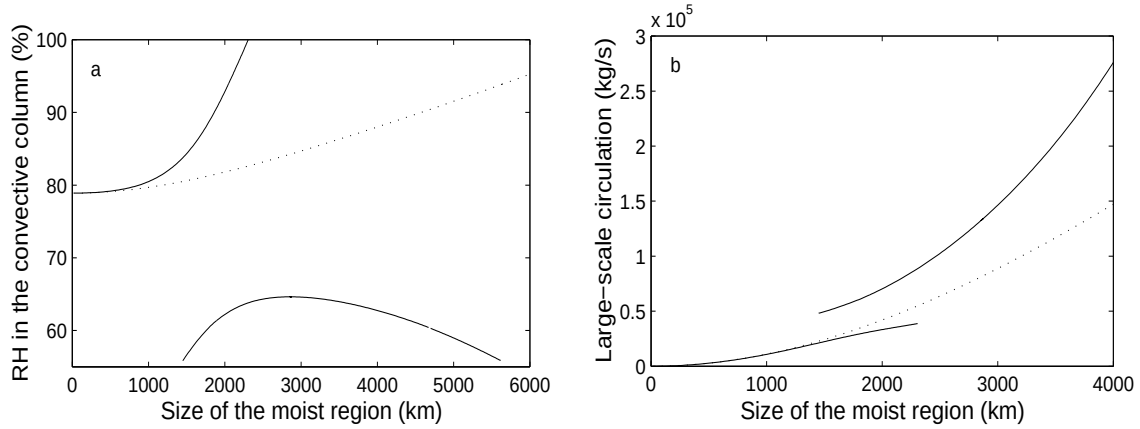

Figure 2.6: Model (a) relative humidity in the convective column and (b) overturning mass-flux m as a function of the horizontal scale of the moist column; solid: case (μ, k)=(8 days, 3.10^{-7} m^{-1}); dotted: same with k=0.

In the absence of Beta convergence (k=0), the model exhibits only the synoptic-scale mode, that extends to larger scales (dotted line in Fig. 2.5 and 2.6). This equilibrium has realistic temperatures (up to 304K) within the realistic range of R_c, but the model humidity is higher than what can be expected for a large-scale moist region, and the rate of growth of the overturning mass flux with R_c does not show any critical scale.

To investigate the conditions for the existence of the two modes, we study the sensitivity of the extreme sizes of the modes to the parameter of the dynamics μ and k. The maximum R_{c_1} for the synoptic-scale mode is associated with the saturation (RH=100%) and a temperature of 306K. The minimum R_{c_2} for the large-scale mode corresponds to a temperature of 293.5K and a humidity of 55%. Figure 2.7 shows the sensitivity of these critical radii for k>0. R_{c_1} is not very sensitive to μ except for small values of μ. It is sensitive to the asymmetry of the system: the more symmetric the system is (the smaller k is), the more the first mode extends towards larger R_c. This is also true for k<0. The

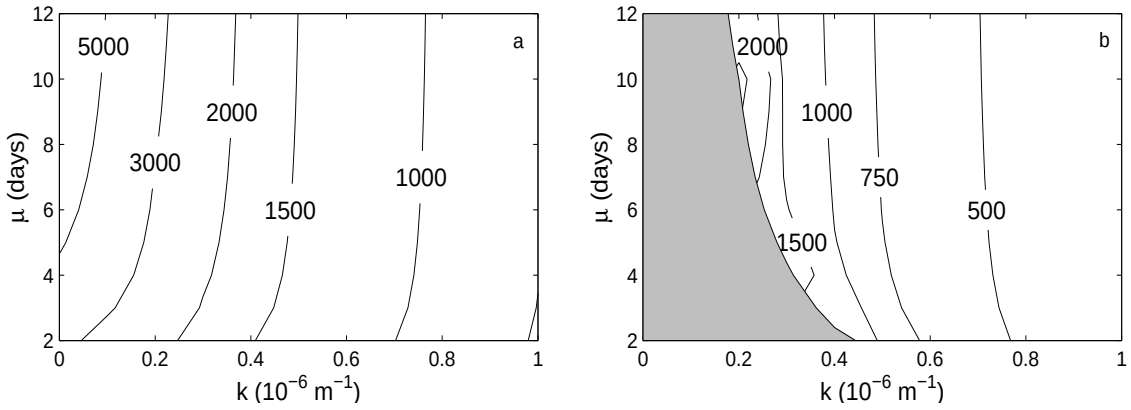

Figure 2.7: Sensitivity to the parameters (μ, k) of (a) the maximum R_{c_1} of the synoptic-scale mode and (b) the minimum R_{c_2} of the large-scale mode; the domain where the large-scale mode does not exist is shaded.

large mode doesn't exist for small k or $k<0$. It appears for $k = k_c$ between 0.2 and 0.4. While R_{c_2} is not very sensitive to μ, the critical k_c decreases significantly with μ. For very large k, the large-scale mode appears at characteristic sizes as small as a few hundreds of kilometers.

Overall, the sensitivity study shows that the two modes coexist in a large part of the parameter domain, and that both modes are restricted to a given range of sizes within this domain. The fact that the observed ξ (Fig. 2.4) is close to zero for the moist regions whose size is about the scale of separation between the two observed modes tend to prove that they correspond to the first mode of the model, with small k ($k \propto \xi$).

The observed regions are likely to be associated with large ranges of the parameters (μ, k). The first model mode is thus expected to represent not only the synoptic-scale systems, but also some of the larger-scale systems. For reasonable values of the parameter k, the large-scale mode can only represent regions of horizontal scale larger than a few hundreds of kilometers, and this can be the cause of the scale separation in the observed distribution of the moist regions: the moist regions with a horizontal scale around 1500km can only be represented by the model for a reduced part of the parameters'domain.

2.3 Evaluation of the reduced-gravity model with reanalysis

As the existence of two modes in the simple model relies on the parameterization of the surface flow, it is important to question the pertinence and limits of this parameterization. As a first step, it is interesting to confront the results of the RG theory, on which the parameterization is based, to observations. This work is also interesting by itself on a theoretical level, to evaluate our understanding of the near-surface dynamics in the tropics.

Lindzen and Nigam (1987) tested their theory considering the perturbations from a state of rest with no wind, but with an zonally averaged meridional gradient of SST, and

found a reasonable agreement between the theory and the data for monthly means of winter and summer 1979 in the Pacific Ocean. Battisti et al. (1999) claims to obtain similar results (without showing them) with the reduced-gravity model in which the state of rest includes mean meridional and zonal gradients of SST. The assumption that the mean gradients do not cause any circulation is not totally consistent: the average gradients are associated with a circulation. Lindzen and Nigam (1987) claim that the neglection of the axisymetric circulation caused by the mean meridional gradients introduces a bias of only 1%. We will show the model and observed monthly means as anomalies from the annual means for January and July.

2.3.1 Data and methodology

For this purpose, we use the monthly NCEP/NCAR reanalysis 2 surface winds and the NOAA Optimum Interpolation SST. We will use monthly data from 1982 to 2002 (21 years) and interpolate the SST data on the 2.5°x2.5° reanalysis grid.

The potential Φ is computed from Equation (2.4) using the SST data and the observed divergence computed from the reanalyzed surface winds. Note that part of the information on the wind field is already contained in the reanalyzed divergence. Furthermore, we will consider that the regions of surface convergence are convective, and that the surface-divergent regions are deprived of convection. A quick study has shown that the model is not very sensitive to this approximation. We further compute the surface winds using Equation (2.1) and compare them to the reanalyzed values. The value of the parameters used in these computations are indicated in the first four lines of Table 2.1. The results are shown as perturbations from the annual mean for the months of January and July.

2.3.2 Surface winds

Figures 2.8 and 2.9 show the results for the long-term meridional winds v for January (Fig. 2.8) and July (Fig. 2.9). The large-scale patterns of the modeled and analyzed winds are in overall agreement, with equatorward motion, particularly along the West coasts of the continent in the summer hemisphere. Nevertheless, the details of the patterns and the intensity of the wind are somewhat different: the intensity of the modeled wind is small compared to the reanalysis in the subtropics, while it exhibits strong winds along the Equator. This is a strong response of the model to potential gradients: close to the Equator, the Coriolis parameter is very small, and the v is well described by the second term of Equation (2.5): $v \approx -\partial_y \Phi / \epsilon_d$. ϵ_d^{-1} is fairly big ($O(10^5)$), and the model wind is quite sensitive to small potential gradients at the Equator. As expected, this bias is smaller during El Niño/Southern Oscillation events, or during intermediary seasons (not shown). Particularly, in the Central and East Pacific, the cold tongue of water that extends westward from the coast of America produces a strong signal.

In January, compared to the reanalysis, the acceleration of the winter trade winds in the Atlantic is confined to a narrow band close to the Equator in the model. Furthermore,

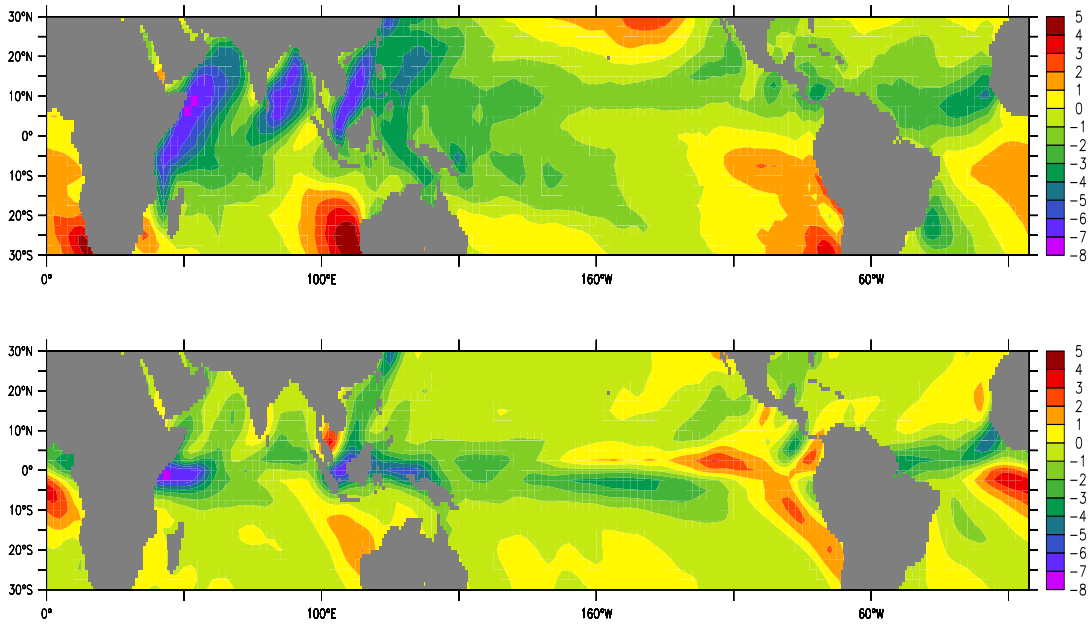

Figure 2.8: Long-term mean reanalyzed (upper panel) and modeled (lower panel) meridional surface wind anomalies for January (in ms^{-1}).

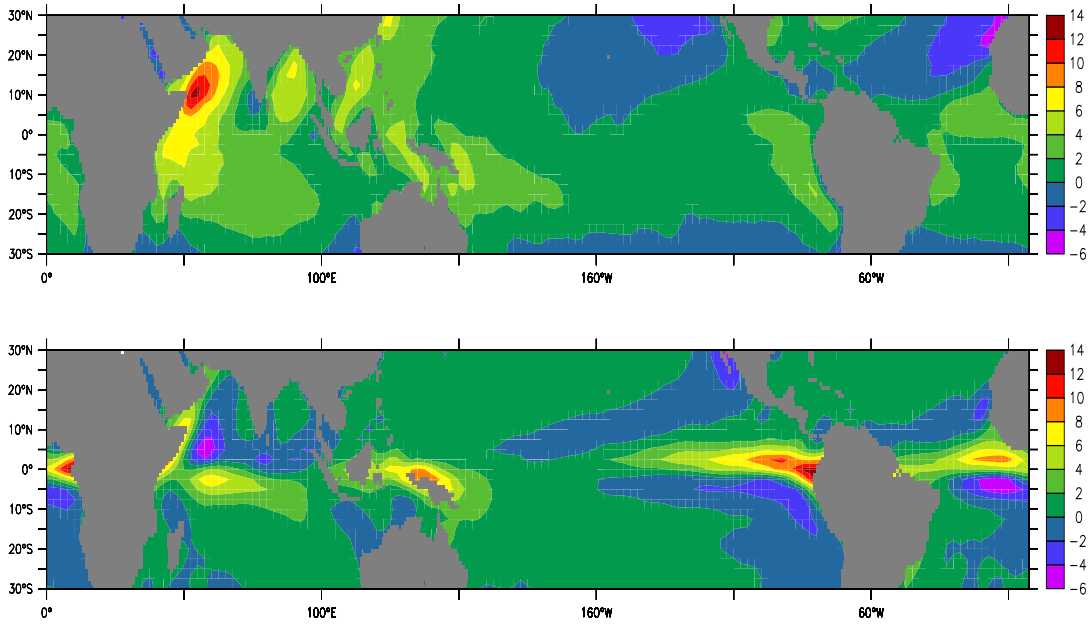

Figure 2.9: Long-term mean reanalyzed (upper panel) and modeled (lower panel) meridional surface wind anomalies for July (in ms^{-1}).

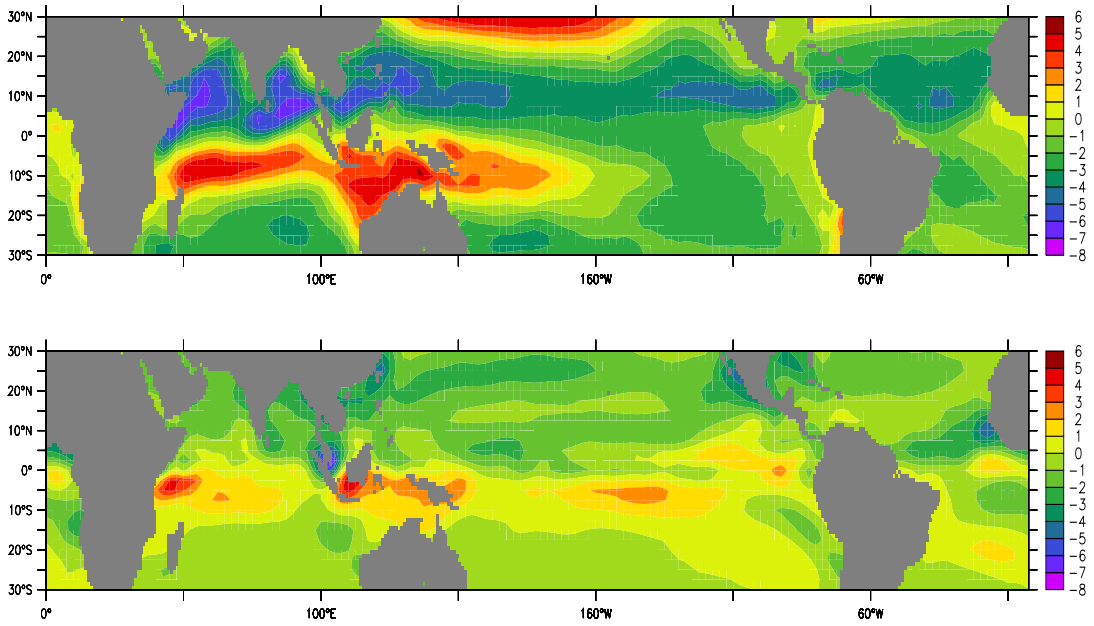

Figure 2.10: Long-term mean reanalyzed (upper panel) and modeled (lower panel) zonal surface windanomalies for January (in ms^{-1}).

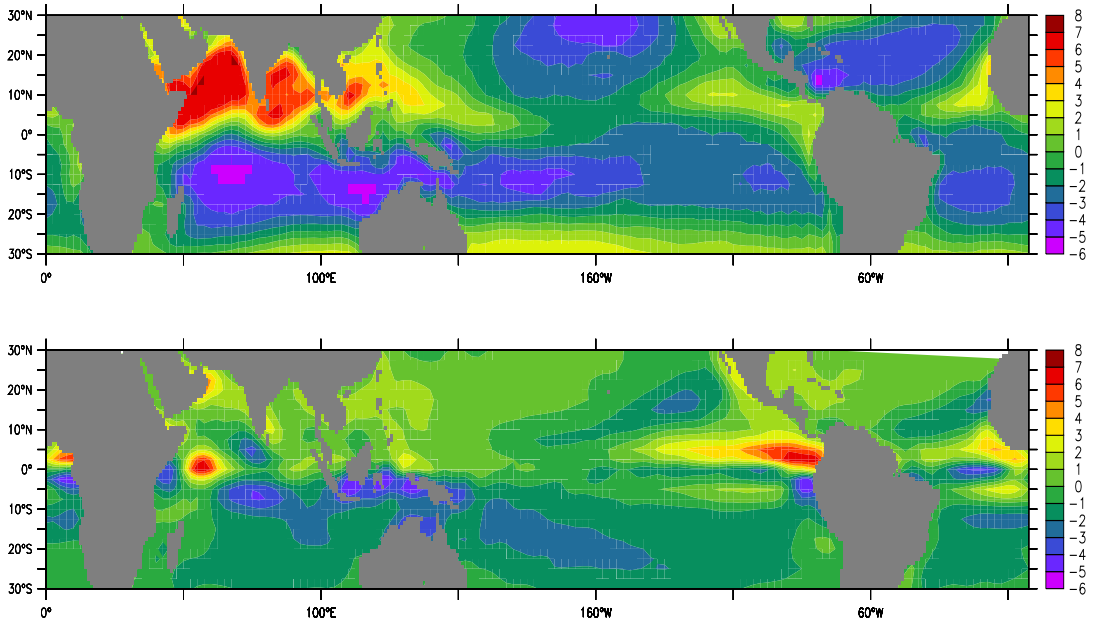

Figure 2.11: Long-term mean reanalyzed (upper panel) and modeled (lower panel) zonal surface wind anomalies for July (in ms^{-1}).

the model produces a weak winter monsoon in the Indian Ocean. In July, the model fails to reproduce the summer monsoon as well: the cross-equatorial flow is limited to the coast of Africa and to a narrow equatorial zone. The perturbation of the model trade winds in the Atlantic and Pacific Oceans show patterns that are closer to the Equator than those of the reanalyzed field. The ability of the model to reproduce the reanalysis seems strongly dependent on the latitude.

Figures 2.10 and 2.11 show the results for the long-term zonal winds u for January (Fig. 2.10) and July (Fig. 2.11). The model field exhibit smaller deviation from the annual mean than the reanalysis. Some discrepancies can still be seen around the Equator where the zonal wind is highly sensitive to zonal gradients of the potential: $u \approx -\partial_x \Phi / \epsilon_d$.

In January, South of the Equator, the eastward perturbation extends much further into the Pacific and poleward in the model than it does in the reanalysis, but its amplitude is weaker. As well, the negative anomaly North of the Equator is more diffuse in the model field than in the reanalysis. In the Atlantic oceans, the model patterns are smaller and closer to the Equator than in the reanalysis. In July, the same bias can be seen: the anomalies are smaller. Their patterns extend on larger regions in the winter hemisphere, and on smaller and lower-latitude regions in the Northern hemisphere. The summer monsoon flux is not well represented in the model u field either.

2.3.3 Surface divergence

As the divergence depends a lot on the details of the wind fields, we expect the quality of the model surface divergence to be worse than the wind fields described in the previous paragraph. Figures 2.12 and 2.13 show the long-term mean of the reanalyzed and modeled divergence for January and July. Except around the Equator, the two fields show some resemblence. Around the Equator, the model produces alternatively zones of intense convergence and zones of intense divergence, as a result of the discrepancies of the wind fields. Except in the Pacific, strong convergence is produced on the Equator and is accompanied by compensating strong divergence next to the Equator in the winter hemisphere. In the East Pacific, the response of the model to the cold tongue of SST is a very intense divergence zone. This divergence is compensated by two convergence zones on each side. This pattern is actually present in the observations, but its reanalyzed magnitude is much smaller than in the model.

In January, the model ITCZ in the Atlantic Ocean is considerably narrower than in the reanalysis. In July, the bias of the model in the Atlantic is quite similar to the situation in the Pacific: the model reproduces the pattens of the reanalyzed divergence, but the amplitude of the anomalies are overestimated.

Figures 2.12 and 2.13 also show the Laplacian and Beta components of the divergence. The two components are of the same order of magnitude. The Laplacian component appears to be dominant almost everywhere, except in the Indian Ocean and the warm pool

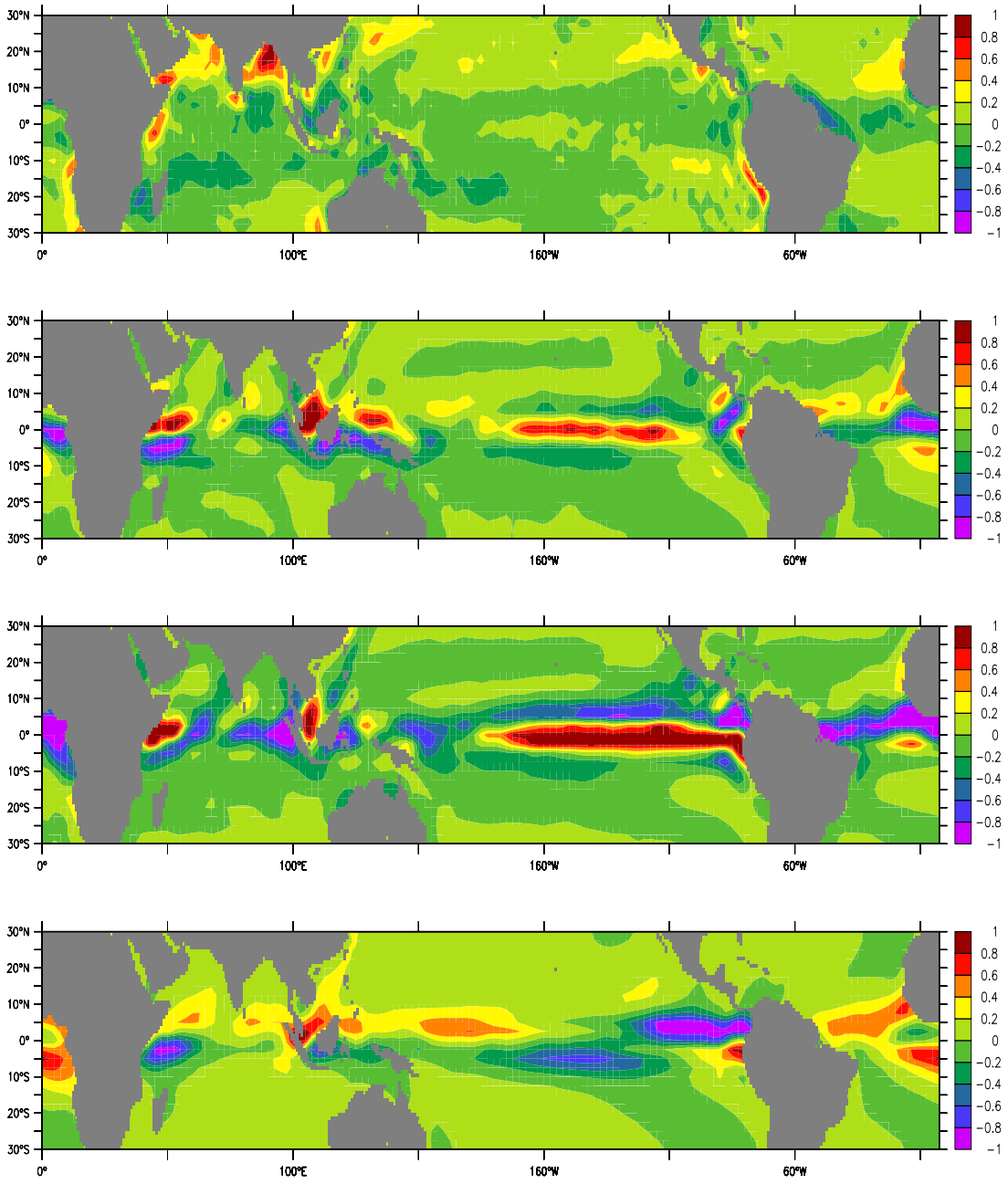

Figure 2.12: Long-term mean reanalyzed (upper panel), modeled (second panel) surface divergence anomalies; Laplacian (third panel) and beta (lower) components of the modeled divergence anomalies for January (in 10^{-5} s^{-1}).

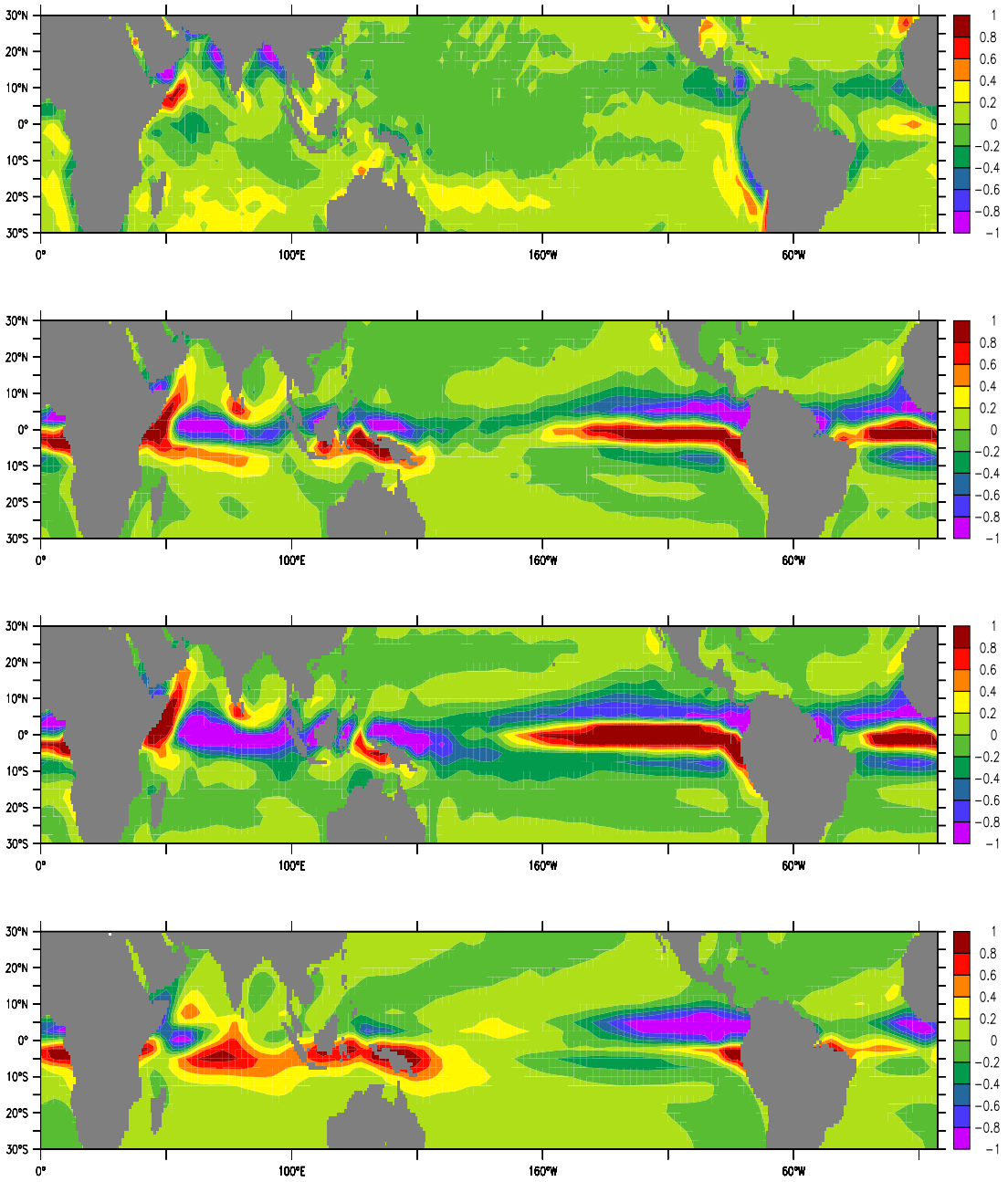

Figure 2.13: Long-term mean reanalyzed (upper panel), modeled (second panel) surface divergence anomalies; Laplacian (third panel) and beta (lower) components of the modeled divergence anomalies for July (in 10^{-5} s^{-1}).

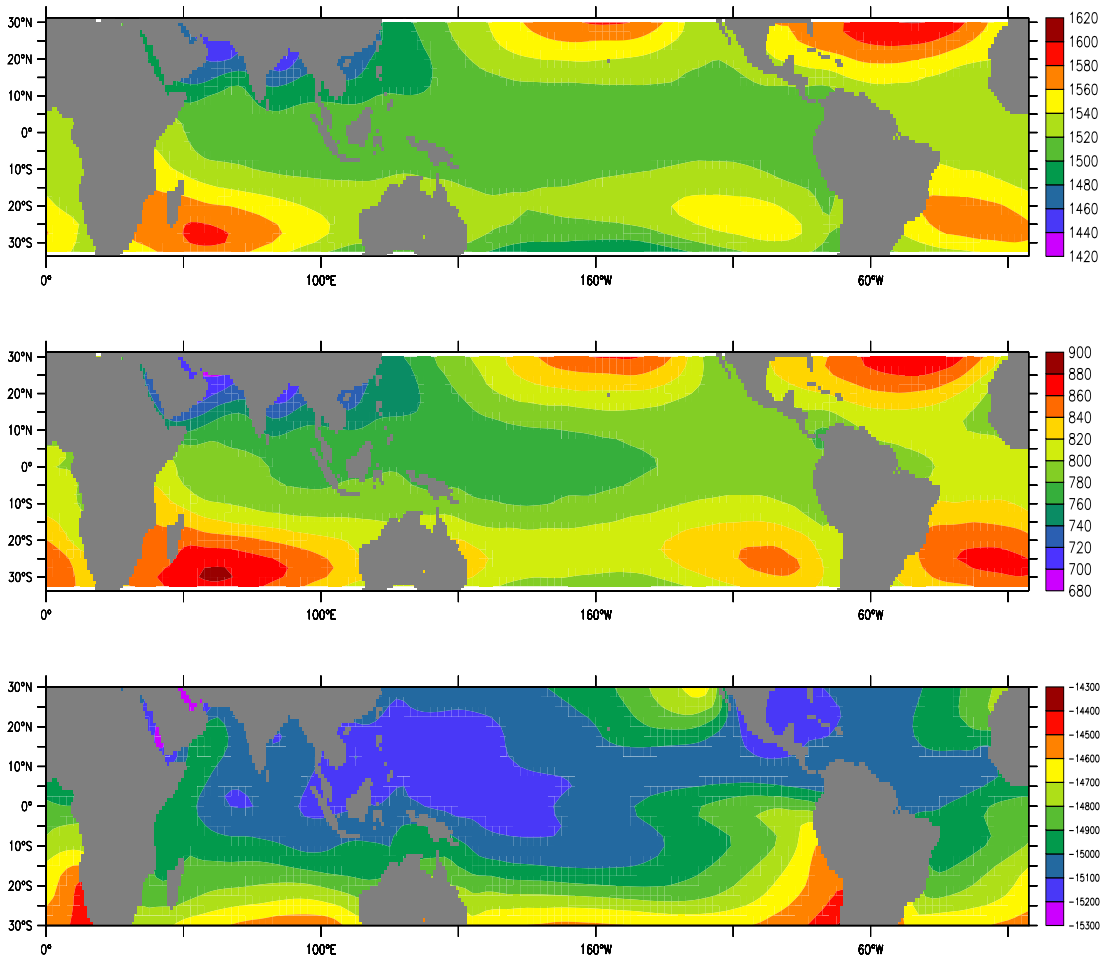

Figure 2.14: Long-term mean reanalyzed 850 mb (upper panel) and 925 mb (second panel) geopotential, and the modeled Φ (lower panel); geopotential in m, Φ in kg s^{-2}

where the Beta term is responsible for the positive anomalies in the winter hemisphere. More generally, the Beta term acts to modify and limit the zones of convergence and divergence due to the Laplacian component. Thus, the competition between the two terms might allow a scale selection for convergence zones.

2.3.4 The theory in question

The results of the model for the January and June anomalies show some systematic bias. Results for the mean annual flow (not shown) are actually worse: they exhibit bias of the same kind around the Equator and around the Indian subcontinent, but the patterns of the bias extend much further into the subtropics. This is in disagreement with the statement of Lindzen and Nigam (1987) who claimed that the mean tropical circulation introduces only a 1% additional bias. Furthermore, the model of Lindzen and Nigam (1987) shows the same bias as the RG model, for the mean and the monthly anomalies (not shown).

Overall, the flaws of the RG and Lindzen-and-Nigam models seem to bring a poor understanding of the tropical surface winds. The main planetary patterns can be reproduced, but the two theories seem unable to simulate accurately regional circulations such as the monsoons and exhibit strong bias on the Equator. Whether the theory can be improved to encompass more observed circulations is beyond the reach of this thesis. Nevertheless, some perspectives seem promising.

The main source of bias is the parameterization of the pressure forcing by the potential Φ. As an illustration, the Figure 2.14 shows the reanalyzed geopotential at 850 and 925 mb, and the model geopotential for long-term mean July. The geopotential at both altitudes show similar patterns and the gradients of geopotential decrease with altitude, thus supporting the idea of an influence of the boundary-layer temperatures on the vertical evolution of the horizontal forcing. But the model potential does not show the same patterns; for example, the reanalyzed geopotential does not exhibit a strong signal for the cold tongue in the Eastern Pacific, while Φ does. The patterns are also quite different in the Equatorial Indian Ocean, and the subtropical anticyclones are not well established in the potential field.

Therefore, the inclusion of a "back-pressure" gradient, as defined in previous works (Lindzen and Nigam 1987; Battisti et al. 1999) does not seem sufficient to reduce the sensitivity of the model Φ to the SST. Part of the problem relies on the fact that the variation of the depth of the boundary layer does not depend exclusively on the large-scale circulation: turbulent processes have a crucial impact on the evolution of the boundary layer. Moreover, these processes are influenced by the underlying SST; this introduces a strong feedback between the two terms of the potential, and further highlights the interest of a better understanding of the boundary layer (see Chapter 3). Furthermore, the impact of the warming of the mid-troposphere by convection has an impact on the surface flow (Chiang et al. 2001) that is poorly taken into account by the reduced-gravity model. A better parameterization of the pressure forcing Φ, used with the linear momentum equation (2.1), would certainly produce more realistic results. The model scale separation obtained

in Section 2.2.3 relies on a scale analysis that is independent of the parameterization of Φ. Therefore, the model scale separation is quite robust. On the contrary, the characteristics of the mesoscale and large-scale moist regions simulated by the model depend on the parameterization of Φ, and are consequently more arguable.

Besides, the non-linearities could be a secondary source of bias. In the total momentum equation, the advection term is quite smaller than the other terms. But the friction term might contain some non-linearity. As we pointed out in Section 2.2.1, it is often parameterized in more complex models as a non-linear term: the bulk formula assumes that the drag coefficient is proportional to the wind speed. This non-linearity would actually introduce a dependency of the drag coefficient on the latitude and potential gradient that would reduce the bias on the Equator: there, $|\mathbf{u}| = |\nabla\Phi|/\epsilon_d$, so $\epsilon_d \propto |\mathbf{u}|$ yields $|\mathbf{u}| \propto \sqrt{|\nabla\Phi|}$: the wind speed vary like the square root of the potential gradient and not like the gradient, and is thus less sensitive to the variations of this gradient.

2.4 Discussion

The analysis of the NCEP/NCAR data allowed us to discover the bimodality in the size distribution of the moist regions. This analysis might be interesting to refine using more precise data such as the products of the NASA Water Vapor Project (NVAP), that combines state-of-the-art multi-channel satellite and radiosonde data. Such an analysis would provide more information about the details of the scale separation and the characteristics of the modes.

The existence of two modes in the observed distribution of the moist regions in the tropics is an interesting feature. It means that the convection associated with the planetary circulations of Hadley and Walker are not only an average picture of the tropics, but they can be seen in the daily data. Furthermore, the existence of a scale separation suggests that the convection and moistening of the atmosphere are differently organized on the large-scale mode and the synoptic-scale. The two modes are characterized by different ranges of humidity, and different dynamical regimes: the synoptic mode is very moist and characterized by an ascending mass flux that varies slowly with the size of the region, while the large-scale regions are less humid and characterized by a larger growth of the vertical circulation with the characteristic radius.

These results can be fairly reproduced by the equilibria of our simple two-column model with a parameterization of the surface flow between the columns, based on a reduced-gravity theory. The existence of two modes and a scale separation relies on the inclusion of parameterized dynamics. The mechanism that the model suggests for the selection of sizes is the competition between the Laplacian and Beta terms of the divergence. The inclusion of the beta-term is necessary to the existence of the large-scale mode, for which the thermodynamical model was originally designed.

Our simple model showed interesting results that are surprisingly resembling the observations. Though, only the model equilibrium is considered, and some systems, especially the small ones, are expected to be time-dependent. Nevertheless, most of the systems are slowly varying during their mature stage and can fairly be described by the equilibrium. More concern rises from the theory on which the parameterization of the surface flow is based: it exhibits some flaws that reduce its validity, and particularly for the synoptic scales. Nevetheless, most of the bias exhibited by the results of the reduced-gravity theory seem due to the modeling of the surface pressure. And, while the spectral properties of the equilibria certainly depend on this parameterization (through Eq. (2.14)), the scale separation is independent of it (Eq. (2.12)), and the existence of two modes is fairly robust.

Chapter 3

On bulk models of shallow cumulus convection

3.1 Introduction

Processes that take place in the cloud-topped boundary layer (CTBL) in the regions of the trade-winds are important to the dynamics and thermodynamics of the tropical atmosphere as a whole, as already noted in the previous chapters. Not only does the depth of the boundary layer condition the low-level convergence of moist energy in the deep tropics, which in turn helps determine the amount of deep convection, as we noted in Chapter 1, but the details of the vertical structure of the CTBL also determines its cloudiness, whose radiative forcing is an important feedback of the tropical system. While regions of boundary-layer stratocumulus are thought to constitute a strong stabilizing feedback in the tropical atmosphere (Miller 1997), the radiative response of the trade-wind regions is crucial to the sensitivity of the tropical climate (Bony et al. 2004). Through their modulation of the tropical climate, trade-wind clouds regulate the climate as a whole. The variability among treatments of CTBL cloud processes is a leading explanation for the varied climate sensitivity of General Circulation Models (GCMs) noted in Cess et al. (1996). Furthermore, the depth and vertical structure of the boundary layer might have an important impact on the surface dynamics, as we pointed out in Chapter 2.

Bulk models of the boundary layer are interesting tools to study the climate sensitivity (Betts and Ridgway 1989). Because they often encapsulate our understanding, bulk models also provide a convenient framework for evaluating parameterization ideas. The steady states of these models can give a good description of the bulk state of a real CTBL, or at least the bulk state to which it tends. Some one-layer models have proven their efficiency in representing the boundary layer. For instance, mixed-layer models (e.g., Lilly 1968) have allowed a better theoretical understanding of the dry convection and the stratocumulus-capped boundary layer.

Later, Betts and Ridgway (1988, 1989) developed the mixing-line model for the CTBL, which is based on empirical relationships describing the mixing of the air rising from the

surface with the air descending from the free troposphere. Notwithstanding that a mixing line does not respect diabatic processes other than mixing, a limitation of this model is that the cloud-layer structure is slaved to the subcloud layer through a fixed parameter β that depends on the nature (cloudy or clear-sky) of the profile. Thus the degrees of freedom exercised by the model are equivalent to that of a single layer model. Because of these limitations, it is interesting to explore two-layer models, or equivalent two-layer models which truly allow extra degrees of freedom in the cloud layer — and typically require additional closure assumptions. In principle, these models should allow a more realistic treatment of the variability in the vertical structure of the cloud layer, thereby improving the representation of cloudiness, and cloud-depth within the CTBL, both of which are critical from the larger scale perspective. In so far as the additional closure assumptions are concerned, these usually take the form of a specification of a mean-field representation of the turbulent fluxes. In large part it is thought that the fidelity of this representation determines the overall degree to which variability in the height and vertical structure of the CTBL are better represented in two-layer models.

The best-known example of a two-layer model of the CTBL is the one developed by Albrecht (1979, 1984, hereafter A79 and A84). This model consists of a well-mixed subcloud layer capped by a cloud layer in which the profiles of the conserved variables are linear and the turbulence is parameterized by a mass-flux scheme. It has been criticized in past work because of its sensitivity to poorly constrained parameters (Bretherton 1993). More recent work calls into question its closure assumptions: the turbulence parameters produced by LES models (Siebesma and Cuijpers 1995, hereafter SC95; Stevens et al 2001) and used in recent parameterizations (Siebesma and Holstag 1996, hereafter SH96) are an order of magnitude bigger than the ones produced by the Albrecht model. This raises the question: do improved models of cloud mixing lessen the sensitivity of the model to tunable parameters? Indeed, to what extent can recent advances in our understanding of the boundary layer improve our theoretical description at a bulk level?

The present chapter is devoted to answering these questions. We begin by reviewing the Albrecht model in Section 3.2 Section 3.3 examines the relationship between the popular models of the cloud layer fluxes, and the assumed cloud layer structure. Section 3.4 discusses the compatibility of Albrecht's framework with more general formulations of the turbulence and Section 3.5 examines the prospects of two-layer models with more degrees of freedom, with the idea of developing insight into remaining challenges confronting attempts to develop consistent bulk theories of the structure of the trade-wind boundary layer. The notations of this chapter are independent of the previous ones; they are listed in Appendix B.

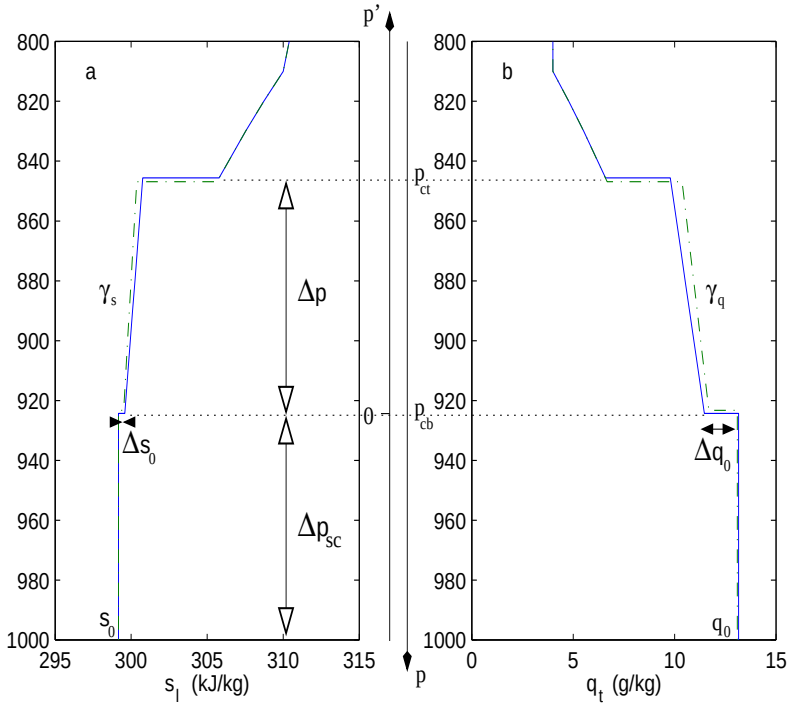

Figure 3.1: Profiles of (a) liquid static energy and (b) total water produced by Albrecht model; solid line: Albrecht model; dash-dotted line: Albrecht model without linearization of the cloud-environment difference.

3.2 A two-layer framework

3.2.1 Thermodynamic structure

The shallow cumulus boundary layer can be represented by two idealized layers, as in Albrecht's model (Fig. 3.1): (i) a well-mixed subcloud layer; (ii) a cloudy layer where average vertical gradients γ_q and γ_s of the conserved variables (i.e. the total water ratio $q_t = q + q_l$ and the static liquid energy $s_l = c_p T + gz - Lq_l$) are independent of height. This assumption will be hereafter called "constant-gradient" hypothesis. (iii) The interface between the two layers, as well as the inversion layer, is characterized by jumps of humidity and temperature. These interfaces are considered here as infinitely thin and represented by the jumps Δq_0 and Δs_0. Such profiles can be described as follows:

$$\begin{array}{lll} p > p_{cb} & q_t(p) = q_0 & s_l(p) = s_0 \\ p_{cb} > p > p_{ct} & q_t(p) = q_0 + \Delta q_0 + \gamma_q p' & s_l(p) = s_0 + \Delta s_0 + \gamma_s p' \end{array}$$

where p is the pressure, the subscript $_{cb}$ (resp. $_{ct}$) indicates the cloud base (resp. cloud top). $p' = p_{cb} - p$ is the pressure difference with the cloud base, which will be hereafter used as a vertical coordinate; note that, following Albrecht, p' increases with height.

3.2.2 Large-scale conditions

Locally, we are looking at how the state of the equilibrium boundary layer depends on the large-scale conditions as measured by the sea surface state, surface divergence D and radiative forcing.

The latter consists of two components: a clear-sky component R and a cloud component ΔF^R that depends on the cloud fraction and the optical depth of the clouds. We assume that R is homogeneous. Following recent work (SH96, Stevens et al. 2001), we further assume that the shallow cumuli cause no radiative forcing, whereas the stratiform clouds cause a cooling at the top of the boundary layer. The cloud radiative forcing can thus be approximated by a discontinuity ΔF^R of the net upward radiative flux at the cloud top:

$$\Delta F^R = f_s * \Delta F_0^R,$$

where f_s is the stratiform cloud fraction and ΔF_0^R=75 Wm^{-2}. It corresponds to a simplified version of the parameterization of the cloud radiative forcing in Stevens et al. (2001), with an average liquid water path of 3 gm^{-2} in the stratocumulus.

In the trade-wind regions the free-troposphere varies on timescales of order days, which is long compared to the turbulent timescale of the CTBL (order tens of minutes). Thus it makes sense to ask how the boundary layer structure develops as a function of some prescribed free-tropospheric state, which we specify as some linear function of p' according to:

$$q_{i+} = q_i^o + \Gamma_q \, p',$$
$$s_{i+} = s_i^o + \Gamma_s \, p',$$

where the subscript $_{i+}$ indicates the value at the top of the inversion, Γ_q and Γ_s are the free-tropospheric vertical gradients of humidity and static energy; q_i^o and s_i^o are the reference humidity and static energy at the cloud base - in our study, choosing the cloud base as a reference altitude is equivalent to choose the surface or tropopause levels, and it simplifies the notations.

To maintain these profiles of the free-tropospheric thermodynamic structure, radiative cooling must be balanced by advection. Usually the balance is enforced only through the consideration of the vertical component of advection, called subsidence and denoted by ω. In the case of a fixed gradient in s_l, a constant radiative cooling implies that $\omega = \omega_{i+}$ for $p \leq p_{ct}$. To have a positive rate of subsidence at, and above, the top of the CTBL, continuity demands that the large-scale divergence D of the horizontal winds is positive within the CTBL. If we further consider that D is constant with height within the CTBL then this is sufficient to completely specify a consistent vertical velocity:

$$\omega = D(p_s - p) = D(\Delta p_{sc} + p'),$$

where p_s is the surface pressure and $\Delta p_{sc} = p_s - p_{cb}$ is the thickness of the subcloud layer. Note that one drawback of this formulation is that because p_{ct} is determined by the model, that the subsidence at cloud top ω_{ct} will adopt a value consistent with the subsidence ω_{i+} above the inversion.

3.2.3 Fluxes and budgets: additional information

Turbulent fluxes needed to compute a constant-gradient model

The time-dependent equation of isentropic invariants (e.g., total water, moist entropy) can be written:

$$\partial_t \phi = \omega \gamma_\phi - g \partial_{p'} F^\phi + \sigma_\phi. \tag{3.1}$$

+Here $\phi \in \{s_l, q_t\}$ denotes one of our thermodynamic state variables, F^ϕ the turbulent flux of ϕ and σ_ϕ is a source associated with irreversible processes acting on ϕ, which for the most part we restrict to be independent of height below p_{ct} such that $\sigma_{s_l} = R$ and $\sigma_{q_t} = 0$. F^ϕ can be thought to include the fluxes due to precipitation, that are negligible at the surface but not at the coud base. For a uniform diabatic source, the prognostic equation of the vertical gradient can be obtained by differentiating (3.1) with respect to p':

$$\partial_t \gamma_\phi = D \gamma_\phi - g \partial_{p'p'} F^\phi. \tag{3.2}$$

If we approximate the last term on the right hand side (RHS) using divided differences, this expression can be written as follows:

$$\partial_t \gamma_\phi = D \gamma_\phi - 4g \frac{F^\phi_{ct} - 2F^\phi_A + F^\phi_{cb}}{\Delta p^2}, \tag{3.3}$$

where Δp is the depth of the cloud and subscript A denotes the mid-point value, e.g., $p_A = 1/2(p_{ct} + p_{cb})$, or $p'_A = 1/2(p_{cb} - p_{ct}) = \Delta p/2$. Because subcloud layer budgets give the time variation of the variables at the surface, once the time evolution of γ_ϕ is known, the time evolution of the jump at cloud base can be derived using the budget of the full cloud layer. The latter involves the flux at cloud base and cloud top — both of which were required to specify $\partial_t \gamma_\phi$. The time evolution of the cloud layer, and its equilibrium, can thus be determined by a parameterization that specifies the fluxes at cloud base, cloud top and at p_A in terms of known quantities. It can be thought of as the closure hypothesis required for the two-layer model.

Profiles of the fluxes in a steady state

Assuming that the cloud layer can be in a steady state and given the large-scale forcing, the turbulent fluxes can be written from (3.1) as a function of the vertical gradient $F^\phi = F^\phi(\gamma_\phi)$:

$$\partial_{p'} F^\phi = \frac{D}{g}(\Delta p_{sc} + p')\gamma_\phi + \frac{\sigma_\phi}{g}, \tag{3.4}$$

which, for constant γ_ϕ, implies that the turbulent fluxes are quadratic in p' :

$$F^\phi = F^\phi_{cb} + \frac{D}{2g}[(\Delta p_{sc} + p')^2 - \Delta p^2_{sc}]\gamma_\phi + \frac{\sigma_\phi}{g} p'. \tag{3.5}$$

This is consistent with the fact the two-layer model requires the values of the flux at three levels in the cloud layer: a quadratic function can be entirely defined by its values at three different points.

3.2.4 Parameterization of the mixing

Albrecht's model, as well as more recent works (Tiedtke 1989; SH96), uses a mass-flux scheme to parameterize the turbulent fluxes, that is based on a one-plume approach. This parameterization is often called "bulk mass-flux" parameterization. It can be written as follows:

$$F^{\phi} = M(\phi^c - \phi), \tag{3.6}$$

$$\partial_{p'} M = (\epsilon - \delta) M, \tag{3.7}$$

$$\partial_{p'} \phi^c = -\epsilon(\phi^c - \phi). \tag{3.8}$$

Here ϕ and F^{ϕ} retain their prior meaning, except that the superscript ^{c} indicates an expected value within the cloud. M is the convective mass flux, ϵ and δ are the fractional entrainment and detrainment rates, respectively. In most of the current parameterizations (A79; A84; Tiedtke 1989; SH96), ϵ is independent of height, in which case (3.8) can then be integrated to obtain the cloud-environment difference:

$$\phi^c - \phi = \Delta\phi_{cb}\, e^{-\epsilon p'} - \frac{\gamma_{\phi}}{\epsilon}\left(1 - e^{-\epsilon p'}\right), \tag{3.9}$$

where $\Delta\phi_{cb}$ is the cloud-environment difference at the cloud base. In Albrecht's model, ϵ is parameterized as $\frac{E}{\Delta p}$ where E is a parameter depending on the buoyancy profile (see Eq. (35) and (36) in A79).

Equations (3.6) and (3.7) can thus also be written:

$$F^{\phi} = F^{\phi}_{cb} f(p') d(p', \zeta_{\phi}), \tag{3.10}$$

$$M = M_{cb} f(p'), \tag{3.11}$$

where f is a function of the pressure that gives the evolution of the mass flux with height ($f(0) = 1$) and d gives the evolution of the cloud-environment difference with height ($d(0) = 1$) which depends also on the ratio $\zeta_{\phi} = \gamma_{\phi}/\Delta\phi_{cb}$ between the vertical gradient and the cloud-environment difference at cloud base:

$$d(p', \zeta_{\phi}) = e^{-\epsilon p'} - \frac{\zeta_{\phi}}{\epsilon}\left(1 - e^{-\epsilon p'}\right). \tag{3.12}$$

Any pair of functions (ϵ,δ),(ϵ,f) and (f,d) uniquely describes the parameterization. Conversely, whatever the profiles of conserved variables may be, any pair of flux profiles (F^q,F^s) can be parameterized by any pair of those functions: the mass-flux formalism *per se* does not place any constraint on the system.

On the contrary, K-diffusion schemes do constrain the turbulent fluxes, since the mixing is described by only one function K (Stevens 2000); in this type of scheme, the turbulent fluxes are parameterized as follows:

$$F^{\phi} = -K\gamma_{\phi}, \tag{3.13}$$

From Equation (3.5), it is readily apparent that the K-diffusion scheme is inconsistent with the assumption of a constant-gradient steady state:

$$\frac{F^\phi}{\gamma_\phi} = \frac{F^\phi_{cb}}{\gamma_\phi} + \frac{D}{2g}[(\Delta p_{sc} + p')^2 - \Delta p_{sc}^2] + \frac{\sigma_\phi}{g\gamma_\phi} p', \tag{3.14}$$

and it is unlikely to be independent of ϕ since it would require F^ϕ_{cb}/γ_ϕ and σ_ϕ/γ_ϕ to be independent of ϕ. Of course, using two different K-profiles is possible, although it takes more elaborate justification than the classical K-diffusion schemes.

It is straightforward to ask what assumptions on the functions describing a mass-flux scheme are compatible with the constant-gradient hypothesis. To start with, we can study whether the parameterizations used in A79 or developed more recently (SH96) can lead to a steady state in such a model.

3.3 Steady-state solutions?

In this section and the next one, we will study how the steady-state solutions of the two-layer constant-gradient model constrain the functions describing the mixing. For this purpose, we will assume that the whole boundary layer is in steady state, and, focusing on the cloud and inversion layer, we will derive necessary conditions on the parameters of the turbulence or the characteristics of the inversion.

3.3.1 Required values of the parameters

Given a mass-flux parameterization as described in the previous section, we can assume the existence of a steady state of the constant-gradient model. In which case Equation (3.5) requires that

$$f(p')d(p', \zeta_\phi) = 1 + \frac{D}{2gM_{cb}}(p'^2 + 2p'\Delta p_{sc})\zeta_\phi + \frac{\sigma_\phi}{gF^\phi_{cb}} p'. \tag{3.15}$$

As we stated in the Section 3.2.3, the model can reach an equilibrium if (3.15) is verified at least at the top and the middle of the cloud.

With those two conditions, we can eliminate the term involving the diabatic forcing and the flux at cloud base to obtain:

$$1 - 2f(\Delta p/2)d(\Delta p/2, \zeta_\phi) + f(\Delta p)d(\Delta p, \zeta_\phi) = \frac{D\Delta p^2}{4gM_{cb}}\zeta_\phi. \tag{3.16}$$

Equation (3.16) can also be derived from (3.3), for the steady state of the vertical gradient.

The expression of d (Eq. (3.12)) shows that the left hand side (LHS) of (3.16) is linear in ζ_ϕ. For Equation (3.16) to be verified for total water and static energy, the following condition is necessary:

$$1 - 2f(\Delta p/2)e^{-\epsilon\frac{\Delta p}{2}} + f(\Delta p)e^{-\epsilon\Delta p} = 0. \tag{3.17}$$

Note that this equation is an expression of the interplay between the fluxes and profiles, and thus depends not at all on the bulk budget, but only on the assumptions on the profiles and in the parameterization of the mixing. Equation (3.17) always yields to the trivial solution $\Delta p = 0$, which reduces the model to a well-mixed one-layer model. We cannot describe the other solutions without specifying the function f. We will analyze two closures that have seemed to be the most reasonable approximations and have been used for two-layer or one-dimensional (1D) models.

- In Albrecht's model, the convective mass flux is supposed to vary linearly with height: $f(p') = 1 + \mu p'$. Equation (3.17) can be rewritten:

$$\left(1 - e^{-\epsilon \frac{\Delta p}{2}}\right)\left(1 - e^{-\epsilon \frac{\Delta p}{2}}(1 + \mu \Delta p)\right) = 0, \tag{3.18}$$

  which yields to either: (i) a mass flux strictly increasing with height:

$$\mu = \frac{e^{\epsilon \frac{\Delta p}{2}} - 1}{\Delta p} > 0,$$

  or (ii) no entrainment: $\epsilon = 0$.

- In SH96, it is suggested that the fractional detrainment rate δ is independent of height, as well as ϵ: the mass flux decreases exponentially: $f(p') = e^{(\epsilon - \delta)p'}$. Equation (3.17) turns into:

$$\left(1 - e^{-\delta \frac{\Delta p}{2}}\right)^2 = 0, \tag{3.19}$$

  which yields to no detrainment $\delta = 0$: the convective mass flux increases strictly with height if the entrainment is not also zero.

Though an increase of the mass flux can be observed in some cases near cloud base or cloud top (Stevens et al. 2001), the monotonic increase of the convective mass flux is far from being the general case. The alternative absence of entrainment is also unrealistic in shallow cumuli (SC95; Stevens et al. 2001; Blyth,1993): even the air in the cloud cores gets somewhat diluted by air from the environment. Thus, the linear profiles seem inconsistent with a bulk mass-flux parameterization of the turbulent fluxes which uses a constant fractional entrainment: the model cannot reach an equilibrium with such a parameterization.

Here, we can see that the constraints on the profiles of the conserved variables can affect the mixing in a way that keeps the system unsteady. In general, the assumptions about the nature of the mixing determine the equilibrium profile. Similarly, assumptions about the state determine or at least constrain the mixing. This raises the question of why Albrecht's model "works".

3.3.2 Why does Albrecht's model work?

Albrecht's simplifications of the parameterization

In A79, an ATEX case is successfully reproduced. However, different mathematical approximations are used in A79 and A84 to simplify the mass flux scheme. Some of them

prove to have a decisive impact on the equilibrium of the model:

(i) The cloud-environment differences $(\phi^c - \phi)$ of the conserved variables q_t and s_l are linearized.

(ii) The flux F_{ct}^q of water at the top of the cloud is constrained to respect the budget of the thin inversion layer.

We reproduce here the base case of A79 except for the closure on E that is taken from A84 (it corresponds to the A84 model without horizontal advection). The equilibrium profiles are shown in Figure 3.1. In order to analyze the impact of the simplifications, we release each of those constraints.

Linearization of the profiles

In Albrecht's model, the cloud-environment differences given by Equation (3.9) are linearized constraining the cloud base values and the total amount of water/liquid static energy in the cloud layer. Note that the approximated cloudy profiles do not verify Equation (3.8). If we release that approximation and use the profiles given by (3.9), the equilibrium total water and temperature profiles are close to the base case (see Fig. 3.1). However, the flux profiles are quite different: the convective mass flux increases with the altitude as stated in Section 3.3.1 (Fig. 3.2.a), and that leads to bigger heat and moisture fluxes at the top of the cloud (Figs. 3.2.b and 3.2.c).

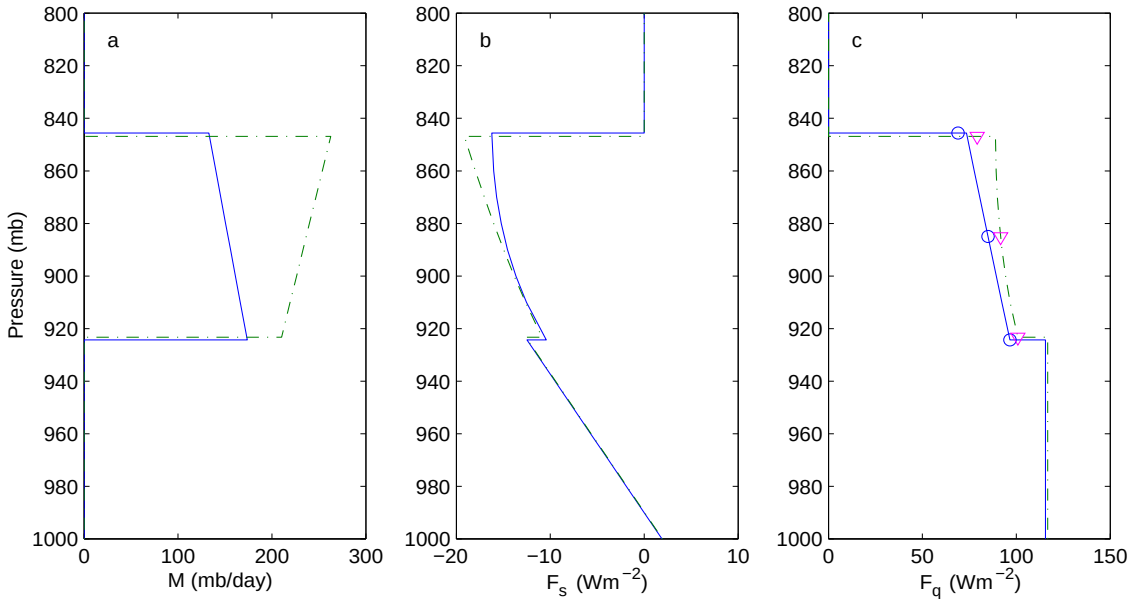

Figure 3.2: Profiles of (a) convective mass flux, (b) turbulent heat flux and (c) turbulent moisture flux; same conventions as previously plus: circles (resp. triangles): moisture fluxes that are actually used in Albrecht model (resp. Albrecht model without linearization).

But the model uses only the water flux at the cloud base, in the middle of the cloud and at the top of the cloud (indicated by circles and triangles on the profile in Figure 3.2.c). The water flux at the top of the cloud is prescribed by the budget of the inversion layer -

constraint (ii) - and this approximation allows the model to find an equilibrium somewhat independently from the mass-flux parameterization.

Flux of water at the top of the cloud

If we release the constraint on the cloud-top water flux (allowing the budget of water in the inversion layer not to be verified), the modeled boundary layer dries up to become dry and well-mixed: the cloud layer disappears ($\Delta p = 0$ as stated in Section 3.3.1).

In the absence of cloud radiative forcing ($\Delta F^R = 0$, which corresponds to BOMEX case), the difference r^q_{ct} between the flux of water prescribed by the balance of the inversion layer and F^q_{ct} computed by the parameterization of the mixing can be written, :

$$r^q_{ct} = F^S_{ct} \left(\frac{q_{i+} - q_{ct}}{S_{i+} - S_{ct}} - \frac{q^c_{ct} - q_{ct}}{S^c_{ct} - S_{ct}} \right), \tag{3.20}$$

This residual flux vanishes if the cloud-environment differences at cloud top, normalized by the jumps across the inversion, are equal for both conserved variables. This is actually a strong boundary condition for the parameterization of the turbulent fluxes. As shown by the circle at cloud top in Figure 3.2, this residual happens to be small in ATEX case when the cloud-environment difference is linearized, but it is larger when this mathematical approximation is not applied (see the triangle in Figure 3.2).

The equilibrium of Albrecht model relies on a mathematical approximation and on an arbitrary constraint that modify the mass-flux scheme. Although these might seem like arcane points, they are critical. The consistency of the theoretical framework allows for a more critical evaluation of the affect of various assumptions on the cloud layer. This weakens Albrecht model's physical pertinence and might explain why its behavior depends so much on the tunable parameters (Bretherton 1993).

3.4 Relaxed flux laws

Parameterizations of the mixing with strong constraints on the flux profiles (constant entrainment, linear or exponential mass flux) fail to represent a constant-gradient cloud layer in steady state, even if they are applied only at three levels. Here we relax these constraints to investigate if there exist some form of f and d which allows a constant-gradient cloud layer capped by an infinitely thin inversion to reproduce the observations. In the most general sense we are exploring the compatibility of the mass-flux equations with the assumption of a constant-gradient cloud layer.

To address this issue we consider the cloud-base altitude and fluxes as parameters which we take from both LES results (SC95; Stevens et al. 2001) and observations (Holland and Rasmusson 1973; Augstein et al. 1973): we further consider that the subcloud layer is in steady state, and that the fluxes at cloud base are constrained by the balance of the subcloud layer. The necessary conditions derived from the equilibrium equations will be

evaluated for conditions observed during the Barbados Oceanographic and Meteorological Experiment (BOMEX; Holland and Rasmusson 1973) and the Atlantic Trade Wind Experiment (ATEX; Augstein et al. 1973). The observed altitude of the cloud top will also be used in the first subsection to bound certain terms in the resultant equations.

3.4.1 Within the cloud: the constant-gradient hypothesis in question

If we assume that a constant-gradient model can reach an equilibrium with more elaborate functions describing the detrainment and entrainment from the clouds, we can build the functions $\epsilon(p')$ and $\delta(p')$ from Equations (3.6) to (3.8), as well as the mass-flux profile $M(p')$. Details of the derivation are given in Appendix A. $M(p')$, $\epsilon(p')$ and $\delta(p')$ can be expressed as a function of the turbulent fluxes and and their derivatives, and the vertical gradients of s_l and q_t:

$$M = -\frac{\frac{\partial_{p'}F^q}{F^q} - \frac{\partial_{p'}F^s}{F^s}}{\frac{\gamma_q}{F^q} - \frac{\gamma_s}{F^s}}, \tag{3.21}$$

$$\delta = -\frac{\frac{\partial_{p'}F^q}{\gamma_q} - \frac{\partial_{p'}F^s}{\gamma_s}}{\frac{F^q}{\gamma_q} - \frac{F^s}{\gamma_s}}, \tag{3.22}$$

$$\epsilon = \frac{\frac{\partial_{p'p'}F^q}{F^q} - \frac{\partial_{p'p'}F^s}{F^s}}{\frac{\partial_{p'}F^q}{F^q} - \frac{\partial_{p'}F^s}{F^s}} - 2\frac{\frac{\partial_{p'}F^q}{\gamma_q} - \frac{\partial_{p'}F^s}{\gamma_s}}{\frac{F^q}{\gamma_q} - \frac{F^s}{\gamma_s}}. \tag{3.23}$$

The physical consistency of the mass flux scheme demands $M > 0$, $\epsilon > 0$ and $\delta > 0$. These constraints reduce the domain of equilibria that can be represented in the constant-gradient framework for a given large-scale forcing and fluxes at the cloud base. Using the expression of the fluxes at equilibrium (Eq. (3.5)), the domain of possible equilibrium (γ_q, γ_s) can be bounded (see the Appendix A for details):

$$\gamma_q\beta_F(1+\frac{\alpha}{\pi}) < \gamma_s < -\frac{R}{\omega_{ct}} + \gamma_q\beta_F\left(1+\frac{\alpha\pi^2}{2(1+\pi)}\right), \tag{3.24}$$

$$\gamma_s < \gamma_q\beta_F\left[1+\alpha\left(\sqrt{1-2\frac{q^e_{cb}}{\gamma_q\Delta p_{sc}}}-1\right)\right], \tag{3.25}$$

where $\pi = \Delta p/\Delta p_{sc}$ is the ratio of the cloud depth to the subcloud layer depth, β_F is the ratio of the sensible to latent heat fluxes at the cloud base (the equivalent of the Bowen ratio at the cloud base) multiplied by L, α is the ratio of the total radiative cooling within the subcloud layer to the warming of this layer by the turbulent flux at cloud base, and q^e_{cb} is the equivalent humidity of the turbulent transport at the cloud base:

$$\beta_F = \frac{F^s_{cb}}{F^q_{cb}}, \quad \alpha = \frac{R\Delta p_{sc}}{gF^s_{cb}}, \quad \text{and} \quad q^e_{cb} = g\frac{F^q_{cb}}{\omega_{cb}}.$$

Furthermore, we can analyze the change of the convective mass flux with height: a decrease of the mass-flux with height corresponds to $\epsilon - \delta < 0$. Using Equations (3.22) and

(3.23), we can write:

$$\epsilon - \delta = \frac{\frac{\partial_{p'p'}F^q}{F^q} - \frac{\partial_{p'p'}F^s}{F^s}}{\frac{\partial_{p'}F^q}{F^q} - \frac{\partial_{p'}F^s}{F^s}} - \frac{\frac{\partial_{p'}F^q}{\gamma_q} - \frac{\partial_{p'}F^s}{\gamma_s}}{\frac{F^q}{\gamma_q} - \frac{F^s}{\gamma_s}}. \tag{3.26}$$

In the common range of forcing, Equation (3.26) yields to both the condition for a strictly decreasing mass-flux (see the Appendix A for details):

$$\gamma_s > \gamma_q \beta_F \left[1 + \frac{\alpha}{2} \left(\sqrt{1 - 2\pi - \pi^2 - 4\frac{q^e_{cb}}{\gamma_q \Delta p_{sc}}} - 1 + \pi \right) \right], \tag{3.27}$$

and the condition for a strictly increasing mass-flux:

$$\gamma_s < \gamma_q \beta_F \left[1 + \frac{\alpha}{2} \left(\sqrt{1 - 4\frac{q^e_{cb}}{\gamma_q \Delta p_{sc}}} - 1 \right) \right]. \tag{3.28}$$

Case	BOMEX	ATEX
D	$3 \cdot 10^{-6}\,\mathrm{s}^{-1}$	$5 \cdot 10^{-6}\,\mathrm{s}^{-1}$
R	-2 K day^{-1}	-2.5 K day^{-1}
f_s	0.0	0.5
p_s	1010 mb	1010 mb
p_{cb}	950 mb	930 mb
p_{ct}	845 mb	855 mb
F^q_{cb}	$125\,\mathrm{Wm}^{-2}$	$100\,\mathrm{Wm}^{-2}$
F^s_{cb}	$-12\,\mathrm{Wm}^{-2}$	$-12\,\mathrm{Wm}^{-2}$

Table 3.1: Large-scale forcing and parameters used in computations.

Figure 3.3 shows the domains of potentially-represented steady states, in ATEX and BOMEX cases, using the large-scale forcings, boundary fluxes and parameters indicated in Table 1. The observations are partly out of the domain: the BOMEX case seems impossible to reproduce. Moreover, in the cases that can be reproduced, a decrease of the convective mass-flux is a marginal case, whereas it is the most common case in the observations. In ATEX case, a constant-gradient model would produce a mass flux that would strictly increase with height, consistently with the results of Section 3.3.1. This is unrealistic: though the convective mass flux increases at the top of the cloud layer because of stratiform clouds (Stevens et al. 2001), it decreases within most of the layer.

The increase of the mass flux with height is a direct consequence of an underestimation of the cloud-environment difference at the top of the cloud, which is due to the constant gradient and appears clearly in (3.9): this difference tends asymptotically towards $-\gamma_\phi/\epsilon$. This limit in the growth of the cloud-environment difference with height requires an increase of the convective mass flux with altitude to produce the equilibrium fluxes.

The increase of the convective mass flux with height is also characteristic of some parameterizations that are used in operational models, as noted in Lenderink et al. (2003);

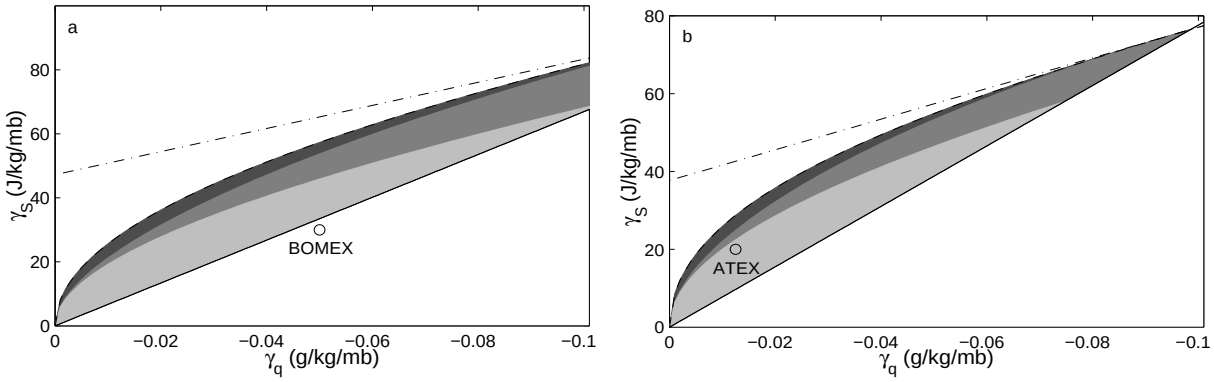

Figure 3.3: Shaded: domains of equilibrium (γ_q, γ_s) that can be simulated by a bulk mass flux parameterization: with (a) BOMEX and (b) ATEX large-scale forcing. Darkest (resp. lightest) shade: mass-flux strictly decreasing (resp. increasing) with height; intermediary shade: non-monotonic mass flux; the limits of the different shades zones are given by (3.27) and (3.28). Solid: LHS of (3.24); dash-dotted: RHS of (3.24); dashed: RHS of (3.25); the circles indicate the observed values.

although it certainly helps represent more steady-state oceanic cases, thisLenderink et al. (2003)'s work shows that it is one of the main problems in the simulation of the diurnal cycle over the continents.

Our result shows that the simple constant-gradient framework can reproduce at best very few observed profiles when it is coupled to a bulk mass-flux scheme, whatever the entrainment and detrainment profiles might be: this type of parameterization depends too much on the details of higher order derivatives of the conserved variables to be used in such a simple framework. Part of the problem might result from our simplifications to the large-scale forcing, or our neglect of transient or advective effects; nonetheless, it illustrates the strength of the physical constraints given by a one-plume scheme.

In general, it seems that a constant gradient is essentially incompatible with the mass flux formalism.

3.4.2 At the top of the cloud: the over-constrained massless inversion

The infinitely thin inversion

In Albrecht's framework, the constant-gradient hypothesis is a strong constraint on the profiles. The assumption of an infinitely thin inversion layer seems less questionable since it has proven so useful in the representation of the stratocumulus-topped boundary layer. Considering that some undetermined parameterization of the turbulence can produce an equilibrium cloud layer, we can investigate to which extent this assumption is compatible with the constant-gradient hypothesis.

Taking the time derivative of ϕ integrated over a thin inversion layer around p_{ct}, and taking the limit where the depth of this layer is zero, the budget of a conserved variable

for the inversion can be written as follows:

$$(\partial_t p'_{ct} + \omega_{ct})(\phi_{i+} - \phi_{ct}) + g(F^{\phi}_{ct} + \Sigma_{\phi}) = 0, \tag{3.29}$$

where Σ_{ϕ} is the diabatic source of ϕ within the inversion layer ($\Sigma_{q_t} = 0$ and $\Sigma_{s_l} = -\Delta F^R$).

The balance of static energy and total water of the infinitely thin inversion layer can thus be written:

$$\frac{F^q_{ct}}{q_{i+} - q_{ct}} = -\frac{\omega_{ct}}{g} = \frac{F^s_{ct} - \Delta F^R}{s_{i+} - s_{ct}}, \tag{3.30}$$

with q_{i+} and s_{i+} assumed to vary linearly with the altitude of the cloud top, as stated in Section 3.2.2.

Case	q^o_i (g kg^{-1})	Γ_q (g kg^{-1} mb^{-1})	s^o_i (kJ kg^{-1})	Γ_s (kJ kg^{-1}mb^{-1})	ω_i (mb day^{-1})
BOMEX	6.0	-0.01	306.6	30.	35.
ATEX	4.0	0.0	306.4	23.	55.

Table 3.2: Free-tropospheric profiles used in computations.

Assuming an equilibrium of the system with an adequate parameterization of the turbulent fluxes, F^q_{ct} and F^s_{ct} are given by Equation (3.5). Knowing the vertical gradients γ_s and γ_q, each part of (3.30) allows to compute independently the thickness of the cloud layer Δp:

$$\Delta p = \frac{\Delta q^o_i + \Gamma_q \Delta p_{sc}}{\gamma_q - 2\Gamma_q} \left(1 - \sqrt{1 - \frac{4(\Gamma_q - \frac{\gamma_q}{2})\Delta p_{sc}}{(\Delta q^o_i + \Gamma_q \Delta p_{sc})^2} \left(\Delta q^o_i + q^e_{cb} \right)} \right), \tag{3.31}$$

$$\Delta p = \frac{\Delta s^o_i + \Gamma_s \Delta p_{sc} + \frac{R}{D}}{\gamma_s - 2\Gamma_s} \left(1 - \sqrt{1 - \frac{4(\Gamma_s - \frac{\gamma_s}{2})\Delta p_{sc}}{(\Delta s^o_i + \Gamma_s \Delta p_{sc} + \frac{R}{D})^2} \left(\Delta s^o_i + s^e_{cb} \right)} \right), \tag{3.32}$$

where s^e_{cb} is the equivalent static energy of the turbulent transport at the cloud base, and $\Delta\phi^o_i$ is the temperature difference between the cloud layer profile and the free-tropospheric profile at cloud base.

$$s^e_{cb} = g\frac{F^s_{cb} - \Delta F^R}{\omega_{cb}} \quad \text{and} \quad \Delta\phi^o_i = \phi^o_i - \phi_0 - \Delta\phi_0.$$

This double equation for Δp is a potential source of inconsistency for the framework, and shows that the system is over-constrained. Let us remind the reader that, in Albrecht's model, the total water flux at cloud top is not parameterized but computed in order to respect (3.30); this allows to get a unique determination of Δp with the energy budget of the inversion layer.

A unique determination of Δp requires the RHS of (3.31) to equal the RHS of (3.32). Given the large-scale conditions and the flux and variables at the cloud base, this equality leads to a constraint on (γ_q,γ_s). Using the observed variables at the cloud base (q_{cb},s_{cb})=(16 g/kg, 302 kJ/kg) and the parameters listed in Table 1 and 2 for BOMEX, the possible

equilibrium pairs (γ_q,γ_s) are shown in Figure 3.4 (solid line). The observed gradients do not seem possible to reproduce. Furthermore, Figure 3.4 shows the equilibrium altitude of the cloud top along the line of possible equilibrium (dots and labels): gradients (γ_q,γ_s) that are close to the observed ones allow the representation of an inversion between 700mb and 500mb, which is much higher than the observed cloud top around 850mb. One could argue that, by suitably choosing the fluxes at the cloud base, a reasonable steady state could be found (see dash-dotted line in Fig. 3.4). However, because these fluxes are constrained by the surface fluxes and the equilibrium of the subcloud layer, it is reasonable to consider them as parameters. Additionally, the gradients and the altitude of the inversion are not too sensitive to changes in these parameters: to reproduce the observed cloud layer, the dash-dotted line in Figure 3.4 was computed with parameters that have been significantly modified: (F^q_{cb},F^s_{cb}) =(100 Wm^{-2},-4 Wm^{-2}).

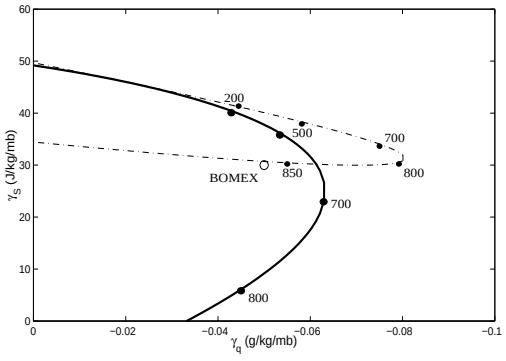

Figure 3.4: Possible steady-state gradients (γ_q,γ_s); solid: with BOMEX large-scale conditions and fluxes; dash-dotted: with BOMEX large-scale conditions and (F^q_{cb},F^s_{cb}) =(100 Wm^{-2},-4 Wm^{-2}); the labeled dots indicate the inversion height along the equilibrium line and the circle indicates the observed gradients.

We do not need to perform the same computation for ATEX: Albrecht's model showed that it is possible to reproduce this case with a constant-gradient model and an infinitely thin inversion layer, using a truncated mass-flux parameterization. Our results show that it is impossible to model BOMEX case. This is consistent with the observations: the inversion was much less abrupt during BOMEX than it was during ATEX, it is thus less likely to be satisfactorily modeled by an infinitely thin layer.

A model for a thin finite inversion

Nevertheless, the model of infinitely thin inversion layer can be simply modified. Let's consider a thin inversion between p_{ct} and p_{i+} where the profiles of conserved variables inside the inversion layer follow a mixing line. This model is slightly more general than an inversion layer with linear profiles. The balance of the layer for a conserved variable ϕ can be written as illustrated in Figure 3.5:

$$\omega_{i+}\ \phi_{i+} - (\omega_{i+} - \omega_{ct})\overline{\phi} - \omega_{ct}\ \phi_{ct} + gF^{\phi}_{ct} + \Sigma_{\phi} = 0 \tag{3.33}$$

where Σ_ϕ is the diabatic source for the whole layer; $\overline{\phi} = \lambda\phi_{i+} + (1-\lambda)\phi_{ct}$ is the vertical average of ϕ in the layer and λ is a mixing coefficient between 0 and 1, which, since the profiles follow a mixing line, does not depend on ϕ. For linear profiles, $\lambda = 1/2$.

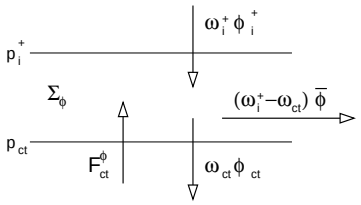

Figure 3.5: Budget of the inversion layer for a conserved variable.

Assuming that the layer is sufficiently thin to neglect the effect of the variation of ϕ_{i+} between p_{i+} and p_{ct}, Equation (3.33) can be written for q_t and s_l to yield to the following equivalent of (3.30):

$$\frac{F^q_{ct}}{q_{i+} - q_{ct}} = -\frac{\overline{\omega}}{g} = \frac{F^s_{ct} - \Delta F^R}{s_{i+} - s_{ct}}, \tag{3.34}$$

where $\overline{\omega} = (1-\lambda)\,\omega_{i+} + \lambda\,\omega_{ct}$ is the equivalent subsidence at the inversion.

This simple model of the inversion gives a additional degree of freedom λ to the system and allows the subsidence at the top of the inversion to be smaller than the subsidence at the top of the cloud, which has been observed (Holland and Rasmusson 1973; Augstein et al. 1973).

The two extreme terms of (3.34) lead to a cubic equation in the cloud depth Δp:

$$\begin{aligned}
&\frac{1}{2\Delta p_{sc}}\left(\frac{\Gamma_q}{\gamma_q} - \frac{\Gamma_s}{\gamma_s}\right)\Delta p^3 \\
&+\left[\frac{\Gamma_q}{\gamma_q} - \frac{\Gamma_s}{\gamma_s} + \frac{1}{2\Delta p_{sc}}\left(\frac{\Delta q^o_i}{\gamma_q} - \frac{\Delta s^o_i}{\gamma_s}\right) + \frac{R}{\omega_{cb}\gamma_s}\left(\frac{\Gamma_q}{\gamma_q} - 1\right)\right]\Delta p^2 \\
&+\left[\frac{\Delta q^o_i}{\gamma_q} - \frac{\Delta s^o_i}{\gamma_s} + \frac{R}{\omega_{cb}\gamma_s}\frac{\Delta q^o_i}{\gamma_q} + \frac{s^e_{cb}}{\gamma_s}\left(\frac{\Gamma_q}{\gamma_q} - 1\right) - \frac{q^e_{cb}}{\gamma_q}\left(\frac{\Gamma_s}{\gamma_s} - 1\right)\right]\Delta p \\
&+\frac{s^e_{cb}}{\gamma_s}\frac{\Delta q^o_i}{\gamma_q} - \frac{q^e_{cb}}{\gamma_q}\frac{\Delta s^o_i}{\gamma_s} = 0.
\end{aligned} \tag{3.35}$$

Figure 3.6 shows the most realistic $p_{ct} = p_{cb} - \Delta p$ (i.e. the closest to 850mb) where Δp is solution of Equation (3.35) and the corresponding mixing-line parameter λ computed with (3.34), using the large-scale conditions and parameters given in Table 1 and 2. If the model can produce plausible altitudes for the inversion, those are underestimated. For the observed vertical gradients, the altitude of the inversion would be about 20mb below the observed altitude. Moreover, the mixing-line parameter λ is supposed to be between 0 and 1, which is not the case for most of the domain including the observed gradients. To the

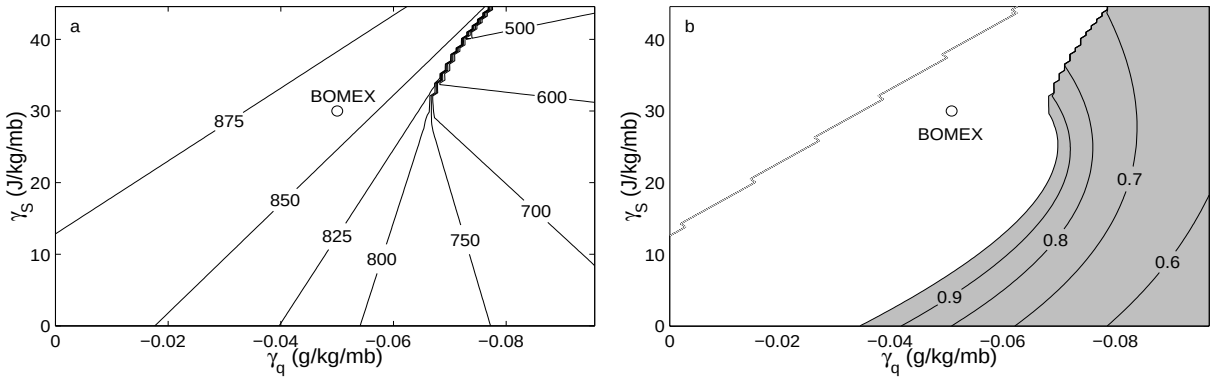

Figure 3.6: (a) Altitude of the inversion (in mb) at the equilibrium, computed from (3.35) and (b) corresponding value of the mixing-line parameter λ; shaded: domain of possible equilibrium ($\lambda \in [0; 1]$).

extent the BOMEX data are representative of a steady solution, this shows that a thin inversion following a mixing line is another incompatible idealization with the constant-gradient hypothesis.

From these results it is unclear whether the source of the incompatibility is the bias on the fluxes at the cloud top which originates from the oversimplification of the profiles inside the cloud, or if the inversion layer needs to be described by models that are more complex than a mixing line. In either case it is evident that the idealization of the profiles, either inside the cloud or in the inversion layer more strongly constrains the evolution of the system than is generally appreciated. The fact that the constant-gradient hypothesis is uncompatible with the mass flux scheme and both idealized models of the inversion points to this assumption as the main overconstraint. It thus seems interesting to study what equilibrium can be reached by releasing this constraint.

3.5 Relaxed gradient laws

In the previous section, we showed that the assumption of a constant gradient in the cloud layer places unrealistic constraints on the model of the turbulent fluxes that keeps the system from reaching an equilibrium. Thus, it makes sense to relax this assumption and study what steady solutions look like given a model of the mixing (e. g. Stevens 2000). Furthermore, we can investigate whether a change of the parameterization of turbulence allows a better representation of the inversion layer.

SH96 showed using a 1D model that a parameterization of the cloudy boundary layer with constant fractional entrainment and detrainment rates ϵ and δ could reproduce the quasi-stationary state observed during BOMEX. The value of ϵ and δ were inspired by a LES run (SC95). It is interesting to analyze the steady profiles obtained by this model, in order to understand the influence of the parameterization on the vertical gradients, and to explain why the parameterization gives satisfactory results in a 1D model and not in

Albrecht's framework. Additionally, we can compute the profiles produced by Albrecht's parameterization of the turbulent fluxes, which corresponds to running Albrecht model without the constant-gradient hypothesis.

3.5.1 General equations of the cloud layer

Without the constant-gradient approximation, Equation (3.1) for the local equilibrium of a conserved variable can be rewritten:

$$\partial_t \phi = \omega \partial_{p'} \phi - g \partial_{p'} F^{\phi} + \sigma_{\phi}. \tag{3.36}$$

With the mass flux parameterization (Eq. (3.6)-(3.8)), it yields a differential equation in $(\phi^c - \phi)$:

$$\partial_{p'}(\phi^c - \phi) + \left(\epsilon - \delta \frac{gM}{\omega + gM}\right)(\phi^c - \phi) = \frac{\sigma_{\phi}}{\omega + gM}, \tag{3.37}$$

which can be solved semi-analytically:

$$\phi^c - \phi = \Delta\phi_{cb} e^{-H(p')} + \sigma_{\phi} e^{-H(p')} I(p'), \tag{3.38}$$

where:

$$H(p') = \int_0^{p'} \left(\epsilon - \delta \frac{gM}{\omega + gM}\right) dp \text{ and } I(p') = \int_0^{p'} \frac{e^{H(p)}}{(\omega + gM)} dp$$

are integration factors. The vertical gradient can thus be written:

$$\partial_{p'} \phi = -\frac{1}{\omega + gM} \left(\sigma_{\phi} + \delta g M e^{-H(p')} [\Delta\phi_{cb} + \sigma_{\phi} I(p')]\right). \tag{3.39}$$

Equations (3.37) to (3.39) are valid whatever the profiles of ω, ϵ and δ. If these functions do not depend on the profiles, these equations can be integrated directly to compute the steady state profiles, as we do in the next subsection.

The inversion will be modeled as described in Section 3.4.2: the altitude of the inversion will be computed using the two extreme terms of Equation (3.34), and the computation of λ using the third term will be used as a test of the improvement of the representation of the inversion layer.

3.5.2 Results for BOMEX case

Figure 3.7 shows the steady-state profiles of the conserved variables and their gradients produced by the following models: (i) SH96's parameterization with $\epsilon = 2.10^{-4}\text{Pa}^{-1}$ and $\delta = 2.7\ 10^{-4}\text{Pa}^{-1}$ (solid line), (ii) Albrecht's parameterization (with parameters from A84: τ_a =1/2 day and A =0.5) (dash-dotted line) and (iii) the functions ϵ and δ tabulated from SC95 (dashed line). The former actually mimics the LES run of SC95. As in the previous experiments, the cloud-base fluxes are prescribed and their values are indicated in Table 3.1. Here, we also prescribe the convective mass-flux at cloud base: it is chosen to match the results of LES (SC95): M_{cb}=0.025kg m^{-2} s^{-1}.

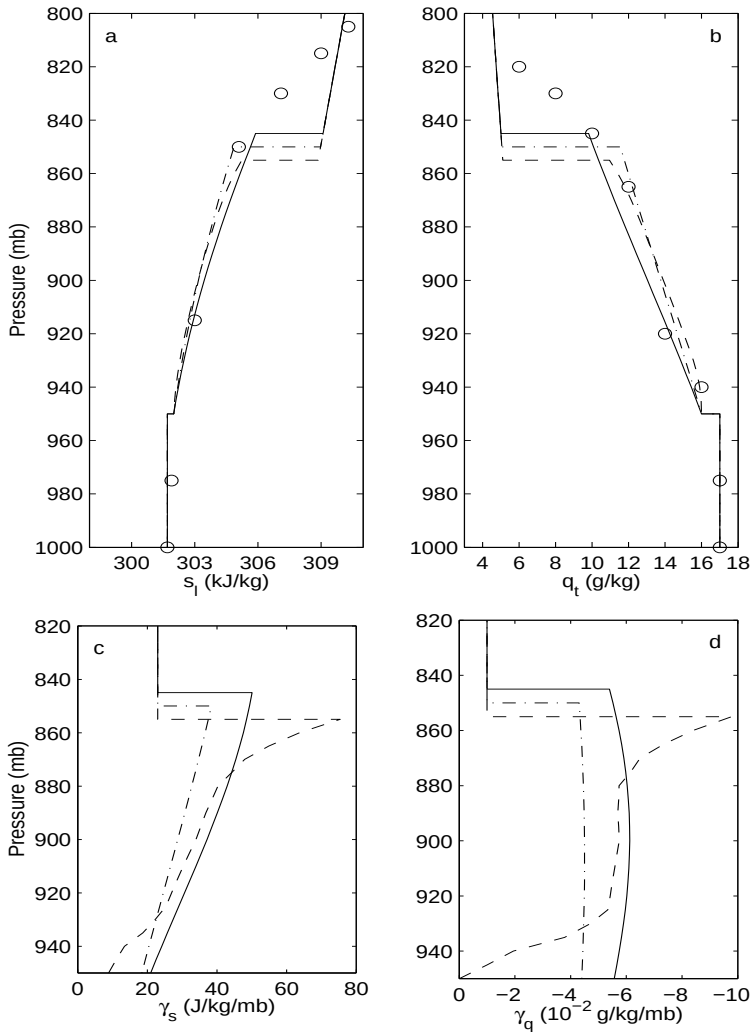

Figure 3.7: Profiles of (a) static liquid energy, (b) total water, (c) and (d) their vertical gradients within the cloud layer, in BOMEX case; circles: observations; dashed: reconstruction of SC95's LES run; solid: SH96's parameterization; dash-dotted: Albrecht's parameterization.

All three profiles look close to linear, but the vertical gradient of liquid static energy actually changes significantly with height (up to an order of magnitude for the reconstruction of the LES run). This change is fundamental in determining the variation of both the vertical advection and the turbulent heating with altitude: the modification of the vertical transport, both the large-scale and the turbulent components, permits a steady state solution that was not possible to reach with a constant gradient.

The variation of the vertical gradients with height, namely the second derivatives of the conserved-variable profiles, has an impact on the turbulence which is unclear in mass-flux parameterizations, while it is an explicit term in K-diffusion schemes. Actually, the cloud-environment difference depends much more on the variations of the gradient with height than the profile does (see Fig. A1 in SH96). As the turbulent fluxes are proportional to this cloud-environment difference in the bulk mass-flux scheme, a good representation of the cloud-environment is thus crucial to the representation of the turbulent mixing. The variation of the vertical gradients within the cloud layer is therefore crucial to the existence of an equilibrium.

Although the three models produce similar profiles of the conserved variables themselves, the gradient profiles are quite different. SH96's parameterization appears to be tuned to resemble the LES run in the middle of the cloud, but the LES produces gradients that are smaller at the cloud base and bigger at the cloud top than the ensuing parameterization. This suggests that the cloud-environment differences at cloud top produced by the LES are likely to be quite different from the ones produced by the parameterization that mimics the LES.

The gradients produced by Albrecht's parameterization are smaller than the ones produced by SH96's parameterization, but their profiles show the same pattern: the liquid static energy gradient increases with height, while the total water gradient is more nearly constant. This similarity reflects the fact that Albrecht's parameterization is a linearized version of SH96's parameterization with modified parameters.

The turbulent-flux profiles (see Figure 3.8) are quite similar in the three different models, except in the upper part of the cloud where they diverge. But the mass-flux profiles exhibit more marked differences. Actually, the gap between the profiles of mass flux is compensated by the gap between the cloud-environment differences. This shows that, given a parameterization of the convective mass flux, the cloud-environment differences tend to adapt themselves to the mass flux in order to produce an appropriate turbulent flux profile. The cloud-environment differences have an important impact on the buoyancy profile, which might be problematic for buoyancy-based closures.

Although the models give different flux profiles at cloud top, all three models produce a realistic inversion around 850mb, which tends to prove that the inversion is well represented by the mixing line model used here. But the mixing line parameter is unrealistic in all three models (SH96's parameterization: $\lambda = 3.2$; Albrecht's parameterization: $\lambda = 2.7$; reconstruction of SC95's LES run: $\lambda = 3.6$). The model of the inversion layer still seems oversimplified.

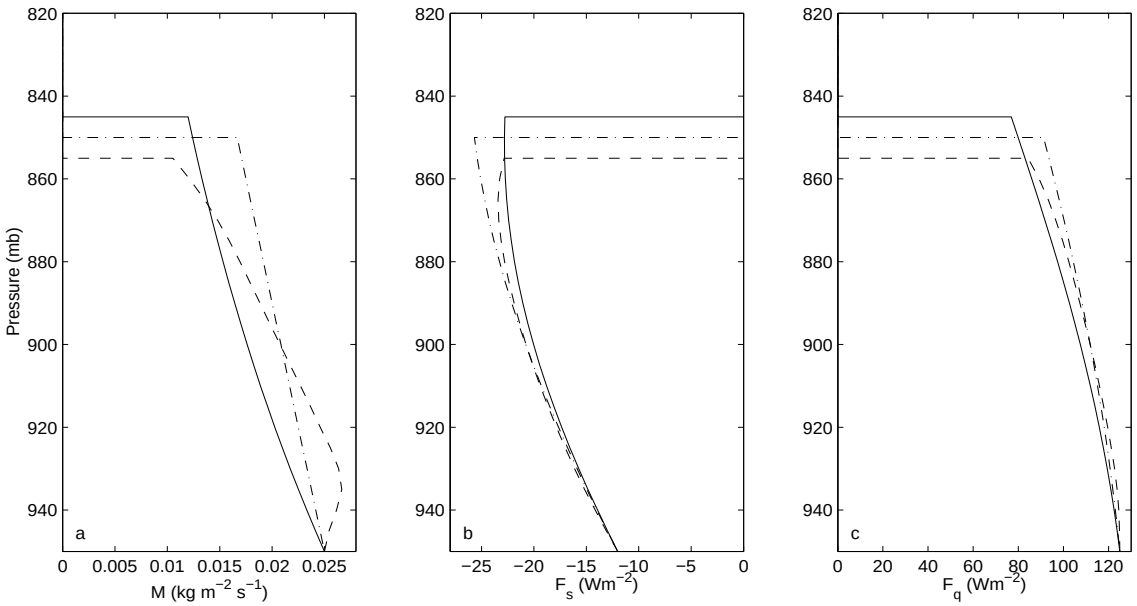

Figure 3.8: Profiles of (a) convective mass flux, (b) turbulent heat flux and (c) turbulent moisture flux in the cloud layer, in BOMEX case; dashed: reconstruction of SC95's LES run; solid: SH96's parameterization; dash-dotted: Albrecht's parameterization.

3.5.3 Sensitivity of λ to the cloud base flux and free-tropospheric profiles

As it has been pointed out (Bretherton, 2004, manuscript in preparation; see also Fig. 4), the issues related to the equilibrium of the inversion layer might be partly due to the strength of the constraints at cloud base. Therefore, it is interesting to study the sensitivity of λ to these fluxes. Figure 3.9 shows this sensitivity for SH96's parameterization. λ is shown as a function of the cloud-base fluxes of water and energy for three values of the cloud-base convective mass flux (M_{cb}=0.02; 0.025 and 0.03 kg m^{-2}s^{-1}). Note that we don't indicate the altitude of the inversion, which of course varies with the cloud-base fluxes.

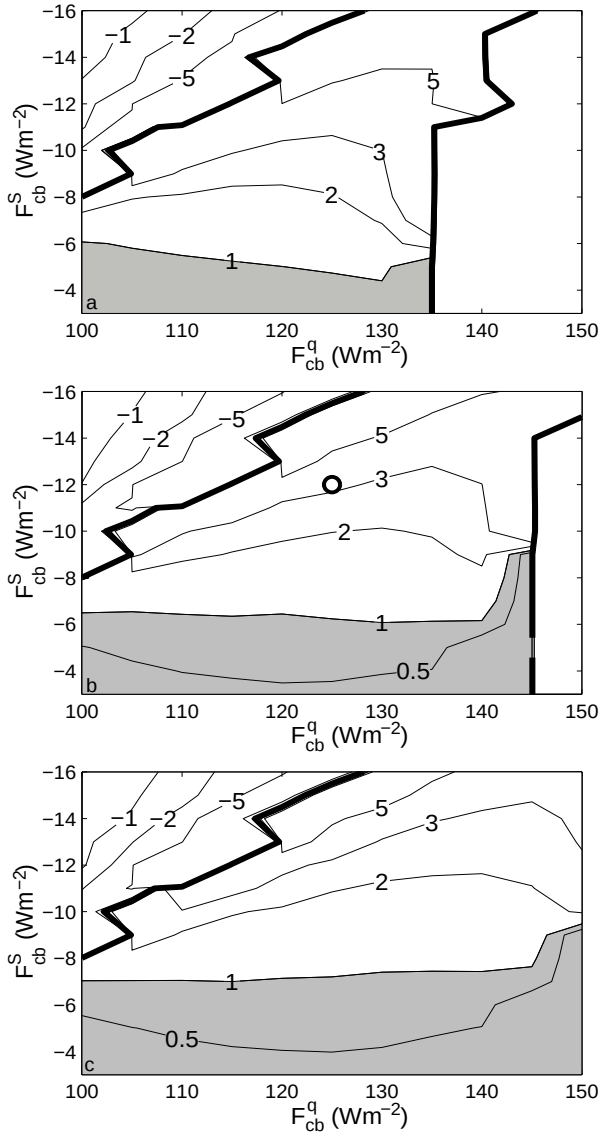

Figure 3.9: Sensitivity of λ to F^S_{cb} and F^q_{cb} for (a) M_{cb}=0.02, (b) M_{cb}=0.025 and (c) M_{cb}=0.03 kg m^{-2} s^{-1}; shaded: domain of consistent equilibrium ($\lambda \in [0;1]$); the thick lines indicate where λ tends to infinity and the circle indicates the values used in the previous section.

λ is not very sensitive to F_{cb}^q in the domain where it is positive. It is much more sensitive to F_{cb}^S: a domain of possible equilibrium appears for low $|F_{cb}^S|$. The size of this domain increases with M_{cb}. In LES experiments, F_{cb}^S is always below -10 W m^{-2}, and M_{cb} tends to be between 0.02 and 0.025 kg m^{-2}s^{-1}, where λ is greater than 1. The result of the previous section seems thus quite robust and encourages further work on the processes at play in the inversion. Furthermore, the sensitivity of λ to F_{cb}^S draws some attention to the closures used at cloud base: they can have a strong impact on the ability of a model to reach an equilibrium in the inversion layer.

Besides, λ is also expected to depend on the free-tropospheric profiles. As a sensitivity experiment, we choose to vary the reference values S_i^o and q_i^o of the free-tropospheric profiles - studies of the sensitivity to the gradients Γ_s and Γ_q show similar results.

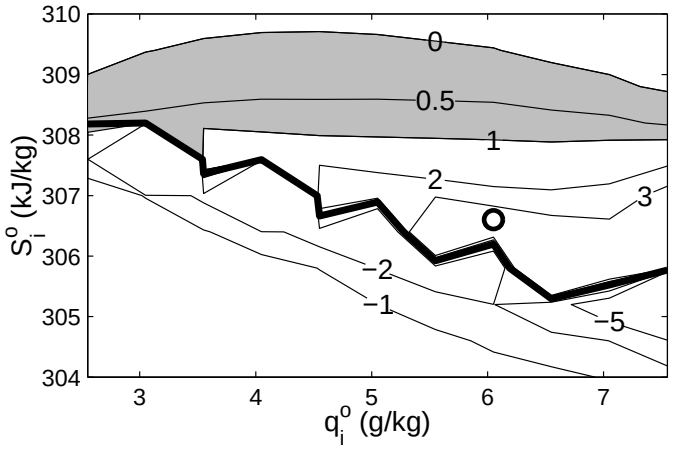

Figure 3.10: Sensitivity of λ to S_i^o and q_i^o; shaded: domain of possible equilibrium ($\lambda \in [0;1]$); the thick line indicates where λ tends to infinity and the circle indicates the values used in the previous section.

Figure 3.10 shows the results of the sensitivity study. The value of λ does not change significantly with q_i^o and much more with S_i^o. A zone of consistent equilibrium of the inversion layer appears for large S_i^o. The inversion layer is thus very sensitive to the free-tropospheric energy profile.

Therefore, the ability of a bulk model to produce a thermodynamically balanced inversion seems to rely on the boundary conditions in static energy, both on the flux at cloud base and the free-tropospheric profile. By suitably choosing both of them, a consistent equilibrium can be reached. Nevertheless, considering the LES results, the required values do not seem realistic.

3.6 Summary and discussion

Our work showed that it is not possible to represent some observed situations with a constant-gradient model when implemented with a bulk mass-flux parameterization. This

framework can produce a limited domain of cases — most of which exhibit a convective mass-flux that unrealistically increases with height. The change of the vertical gradient with height seems to be crucial to the existence of a steady state. SH96's parameterization of the mixing, as well as Albrecht's, allows the cloud layer to reach an equilibrium, mainly by increasing the vertical gradient of dry static energy with height.

The ability of different parameterizations to simulate realistic profiles of the conserved variables and their fluxes suggests that those profiles are not sufficient to validate a parameterization. The profiles of the gradient and cloud-environment differences appear as a better test. Unfortunately, they are difficult to be observed directly, with although LES may provide useful information in this respect.

In the absence of diabiatic sources, the approximation of an infinitely-thin inversion layer is also shown to overconstrain the system. Modeling the inversion as a thin layer following a mixing line allows to simulate well the altitude of the inversion, with cloud-layer profiles that are either linear or produced by Albrecht's or SH96's parameterizations. But, in all cases, the thermodynamic structure of the inversion is unrealistic. This is problematic because the vertical structure at the top of the cloud layer and in the inversion is crucial to determine the presence or absence of stratiform cloudiness, whose radiative forcing is important.

Of course, the constraints resulting from the constant-gradient hypothesis or from these parameterizations, which are tuned to represent well the middle of the cloud, leads to a loose representation of the conserved variables and their fluxes at the top of the cloud. But it seems that the main reason of the misrepresentation of the inversion is the fact that the processes at play in the inversion layer need to be addressed more accurately. Some of the processes are not well understood: possible decrease of the subsidence speed with height, radiative cooling at the top of the cloud, but most of them are actually the same as in the cloud layer. It seems thus natural to take a unified approach, considering a unique layer extending from the cloud base to the top of the inversion.

So far, no consistent theory including the inversion layer has been developed: most of the parameterizations strive to reproduce the profiles within the cloud layer, and the inversion layer is thought as a buffer that links the cloud layer to the free troposphere. A unified approach would require the parameterizations of the mixing to produce, at the top of the inversion, turbulent fluxes that vanish and profiles of the conserved variables that merge with the free-tropospheric profiles. The challenge in the construction of such a bulk model is to establish plausible hypotheses on the profiles of the conserved and their fluxes that are (i) of the same order of complexity, (ii) consistent within the cloud layer and (iii) meeting the boundary conditions at the top of the inversion.

The unresolved issue of the balance of the inversion layer points out the necessity of a better modeling of this layer at any level of complexity. In LES experiments, the inversion layer is often represented as a buffer, where the large-scale forcing decreases linearly until it vanishes (see Fig. 3.11). This is supposed to represent the transition to the free troposphere, which is assumed to be in steady state: the subsidence compensates the

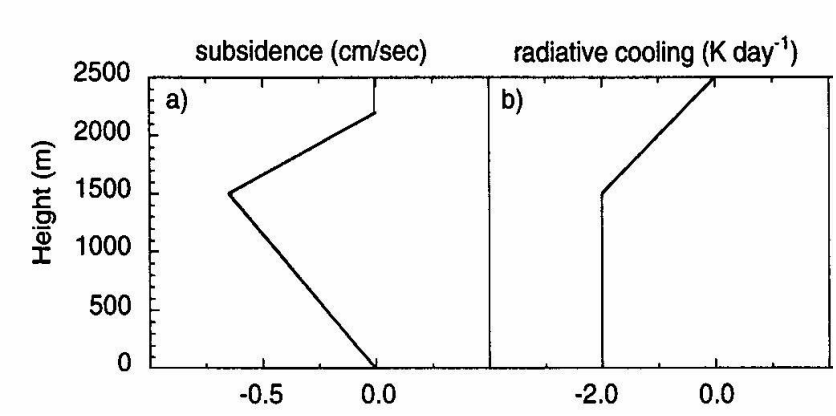

Figure 3.11: Example of profiles of (a) large-scale subsidence and (b) radiative cooling used in LES experiments (from Fig. 2 in Siebesma and Holtslag 1996).

radiative cooling. But these arbitrary large-scale profiles are not consistent if one considers the water budget, and they thus limit the LES insight in the budgets of the inversion layer.

Lastly, one can only speculate how the vertical resolution of the GCMs can affect the parameterization of the shallow convection. In general, the parameterization of the CTBL is very sensitive to this resolution (Lenderink et al. 2003). Our work also suggests that some precision in the vertical profiles of the thermodynamic variables is needed to obtain a good representation of the shallow convection. Low vertical resolutions in climate versions of the GCMs give a representation of the vertical profiles that are hardly better than a linear profile, and the inversion layer is not well represented either. In this case, the parameterization of the shallow convection is unlikely to produce realistic profiles or cloud fields, thus imperiling attempts to rationalize the role of clouds in climate change.

Conclusion

L'identification des processus clefs qui régule la température tropicale et sa sensibilité dans le cadre de changements climatiques, et notamment celui causé par les activités humaines, requière une compréhension d'interactions complexes entre processus d'échelles variées, dont l'effet moyen reste difficile à évaluer. Néanmoins, le travail de thèse présenté ici apporte des éléments de réponse et des pistes de réflexions qui sont résumés ci dessous.

Régions humides et dynamique dans les tropiques

Rétroactions climatiques

L'aire couverte par les régions humides, en effet de serre emballé, apparaît comme une variable intéressante pour évaluer la rétroaction de la vapeur d'eau dans les Tropiques. En effet, dans les observations, la variabilité interannuelle de l'aire A_c des régions humides, normalisée par l'aire de la zone intertropicale, semble liée à celle de la température de surface. De plus, les modèles à deux boîtes montrent une sensibilité marquée à cette aire, si elle est considérée comme un paramètre. Notamment, la réponse du modèle à une variation modérée de A_c est comparable à la réponse à une perturbation radiative du type de celle que subira à moyen terme l'atmosphère tropicale, c'est-à-dire un doublement de la concentration en dioxyde de carbone.

Ces sensibilités comparables s'expliquent par des rétroactions dynamiques différentes selon le type de perturbation. La circulation de grande échelle régule le climat tropical : plus elle est intense, plus la température moyenne refroidit. Or, cette circulation est contrôlée par le bilan radiatif de la troposphère libre sèche. De ce fait, elle augmente avec un réchauffement, et elle est fonction (dé)croissante de l'aire relative des régions sèches (humides). Alors que seul le premier effet intervient dans le cas d'une perturbation radiative, le second est aussi mis en jeu dans le cas d'une augmentation de A_c des régions convectives. Par suite, la rétroaction de la dynamique est négative pour une perturbation de la concentration des gaz à effet de serre ou de la constante solaire, et elle est positive pour une perturbation de A_c.

Par ailleurs, la dynamique a un rôle supplémentaire dans la régulation des flux de surface par le vent. Une intensification de la circulation entraîne en effet un accroissement des flux d'énergie sensible et latente à la surface de l'océan. Cette énergie injectée dans l'atmosphère est transportée vers la troposphère libre sèche via les zones humides et rayon-

née vers l'espace. Il en résulte un refroidissement de la température moyenne du système. Cet effet "vent-évaporation" accroît l'efficacité de la rétroaction due à la circulation de grande échelle.

La grande sensibilité du climat à une variation de A_c en fait une source potentielle de rétroactions importantes pour le climat tropical. Parmi les processus influençant la convection, et donc l'aire des régions humides, la convergence de l'humidité dans les basses couches est un mécanisme déterminant. Celui-ci est majoritairement associé à une convergence de masse. La compétition entre la convergence dans la couche limite et la circulation thermodynamiquement forcée par le refroidissement radiatif de la troposphère libre sèche est donc cruciale dans la modulation de A_c. A la fin du Chapitre 1, une expérience menée avec une paramétrisation très simple de la dynamique de surface en fonction des gradients de température de surface a montré que la modulation de A_c par la dynamique peut constituer une importante rétroaction positive pour un réchauffement occasionné par une augmentation de la concentration des gaz à effet de serre dans l'atmosphère.

Néanmoins, l'amplitude et même le signe de cette rétroaction modélisée dépend de façon claire des paramétrisations de l'épaisseur de la couche limite et de la dynamique. De fait, une étude présentée à la fin du Chapitre 2 montre que la dynamique des basses couches de l'atmosphère est relativement mal décrite par les théories reposant sur les gradients de température, même en incluant un terme "back pressure" comme dans le modèle de Lindzen et Nigam (1987) et les théories dérivées. Dans celles-ci, la modélisation du forçage de la pression est sans doute le principal point faible. Comprendre les facteurs intervenant dans la dynamique en surface au delà de ces modèles est un chantier de recherche en soi, que certaines études ont déjà entrepris (Wu et al. 2001). Obtenir une représentation fiable de la dynamique de surface qui puisse être adapté à un système bicolonne est un pas supplémentaire qui permettrait d'appréhender plus précisément le rôle de A_c dans la régulation du climat tropical.

L'aire A_c peut être aussi considérée comme une variable de diagnostique pour les simulations utilisant des MCG. La capacité d'un MCG à simuler la fraction des tropiques en effet de serre emballé est une indication de la qualité de la représentation du cycle de l'eau. Par exemple, ce type de diagnostic peut être réalisé en étudiant la variabilité interannuelle du A_c modélisé. Des expériences de doublement de CO_2 utilisant des MCG pourraient aussi apporter des éléments supplémentaires pour la compréhension de la réponse de A_c à une perturbation climatique.

Bimodalité de la distribution des tailles des régions humides

Afin d'obtenir une meilleure compréhension des mécanismes modulant l'aire relative des régions humides, il est intéressant de regarder la distribution des régions humides dans les Tropiques. Il apparaît que les tailles des régions humides ont une distribution bimodale. Le premier mode correspond aux zones meso-échelle et synoptiques fortement humidifées par des systèmes convectifs organisés, et le second aux branches ascendantes des circulations

planétaires, relativement moins humides. Ces deux modes semblent caractérisés par des régimes dynamiques différents : l'augmentation de la circulation de grande échelle avec la taille est plus marquée pour les grandes régions humides que pour les régions d'échelle synoptique. Il serait intéressant de vérifier si ce résultat, obtenu à partir de réanalyses, est reproduit dans des données plus précises d'humidité de la troposphère, comme celles du Projet Vapeur d'Eau de la NASA (NVAP).

Les deux modes observés semblent pouvoir s'expliquer par une sélection d'échelles due à la dynamique atmosphérique. Une paramétrisation simple de celle-ci, basée sur les gradients de température de surface, mais incluant aussi un terme "back pressure", permet de reproduire ces modes dans un modèle bicolonne. Ces modes modélisés sont associés à une séparation d'échelle si l'on considère l'extension du système bicolonne. Une meilleure compréhension de ces deux modes peut apporter beaucoup à l'étude des processus d'humidification de l'atmosphère tropicale et à l'évaluation de la rétroaction de la vapeur d'eau dans les Tropiques. Notamment, la réponse à un changement climatique de la distribution des zones humides selon leur taille influence certainement la réponse de la fraction des tropiques en effet de serre emballé.

Là encore, une meilleure représentation de la dynamique de surface permettrait une caractérisation plus précise des deux modes modélisés. La séparation d'échelles est certes un résultat robuste, mais les propriétés des deux modes sont sensibles à la paramétrisation du forçage de pression.

Compétition entre différents systèmes

L'étude de sensibilité du modèle au transport horizontal d'énergie a montré le comportement fortement non-linéaire du modèle. Au delà des comportements purement liés à la paramétrisation de la couche limite, cette sensibilité attire l'attention sur les potentielles interactions entre différents systèmes à deux colonnes. Ces interactions peuvent être une façon de considérer la circulation de Walker, et les téléconnections liées à El Niño-Oscillation Australe.

Par ailleurs, la variabilité intrasaisonnière de la mousson peut-être considérée comme une compétition entre deux zones de convergence, l'une sur l'Océan Indien Equatorial, l'autre sur le subcontinent Indien, qui partagent la même zone de subsidence. Cette compétition entraîne une alternance de périodes de pluies intenses (phase actives) et de périodes sèches (les pauses) au cours de la mousson. Ces deux états extrêmes sont considérés comme deux quasi-équilibres. Une modélisation simplifiée, analogue au modèle utilisé dans cette thèse, pourrait apporter un éclairage nouveau sur le fonctionnement de ce système.

Influence de l'humidité de la troposphère libre subsidente

L'effet de serre de la troposphère libre des zones sèches a été identifié par Pierrehumbert (1995) comme un processus important mais difficile à évaluer dans le cadre d'un modèle bicolonne. En effet, l'humidité de cette troposphère libre est contrôlée par l'advection de

grande échelle dans les couches supérieures de l'atmosphère, et une représentation adéquate de ce transport nécessiterait une meilleure paramétrisation de processus d'échelles variées comme le détrainement et la dynamique de la haute troposphère. Le travail de thèse présenté ici apporte peu d'éléments à ce sujet.

Mais il apparaît que l'humidité dans cette partie de l'atmosphère a des effets indirects au moins aussi importants que son influence directe sur le bilan radiatif des zones subsidentes, et donc sur la température moyenne. Le refroidissement radiatif de la troposphère libre sèche, qui dépend de la concentration des gaz à effet de serre et donc en premier lieu de la vapeur d'eau, contrôle la circulation de grande échelle et par conséquent les rétroactions dynamiques agissant sur une perturbation. De plus, la réponse de l'humidité au dessus de l'inversion à une perturbation a un impact déterminant sur la réponse du gradient horizontal de température en surface entre les colonnes sèche et humide via le bilan radiatif de l'océan et la ventilation de la couche limite. Cet impact est d'une influence décisive sur la dynamique de surface, et donc sur le signe et l'amplitude des rétroactions qui peuvent être attendues de variations de l'extension des régions humides. De nombreuses études climatiques se sont concentrées sur les rétroactions inhérentes aux régions humides de l'atmosphère tropicale ; la troposphère libre des régions sèches apparaît comme le lieu de processus potentiellement tout aussi intéressants.

Les mystères de la couche limite

Les nuages de couches limites ont été identifiés comme une source de rétroactions importantes pour la régulation du climat tropical (Miller 1997; Larson et al. 1999; Bony et al. 2004). De plus, au cours des études climatiques de cette thèse, la couche limite des alizés est apparue déterminante pour le contrôle de l'intensité et de l'extension spatiale de la convection par son rôle d'extracteur de vapeur d'eau des océans subtropicaux et le transport de celle-ci vers les zones de convergence. L'advection d'humidité des zones subsidentes vers les régions convectives dépend principalement de l'altitude de l'inversion et de l'intensité des vents de grande échelle en surface. A la lumière de notre étude de théories classiques héritières de celle de Lindzen et Nigam (1987), il semble que le second facteur soit relativement mal compris, et que ses variations soient elles-mêmes fortement modulées par la hauteur de la couche limite ainsi que par les variations spatiales des profils thermodynamiques à l'intérieur de la couche limite.

Or, la compréhension des phénomènes de convection peu profonde est encore incomplète. Le travail présenté au chapitre 3 a montré l'inadéquation de certaines simplifications pour obtenir des résultats réalistes, et particulièrement les problèmes liés à l'idéalisation de la couche d'inversion. Or, si l'on peut considérer en première approximation que l'altitude de l'inversion est contrôlée principalement par la flottabilité des particules nuageuses et les profils thermodynamiques de la troposphère libre, le mélange de l'air subsident et de l'air de la couche limite dans l'inversion module cette altitude. De plus, le détail des profils d'énergie et d'humidité au sommet du nuage et dans l'inversion conditionnent l'apparition

de stratocumulus; et c'est cette nébulosité stratiforme qui a un impact climatique important.

Notre analyse se base sur des modèles diagnostics simplifiés, mais leur validité s'étend au delà : ainsi, les questions soulevées sur la simplification des profils concernent les MCG, dont le nombre limité de niveaux sur la verticale exige d'être particulièrement précautionneux dans la paramétrisation de la couche limite. Par ailleurs, les problématiques liées à l'équilibre thermodynamique de l'inversion peuvent être transposées dans le cas des modèles de Simulation des Grands Tourbillons (LES), qui utilisent le plus souvent des forçages arbitraires dans la couche d'inversion. La sensibilité de ces modèles aux conditions de grande échelle, et particulièrement dans la couche d'inversion, a été jusqu'à présent peu étudiée. De telles études pourraient permettre une meilleure compréhension des processus en jeu dans la transition entre la convection peu profonde et la troposphère libre.

Questions climatiques sur la dynamique tropicale

Ce travail de thèse montre que les rétroactions radiatives-convectives sont couplées à des rétroactions dynamiques par de multiples aspects : non seulement par les transports horizontaux d'énergie et d'humidité, mais aussi par la modulation de la convection, profonde ou peu profonde, et par les flux de surfaces. La compréhension de la stabilité du climat tropical passe donc tout autant par la compréhension de sa dynamique humide, que par l'étude des mécanismes radiatifs-convectifs.

La compréhension conceptuelle de la dynamique tropicale est encore imparfaite. De nombreux travaux théoriques ont été menés, mais leur confrontation aux données reste insuffisante. L'étude rapide menée au cours de cette thèse souligne l'intérêt de cette confrontation.

Appendix

A Derivation of the domain of possible equilibrium for the relaxed flux laws

Replacing Equations (3.7) and (3.8) in the derivative of Equation (3.8) gives:

$$\begin{aligned}\partial_{p'}F^{\phi} &= \partial_{p'}M(\phi^c-\phi)+M(\partial_{p'}\phi^c-\gamma_\phi)\\ &= (\epsilon-\delta)M(\phi^c-\phi)+M[-\epsilon(\phi^c-\phi)-\gamma_\phi]\\ &= -\delta F^{\phi}-M\gamma_\phi. \end{aligned} \tag{A1}$$

Using this equation for s_l and q_t yields a linear system in M and δ which allows us to express the functions $M(p')$ and $\delta(p')$ as functions of the turbulent fluxes, their derivatives and the vertical gradients (Eqs. (3.21) and (3.22)).

Furthermore, Equation (3.7) can be rewritten:

$$\epsilon-\delta=\frac{\partial_{p'}M}{M}=\partial_{p'}(\ln(M)), \tag{A2}$$

which yields:

$$\begin{aligned}\epsilon-\delta &= \partial_{p'}\ln\left(\frac{\partial_{p'}F^q}{F^q}-\frac{\partial_{p'}F^s}{F^s}\right)-\partial_{p'}\ln\left(-\frac{\gamma_q}{F^q}+\frac{\gamma_s}{F^s}\right)\\ &= \frac{\frac{\partial_{p'p'}F^q}{F^q}-\frac{\partial_{p'p'}F^s}{F^s}}{\frac{\partial_{p'}F^q}{F^q}-\frac{\partial_{p'}F^s}{F^s}}-\frac{\frac{\partial_{p'}F^q}{\gamma_q}-\frac{\partial_{p'}F^s}{\gamma_s}}{\frac{F^q}{\gamma_q}-\frac{F^s}{\gamma_s}}.\end{aligned}$$

Replacing the expression of δ by the previous result (Eq. (3.22)) give the expression of ϵ (Eq. (3.23)).

The conditions of sign on M and δ can be turned into conditions on the ratios of the fluxes, their derivatives and the gradients of conserved variables, using their physically consistent signs ($F^q>0$, $\gamma_q<0$, $F^s<0$ and $\gamma_s>0$) :

$$M>0 \quad \Leftrightarrow \left(\frac{\partial_{p'}F^q}{F^q}<\frac{\partial_{p'}F^s}{F^s} \text{ and } \frac{F^q}{\gamma_q}<\frac{F^s}{\gamma_s}\right) \text{or} \left(\frac{\partial_{p'}F^q}{F^q}>\frac{\partial_{p'}F^s}{F^s} \text{ and } \frac{F^q}{\gamma_q}>\frac{F^s}{\gamma_s}\right), \tag{A3}$$

$$\delta>0 \quad \Leftrightarrow \left(\frac{\partial_{p'}F^q}{\gamma_q}>\frac{\partial_{p'}F^s}{\gamma_s} \text{ and } \frac{F^q}{\gamma_q}<\frac{F^s}{\gamma_s}\right) \text{or} \left(\frac{\partial_{p'}F^q}{\gamma_q}<\frac{\partial_{p'}F^s}{\gamma_s} \text{ and } \frac{F^q}{\gamma_q}>\frac{F^s}{\gamma_s}\right). \tag{A4}$$

Using the expression of the derivative of the fluxes and the fact that the radiative rate is negative ($R<0$), we can discriminate one of the conditions:

$$\frac{\partial_{p'}F^q}{\gamma_q}=\frac{\omega}{g}>\frac{\omega}{g}+\frac{R}{g\gamma_s}=\frac{\partial_{p'}F^s}{\gamma_s}. \tag{A5}$$

Consequently, considering the signs of the γ_ϕ and F^ϕ, the conditions (A3) and (A4) combine into:

$$M > 0 \text{ and } \delta > 0 \quad \Leftrightarrow \frac{F^q}{\gamma_q} < \frac{F^s}{\gamma_s} \text{ and } \frac{\partial_{p'} F^q}{F^q} < \frac{\partial_{p'} F^s}{F^s}. \tag{A6}$$

We will refer to the first condition of the RHS as (C1) and the second as (C2). (C1) and (C2) imply $\frac{\partial_{p'} F^q}{\gamma_q} > \frac{\partial_{p'} F^s}{\gamma_s}$, which can be written $\partial_{p'}\left(\frac{F^q}{\gamma_q} - \frac{F^s}{\gamma_s}\right) > 0$. Therefore, $\frac{F^q}{\gamma_q} - \frac{F^s}{\gamma_s}$ increases with p' and will be negative over the whole cloud layer if it is negative at cloud top. (C1) is thus equivalent to:

$$\frac{F^q_{ct}}{\gamma_q} - \frac{F^s_{ct}}{\gamma_s} < 0. \tag{A7}$$

Using the equilibrium flux profiles (Eq. (3.5)), we can further write (C1) as follows:

$$\frac{F^q_{cb}}{\gamma_q} - \frac{F^s_{cb} + \frac{R\Delta p}{g}}{\gamma_s} < 0, \tag{A8}$$

which leads to the LHS in inequality (3.24).

Furthermore, considering the opposite signs of the fluxes, (C2) is equivalent to $F^s \partial_{p'} F^q - F^q \partial_{p'} F^s > 0$. Besides, we note that, according to the equilibrium flux profiles and their derivatives (Eq. (3.5) and (3.4)), the second derivative of the flux is expressed:

$$\partial_{p'p'} F^\phi = \frac{D}{g}\gamma_\phi. \tag{A9}$$

Thus, considering the opposite signs of the gradients and (C1) $\partial_{p'}(F^s \partial_{p'} F^q - F^q \partial_{p'} F^s) = -\frac{D}{g}\gamma_q\gamma_s\left(\frac{F^q}{\gamma_q} - \frac{F^s}{\gamma_s}\right) < 0$: $F^s \partial_{p'} F^q - F^q \partial_{p'} F^s$ decreases with p', and will be positive over the whole cloud layer if it is positive at cloud top. (C2) is thus equivalent to:

$$F^s_{ct} \partial_{p'} F^q(\Delta p) - F^q_{ct} \partial_{p'} F^s(\Delta p) > 0. \tag{A10}$$

Using the equilibrium flux profiles and its derivative (Eq. (3.5) and (3.4)), we can further write (C2) as follows:

$$\frac{F^q_{cb}}{\gamma_q}\left(1 + \frac{R}{\omega_{ct}\gamma_s}\right) - \frac{F^s_{cb}}{\gamma_s} - \frac{R}{g\gamma_s}\frac{\Delta p^2}{2(\Delta p + \Delta p_{sc})} > 0, \tag{A11}$$

which leads to the RHS in inequality (3.24).

The second term of the RHS of (3.23) is actually twice δ. Therefore, we can write $\epsilon = h(p', 2)$ and $\epsilon - \delta = h(p', 1)$ with:

$$h(p', n) == -\frac{D}{g}\frac{\gamma_q\gamma_s}{F^q F^s}\frac{\frac{F^q}{\gamma_q} - \frac{F^s}{\gamma_s}}{\frac{\partial_{p'} F^q}{F^q} - \frac{\partial_{p'} F^s}{F^s}} + n\frac{\frac{R}{g\gamma_s}}{\frac{F^q}{\gamma_q} - \frac{F^s}{\gamma_s}}, \tag{A12}$$

where the second derivatives of the equilibrium flux profiles have been replaced by their expression (A9), as well as the first derivatives in the second term: $\frac{\partial_{p'} F^q}{\gamma_q} - \frac{\partial_{p'} F^s}{\gamma_s} = -\frac{R}{g\gamma_s}$.

The conditions on the signs of ϵ and $\epsilon - \delta$ can thus be assessed by studying the sign of h. Using the conditions derived from $M > 0$ and $\delta > 0$, we can write:

$$h > 0 \Leftrightarrow H(p', n) = \left(\frac{F^q}{\gamma_q} - \frac{F^s}{\gamma_s}\right)^2 - n\frac{R}{D\gamma_s}\left(\frac{F^s}{\gamma_s}\frac{\partial_{p'}F^q}{\gamma_q} - \frac{F^q}{\gamma_q}\frac{\partial_{p'}F^s}{\gamma_s}\right) < 0. \tag{A13}$$

We derive H to assess its variation with p':

$$\begin{aligned}\partial_{p'}H \quad &= 2\left(\frac{\partial_{p'}F^q}{\gamma_q} - \frac{\partial_{p'}F^s}{\gamma_s}\right)\left(\frac{F^q}{\gamma_q} - \frac{F^s}{\gamma_s}\right) - n\frac{R}{D\gamma_s}\left(\frac{F^s}{\gamma_s}\frac{\partial_{p'p'}F^q}{\gamma_q} - \frac{F^q}{\gamma_q}\frac{\partial_{p'p'}F^s}{\gamma_s}\right) \\ &= (n-2)\frac{R}{D\gamma_s}\left(\frac{F^q}{\gamma_q} - \frac{F^s}{\gamma_s}\right). \end{aligned} \tag{A14}$$

So, for $n = 2$, H is independent of p', therefore, the condition $\epsilon > 0$ can be computed anywhere within the cloud. We will compute it at the cloud base ($H(0,2) < 0$). For $n = 1$, H decreases with p'. The condition for increasing mass-flux ($\epsilon - \delta > 0$) for the whole cloud layer is thus equivalent to $H(0,1) < 0$ and the condition for a strictly decreasing mass flux is equivalent to $H(\Delta p, 1) > 0$. H is quadratic in γ_q and γ_s and can be rewritten, replacing the fluxes and their derivatives by their equilibrium profiles (3.5) and (3.4):

$$\begin{aligned} H(p', n) \quad &= \frac{F_{cb}^{q\,2}}{\gamma_q^2\gamma_s^2}\left\{\gamma_s^2 + \gamma_s\frac{\gamma_q}{F_{cb}^q}\left[n\frac{R}{g}(\Delta_{sc} + p') - 2\left(F_{cb}^s + \frac{R}{g}p'\right)\right]\right. \\ &\left. + \frac{\gamma_q^2}{F_{cb}^{q\,2}}\left[\left(F_{cb}^s + \frac{R}{g}p'\right)^2 - n\frac{R}{g}\left(\left(F_{cb}^s + \frac{R}{g}p'\right)(\Delta p_{sc} + p') - \frac{R}{D}\left(\frac{F_{cb}^q}{\gamma_q} + \frac{DD_2(p')}{2g}\right)\right)\right]\right\} \end{aligned} \tag{A15}$$

with $D_2(p') = (\Delta p_{sc} + p')^2 - \Delta p_{sc}^2$. H is negative for γ_s between the roots γ_s^- and γ_s^+ of this quadratic equation, and positive elsewhere. The roots can be expressed as a function of γ_q, the cloud base fluxes, and the large-scale forcing:

$$\gamma_s^{\pm} = \frac{\gamma_q}{F_{cb}^q}\left[F_{cb}^s + \frac{R}{g}p' - \frac{nR}{2g}(\Delta p_{sc} + p')\left(1 \mp \sqrt{1 - \frac{4\frac{gF_{cb}^q}{D\gamma_q} + 2D_2(p')}{n(\Delta p_{sc} + p')^2}}\right)\right]. \tag{A16}$$

For the parameter range of interest, γ_s^- is negative. The cloud layer is only conditionally unstable, so γ_s is positive, and we will focus on its position with respect to γ_s^+.

We can deduce the three following conditions, which are reproduced in a more concise form in Equations (3.25), (3.27) and (3.28) :

$$\begin{aligned} \epsilon > 0 \quad &\Leftrightarrow \quad \gamma_s < \frac{\gamma_q}{F_{cb}^q}\left[F_{cb}^s + \frac{R}{g}\Delta p_{sc}\left(\sqrt{1 - 2\frac{gF_{cb}^q}{D\gamma_q\Delta p_{sc}^2}} - 1\right)\right], \\ \epsilon - \delta > 0 \quad &\Leftrightarrow \quad \gamma_s < \frac{\gamma_q}{F_{cb}^q}\left[F_{cb}^s + \frac{R}{2g}\Delta p_{sc}\left(\sqrt{1 - 4\frac{gF_{cb}^q}{D\gamma_q\Delta p_{sc}^2}} - 1\right)\right], \\ \epsilon - \delta < 0 \quad &\Leftrightarrow \quad \gamma_s > \frac{\gamma_q}{F_{cb}^q}\left[F_{cb}^s + \frac{R}{2g}\left(\frac{\Delta p}{\Delta p_{sc}} - 1 + \sqrt{1 - 2\frac{\Delta p}{\Delta p_{sc}} - \frac{\Delta p^2}{\Delta p_{sc}^2} - 4\frac{gF_{cb}^q}{D\gamma_q\Delta p_{sc}^2}}\right)\right]. \end{aligned}$$

B Summary of symbols

Vertical coordinates

$p' \equiv p_{cb} - p$: difference of pressure from the cloud base;
Δp_{sc}: depth of the subcloud layer;
Δp: depth of the cloud layer;
$\pi \equiv \Delta p / \Delta p_{sc}$: normalized depth of the cloud layer.
Subscripts:
0: subcloud; *cb*: cloud base; *A*: middle of the cloud; *ct*: cloud top; i^+: top of the inversion.

Conserved-variable profiles

ϕ: conserved variable, either $s_l = C_P T + gz - Lq_l$ or $q_t = q + q_l$. The subscripts $_l$ and $_t$ are omitted when ϕ has another subscript or when ϕ itself is a subscript or superscript; ϕ is used for the clear sky profile in the cloud layer.
$\Delta\phi_0$: jump at cloud base;
γ_ϕ: gradient of ϕ in the cloud layer ;
ϕ_i^o: reference free-tropospheric profile ϕ at cloud base;
$\Delta\phi_i^o \equiv \phi_i^o - \phi_0 - \Delta\phi_0$: reference free-troposphere/boundary layer difference at cloud base;
Γ_ϕ: free-tropospheric gradient of ϕ;
$\overline{\phi} \equiv \lambda\phi_{i^+} + (1-\lambda)\phi_{ct}$: divergence-averaged ϕ of the inversion layer;
ϕ^c: cloud profile;
$\Delta\phi_{cb}$: cloud-environment difference at cloud base;
$d \equiv (\phi^c - \phi)/\Delta\phi_{cb}$: normalized cloud-environment difference;
$\zeta_\phi \equiv \gamma_\phi / \Delta\phi_{cb}$: ratio of the stratification to the cloud base difference.

Large-scale forcing

ω: vertical speed;
D: rate of divergence;
$\overline{\omega} \equiv (1-\lambda)\omega_{i^+} + \lambda\omega_{ct}$: equivalent subsidence at the inversion;
σ_ϕ: adiabatic source of ϕ;
$R \equiv \sigma_{s_l}$: radiative cooling;
Σ_ϕ: adiabiatic source integrated over the inversion layer;
$\Delta F^R \equiv -\Sigma_{s_l}$: jump of the upward net radiative flux at the inversion.

Turbulent mixing

F^ϕ: upward turbulent flux of ϕ;
M: convective mass flux;
$f \equiv M/M_{cb}$: normalized convective mass flux;
ϵ: entrainement rate;
δ: detrainment rate.

Miscanelous

α: ratio of the cooling of the subcloud layer to the warming of this layer due to the turbulent flux at cloud base;

β_F: Bowen ratio at cloud base;

q^e_{cb}: equivalent humidity of the turbulent water flux at cloud base;

s^e_{cb}: equivalent energy of the turbulent sensible flux at cloud base.

Bibliography

Albrect, B. A., 1984: A model study of downstream variations of the thermodynamic structure of the trade winds. *Tellus*, **36A**,187–202.

Albrect, B. A., K. Betts, W. Schubert, and S. K. Cox, 1979: A model of the thermodynamic structure of the trade-wind boundary layer: Part i: Theoretical framework and sensitivity tests. *Journal of the Atmospheric Sciences*, **36**,73–89.

Arakawa, A., and W. H. Schubert, 1974: Interaction of a cumulus cloud ensemble with the large-scale environment, part i. *Journal of the Atmospheric Sciences*, **31**,674–701.

Augstein, E., H. Riehl, F. Ostapoff, and V. Wagner, 1973: Mass and energy transports in an undisturbed atlantic trade-wind flow. *Monthly Weather Review*, **101**,101–111.

Barron, E. J., and W. M. Washington, 1985: Warm cretaceous climates: High atmospheric CO_2 as a plausible mechanism. *The carbon cycle and atmospheric CO_2: Natural variations Archean to present*, E. T. Sundquist, and W. S. Broecker, Eds., pp. 546–553. American Geophysical Union.

Bates, J. R., 1999: A dynamical stabilizer in the climate system: a mechanism suggested by a simple model. *Tellus*, **51A**,349–372.

Battisti, D. S., E. S. Sarachik, and A. C. Hirst, 1999: A consistent model for the large-scale steady surface atmospheric circulation in the tropics. *Journal of Climate*, **12**,2956–2964.

Bellon, G., H. Le Treut, and M. Ghil, 2003: Large-scale and evaporation-wind feedbacks in a box model of the tropical climate. *Geophysical Research Letters*, **30**,2145.

Betts, A. K., and W. Ridgway, 1988: Coupling of the radiative, convective, and surface fluxes over the equatorial pacific. *Journal of the Atmospheric Sciences*, **45**,522–546.

Betts, A. K., and W. Ridgway, 1989: Climatic equilibrium of the atmospheric convective boundary layer over a tropical ocean. *Journal of the Atmospheric Sciences*, **46**,2621–2641.

Betts, A. K., and W. Ridgway, 1992: Tropical boundary layer equilibrium in the last ice age. *Journal of Geophysical Research*, **97(2)**,2529–2534.

Blyth, A. M., 1993: Entrainment in cumulus clouds. *J. Appl. Meteor*, **32**,626–641.

Bony, S., J.-L. Dufresne, H. L. Treut, J.-J. Morcrette, and C. Senior, 2004: On dynamic and thermodynamic components of cloud changes. *Climate Dynamics*, **22 (2/3)**,71–76.

Bony, S., J.-P. Duvel, and H. Le Treut, 1995: Observed dependence of the water-vapor and clear-sky greenhouse-effect on sea-surface temperature - comparison with climate warming experiments. *Climate Dynamics*, **11**,307–320.

Bony, S., K.-M. Lau, and Y. C. Sud, 1997: Sea surface temperature and large-scale circulation influences on tropical greenhouse effect and cloud radiative forcing. *Journal of Climate*, **10**,2055–2077.

Bretherton, C. S., 1993: Understanding albrecht's model of trade cumulus cloud fields. *Journal of the Atmospheric Sciences*, **50**,2264–2283.

Bretherton, C. S., and A. H. Sobel, 2002: A simple model of a convectively coupled walker circulation using the weak temperature gradient approximation. *Journal of Climate*, **15**,2907–2919.

Broecker, W., 1996: Glacial climate in the tropics. *Science*, **272**,1902–1904.

Cahalan, R. F., and J. H. Joseph, 1988: Fractal statistics of cloud fields. *Monthly Weather Review*, **117**,261–272.

Cess, R. D., G. L. Potter, J. P. Blanchet, A. D. D. Genio, M. Deque, V. Dymnikov, V. Galin, W. L. Gates, S. J. Ghan, J. T. Kiehl, A. Lacis, H. L. Treut, Z.-X. Li, X.-Z. Liang, B. J. McAvaney, V. P. Meleshko, J. F. B. Mitchell, J.-J. Morcrette, D. A. Randall, L. Rikus, E. Roeckner, J. F. Royer, U. Schlese, D. A. Sheinin, A. Slingo, A. P. Sokolov, K. E. Taylor, W. M. Washington, R. T. Wetherald, I. Yagai, and M.-H. Zhang, 1990: Intercomparison and interpretation of climate feedback processes in 19 atmospheric general circulation models. *Journal of Geophysical Research*, **95**,16601–16615.

Cess, R. D., M. H. Zhang, W. J. Ingram, G. L. Potter, V. Alekseev, H. W. Barker, E. Cohen-Solal, R. A. Colman, D. A. Dazlich, A. D. D. Genio, M. R. Dix, V. Dymnikov, M. Esch, L. D. Fowler, J. R. Fraser, V. Galin, W. L. Gates, J. J. Hack, J. T. Kiehl, H. L. Treut, K. K.-W. Lo, B. J. McAvaney, V. P. Meleshko, J.-J. Morcrette, D. A. Randall, E. Roeckner, J.-F. Royer, M. E. Schelsinger, P. V. Sporyshev, B. Timbal, E. M. Volodin, K. E. Taylor, W. Wang, and R. T. Wetherald, 1996: Cloud feedback in atmospheric general circulation models: An update. *Journal of Geophysical Research*, **101**,12791–12794.

Chiang, J. C. H., S. E. Zebiak, and M. A. Cane, 2001: Relative roles of elevated heating and surface temperature gradients in driving anomalous surface winds in over tropical oceans. *Journal of the Atmospheric Sciences*, **58**,1371–1394.

Chou, C., and J. D. Neelin, 1999: Cirrus detrainment temperature. *Geophysical Research Letters*, **26**,1295–1298.

Chou, M.-D., and R. S. Lindzen, 2002: Comments on "tropical convection and the energy balance of the top of the atmosphere". *Journal of Climate*, **15**,2566–2570.

Chou, M.-D., R. S. Lindzen, and A. Y. Hou, 2002: Comments on "The Iris hypothesis: A negative or positive cloud feedback?". *Journal of Climate*, **15**,2713–2715.

Clement, A. C., and R. Seager, 1999: Climate and the tropical oceans. *Journal of Climate*, **12**,3383–3401.

CLIMAP, 1976: The surface of the ice-age earth. *Science*, **191**,1131–1137.

Crowley, T. J., 2000: Climap SSTs re-revisited. *Climate Dynamics*, **16**,241–255.

Del Genio, A. D., and W. Kovari, 2002: Climatic properties of tropical precipitating convection under varying environmental conditions. *Journal of Climate*, **15**,2597–2615.

Emanuel, K. A., J. D. Neelin, and C. S. Bretherton, 1994: On large-scale circulations in convecting atmospheres. *Quarterly Journal of the Royal Meteorological Society*, **120**,1111–1143.

Fouquart, Y., 1988: Radiative transfer in climate modeling. *Physically-Based Modeling and Simulation of Climate and Climatic Change*, M. Schlesinger, Ed., pp. 223–283. Kluwer Academic Publishers.

Fu, Q., M. Baker, and D. L. Hartmann, 2002: Tropical cirrus and water vapor: an effective earth infrared iris feedback. *Atmospheric Chemistry and Physics*, **2**,31–37.

Fu, R., A. D. Del Genio, W. B. Rossow, and W. T. Liu, 1992: Cirrus-cloud thermostat for tropical sea surface temperatures tested using satellite data. *N*, **358**,394–397.

Gagan, M. K., L. K. Ayliffe, J. W. Beck, J. E. Cole, E. R. M. Druffel, R. B. Dunbar, and D. P. Shrag, 2000: New views of tropical paleoclimates from corals. *Quaternary Science Reviews*, **16**,241–255.

Hartmann, D. L., and M. L. Michelsen, 1993: Large-scale effects on the regulation of tropical sea surface temperature. *Journal of Climate*, **6**,2049–2062.

Hartmann, D. L., and M. L. Michelsen, 2002: No evidence for iris. *Bulletin of the American Meteorological Society*, **83**,249–254.

Hartmann, D. L., L. A. Moy, and Q. Fu, 2001: Tropical convection and the energy balance at the top of the atmosphere. *Journal of Climate*, **14**,4495–4511.

Hartmann, D. L., L. A. Moy, and Q. Fu, 2002: Reply. *Journal of Climate*, **15**,2571–2572.

Held, I. M., and A. Y. Hou, 1980: Nonlinear axially symmetric circulations in a nearly inviscid atmosphere. *Journal of the Atmospheric Sciences*, **37**,515–533.

Held, I. M., and B. J. Soden, 2000: Water vapor and global warming. *Annual Review of Energy and the Environment*, **25**,441–475.

Hodges, K. I., 1994: A general method for tracking analysis and its application to meteorological data. *Monthly Weather Review*, **122**,2573–2586.

Holland, J. Z., and E. M. Rasmusson, 1973: Measurements of the atmospheric mass, energy, and momentum budgets over a 500-kilometer square of tropical ocean. *Monthly Weather Review*, **101**,44–55.

Ide, K., H. L. Treut, Z.-X. Li, and M. Ghil, 2001: Atmospheric radiative equilibria. part ii: Bimodal solutions for atmospheric optical properties. *Climate Dynamics*, **18**,29–49.

Keigwin, L., 1996: The little ice age and medieval warm period in the sargasso sea. *Science*, **274**,1504–1508.

Kelly, M. A., and D. A. Randall, 2001: A two-box model of a zonal atmospheric circulation in the tropics. *Journal of Climate*, **14**,3944–3964.

Kiehl, J. T., 1994: On the observed near cancellation between longwave and shortwave cloud forcing in tropical regions. *Journal of Climate*, **7**,559–565.

Kistler, R., E. Kalnay, W. Collins, S. Saha, G. White, J. Woollen, M. Chelliah, W. Ebisuzaki, M. Kanamitsu, V. Kousky, H. van den Dool, R. Jenne, and M. Fiorino, 2001: The ncep/ncar 50-year reanalysis: Monthly means CD-ROM and documentation. *Bulletin of the American Meteorological Society*, **82**,247–268.

Klein, S. A., and D. L. Hartmann, 1993: The seasonal cycle of low stratiform clouds. *Journal of Climate*, **6**,1587–1606.

Larson, K., D. L. Hartmann, and S. A. Klein, 1999: The role of clouds, water vapor, circulation, and boundary layer structure in the sensitivity of the tropical climate. *Journal of Climate*, **12**,2359–2374.

Le Treut, H., and G. Bellon, 2004: Radiative feedbacks and monsoon circulations: a view from simplified models. accepted by *PAGEOPH*.

Lenderink, G., A. P. Siebesma, S. Cheinet, S. Irons, C. G. Jones, P. Marquet, F. Muller, D. Olmeda, J. Calvo, E. Sanchez, and P. M. Soares, 2004: The diurnal cycle of shallow cumulus clouds over land: a single column model intercomparison study. *Submitted to the Quarterly Journal of the Royal Meteorological Society.*

Li, T., T. F. Hogan, and C.-P. Chang, 2000: Dynamic and thermodynamic regulation of ocean warming. *Journal of the Atmospheric Sciences*, **57**,3353–3365.

Li, Z.-X., K. Ide, H. L. Treut, and M. Ghil, 1997: Atmospheric radiative equilibria in a single column model. *Climate Dynamics*, **13**,429–440.

Liebmann, B., and C. Smith, 1996: Description of a complete (interpolated) outgoing longwave radiation dataset. *Bulletin of the American Meteorological Society*, **77**,1275–1277.

Lilly, D. K., 1968: Models of cloud-topped mixed layers under a strong inversion. *Quarterly Journal of the Royal Meteorological Society*, **94**,292–309.

Lin, B., B. Wielicki, L. Chambers, Y. Hu, and K.-M. Xu, 2002: The iris hypothesis: A negative or positive cloud feedback? *Journal of Climate*, **15**,3–7.

Lindzen, R. S., 1990: Some coolness concerning global warming. *Bulletin of the American Meteorological Society*, **71**,288–299.

Lindzen, R. S., M.-D. Chou, and A. Y. Hou, 2001: Does the earth have an adaptative infrared iris? *Bulletin of the American Meteorological Society*, **82**,417–432.

Lindzen, R. S., M.-D. Chou, and A. Y. Hou, 2002: Comment on "No evidence for iris". *Bulletin of the American Meteorological Society*, **83**,1345–1348.

Lindzen, R. S., and A. Y. Hou, 1988: Hadley circulations for zonally averaged heating centered off the equator. *Journal of the Atmospheric Sciences*, **45**,2416–2427.

Lindzen, R. S., and S. Nigam, 1987: On the role of the sea surface temperature gradients in forcing the low-level winds and convergence in the tropics. *Journal of the Atmospheric Sciences*, **44**,2418–2436.

Lovejoy, S., 1982: Area-perimeter relation for rain and cloud areas. *Science*, **216**,185–187.

Machado, L. A. T., M. Desbois, and J.-P. Duvel, 1992: Structural characteristics of deep convective systems over tropical africa and the atlantic ocean. *Monthly Weather Review*, **120**,392–406.

Machado, L. A. T., and W. B. Rossow, 1993: Structural characteristics and radiative properties of tropical cloud clusters. *Monthly Weather Review*, **121**,3234–3260.

Mapes, B. E., and R. A. Houze, 1993: Cloud clusters and superclusters over the oceanic warm pool. *Monthly Weather Review*, **121**,1398–1415.

Meehl, G. A., W. D. Collins, B. A. Boville, J. T. Kiehl, T. M. L. Wigley, and J. M. Arblaster, 2000: Response of the ncar climate system model to increased CO_2 and the role of physical processes. *Journal of Climate*, **13**,1879–1898.

Miller, R. L., 1997: Tropical thermostats and low cloud cover. *Journal of Climate*, **10**,409–440.

Nakajima, S., Y.-Y. Hayashi, and Y. Abe, 1992: A study on the "runaway greenhouse effect" with a one-dimensional radiative-convective equilibrium model. *Journal of the Atmospheric Sciences*, **49**,2256–2266.

Neelin, J. D., 1989: On the interpretation of the gill model. *Journal of the Atmospheric Sciences*, **46**,2466–2468.

Neelin, J. D., and C. Chou, 2001: Mechanisms limiting the southward extent of the South American monsoon. *Geophysical Research Letters*, **28**,2433–2436.

Neelin, J. D., I. M. Held, and K. H. Cook, 1987: Evaporation-wind feedback and low frequency variability in the tropical atmosphere. *Journal of the Atmospheric Sciences*, **44**,2341–2348.

Nilsson, J., and K. A. Emanuel, 1999: Equilibrium atmospheres of a two-column radiative-convective model. *Quarterly Journal of the Royal Meteorological Society*, **125**,2239–2264.

Peixoto, J. P., and A. H. Oort, 1992: *Physics of Climate*. American Institute of Physics, New York, Oxford.

Philander, S. G. H., 1990: *El Niño, La Niña and the Southern Oscillation*. Academic Press, New York.

Pierrehumbert, R. T., 1995: Thermostats, radiator fins, and the local runaway greenhouse. *Journal of the Atmospheric Sciences*, **52**,1784–1806.

Pierrehumbert, R. T., and R. Roca, 1998: Evidence for the control of atlantic subtropical humidity by large-scale advection. *Geophysical Research Letters*, **25**,4537–4540.

Ramanathan, V., R. D. Cess, E. F. Harrison, P. Minnis, B. R. Barkstrom, E. Ahmad, and D. Hartmann, 1989: Cloud-radiative forcing and climate: Results from the earth radiation budget experiment. *Science*, **243**,57–63.

Ramanathan, V., and W. Collins, 1991: Thermodynamic regulation of ocean warming by cirrus clouds deduced from the 1987 el Niño. *Nature*, **351**,27–32.

Reynolds, R. W., N. A. Rayner, T. M. Smith, D. C. Stokes, and W. Wang, 2002: An improved in situ and satellite SST analysis for climate. *Journal of Climate*, **15**,1609–1625.

Rheinboldt, W. C., and J. V. Burkardt, 1983: A locally parameterized continuation process. *Association for Computing Machinery Transactions on Mathematical Software*, **9**,215–235.

Roca, R., and V. Ramanathan, 2000: Scale dependence of monsonal convective systems over the indian ocean. *Journal of Climate*, **13**,1286–1298.

Roca, R., M. Viollier, L. Picon, and M. Desbois, 2002: A multi satellite analysis of deep convection and its moist environment over the indian ocean during the winter monsoon. *Journal of Geophysical Research*, **107**,N°10.1029/2000JD000040.

Rosenfeld, A., and A. C. Kak, 1976: *Digital picture processing*. Academic Press, New York.

Salathe, E. P., and D. L. Hartmann, 2000: Subsidence and upper-tropospheric drying along the trajectories in a general circulation model. *Journal of Climate*, **13**,257–263.

Samet, H., 1989: *Applications of spatial data structures: computer graphics, Image processing and GIS*. Addison-Wesley Publishing Company, Boston.

Sarachik, E. S., 1985: A simple theory for the vertical structure of the tropical atmosphere. *Pure and Applied Geophysics*, **123**,261–271.

Selwood, B. W., G. D. Price, and P. J. Valdes, 1994: Cooler estimates of cretaceous temperatures. *N*, **370**,453–455.

Sherwood, S. C., 1996: Maintenance of the free-tropospheric water vapor distribution. part ii: simulation by large-scale advection. *Journal of Climate*, **9**,2903–2918.

Shine, K. P., and A. Sinha, 1991: Sensitivity of the Earth's climate to height-dependent changes in the water vapour mixing ratio. **354**,382–384.

Siebesma, A. P., and J. W. M. Cuijpers, 1995: Evaluation of parametric assumptions for shallow cumulus convection. *Journal of the Atmospheric Sciences*, **52**,650–666.

Siebesma, A. P., and A. A. M. Holtslag, 1996: Model impact of entrainment and detrainment rates in shallow cumulus convection. *Journal of the Atmospheric Sciences*, **53**,2354–2364.

Stevens, B., 2000: Quasi-steady analysis of a pbl model with an eddy-diffusivity profile and non-local fluxes. *Monthly Weather Review*, **128**,824–836.

Stevens, B., A. S. Ackerman, B. A. Albrecht, A. R. Brown, A. Chlond, J. Cuxart, P. G. Duynkerke, D. C. Lewellen, M. K. Macvean, R. A. J. Neggers, E. Sánchez, A. P. Siebesma, and D. E. Stevens, 2001: Simulation of trade-wind cumuli under a strong inversion. *Journal of the Atmospheric Sciences*, **58**,1870–1891.

Sun, D. Z., and R. S. Lindzen, 1993: Distribution of tropical tropospheric water vapor. *Journal of the Atmospheric Sciences*, **50**,1644–1660.

Sun, D.-Z., and Z. Liu, 1996: Dynamic ocean-atmosphere coupling: a thermostat for the tropics. *Science*, **272**,1148–1150.

Thompson, L. G., 2000: Ice core evidence for climate change in the tropics: implications for our future. *Quaternary Science Reviews*, **19**,19–35.

Tiedtke, M., 1989: A comprehensive mass flux scheme for cumulus parameterization in large-scale models. *Monthly Weather Review*, **117**,1779–1800.

Tomas, R. A., and O. J. Webster, 1997: The role of inertial instability in determining the location and strength of near-equatorial convection. *Quarterly Journal of the Royal Meteorological Society*, **123**,1445–1482.

Tompkins, A. M., and G. C. Craig, 1999: A sensitivity study of tropical convection to sea-surface temperature in the absence of large-scale flow. *Journal of Climate*, **12**,462–476.

Wallace, J. M., 1992: Effect of deep convection on the regulation of tropical sea surface temperature. *Nature*, **357**,230–231.

Webster, P. J., V. O. M. na, T. N. Palmer, J. Shukla, R. A. Tomas, M. Yanai, and T. Yatsunari, 1997: Monsoons: Processes, predictability and the prospects for prediction. *Journal of Geophysical Research*, **103**,14451–14510.

Wu, Z., E. S. Sarachik, and D. S. Battisti, 2001: Thermally driven circulation under Rayleigh friction and Newtonian cooling: analytic solutions. *Journal of the Atmospheric Sciences*, **58**,724–741.

Yano, Y.-I., W. W. Grabowski, and M. W. Montcrieff, 2002: Mean-state convective circulations over large-scale tropical SST gradients. *Journal of the Atmospheric Sciences*, **59**,1578–1592.

Zebiak, S. E., 1982: Atmospheric convergence feedback in a simple model for el niño. *Monthly Weather Review*, **114**,1263–1271.

Zhang, C., B. E. Mapes, and B. J. Soden, 2003: Bimodality in tropical water vapour. *Quarterly Journal of the Royal Meteorological Society*, **129**,2849–2866.

Zhu, Y., R. E. Newell, and W. G. Read, 2000: Factors controlling upper-tropospheric humidity. *Journal of Climate*, **13**,836–848.